THE INITIAL EFFECTS OF WATER JET CLEANING ON SUPERHEATER TUBES

BY: *M H Melksham, BSc(Eng)(Hons)*

A thesis presented to the faculty of Engineering of the University of Adelaide in partial fulfillment of the requirements for the Degree of Master of Engineering Science.

Civil Engineering Department
University of Adelaide

JULY 1976

THE UNIVERSITY OF ADELAIDE

This thesis embodies the results of project work which made up two-thirds of the work for the degree of Master of Engineering Science.

CONTENTS

THE INITIAL EFFECTS OF WATER JET CLEANING ON SUPERHEATER TUBES

by

M H Melksham

SUMMARY

A finite element transient heat-conduction analysis was carried out to determine the temperature distribution at selected time-steps for a superheater tube subjected to localised surface quenching. Initially, a 2D analysis was undertaken so that alternative time-stepping schemes could be assessed and also sensitivity to temperature dependent material properties could be investigated. Then a 3D heat conduction analysis was carried out and the temperatures from this were used to determine the elastic stresses in the tube at the corresponding time stations. The linear elastic stress analysis, although being 3D was reduced to the superposition of a number of harmonic 2D analyses in order to investigate the economy of this approach to this type of problem.

All computing was carried out on the CDC 6400 at the Adelaide University Computing Centre.

DECLARATION

To the best of the candidate's knowledge and belief, this thesis contains no material which has been accepted for the award of any other degree or diploma in any University, and contains no material previously published or written by another person, except where due reference is made in the text.

M H MELKSHAM

ACKNOWLEDGEMENTS

The author wishes to express his appreciation for the suggestions and guidance given by Professor Y K Cheung, Dr M F Yeo and Mr G Sved.

Thanks are also extended to the State Electricity Commission of Victoria for enabling this work to be carried out.

1 INTRODUCTION

The use of finite elements for transient heat-conduction analysis and the determination of thermal stresses is well established. A means is provided by this method for obtaining answers to engineering problems which could not be obtained from alternative analytical solutions because of complex boundary conditions and material properties. Such a problem occurs in the on-load, water jet deslagging of furnace and superheater tubes.

Power stations in the State of Victoria operate primarily on brown coals from the Latrobe Valley obtained by open cut dredging. Combustion of the brown coal unfortunately results in the build-up of deposits on the furnace and superheater tubes leading eventually to a severe reduction in the efficiency of the heat transfer process. On-load cleaning of the furnace tubes is carried out effectively by using the impingement of water jets to quench and break away the offending surface deposits. This water washing process consists essentially of feeding a rotating water lance into the furnace so that the impinging water jets create an increasing spiral quench path on the furnace wall as indicated in Figure 1.1. The velocity v varies from 0.1 to 1.0 m/s

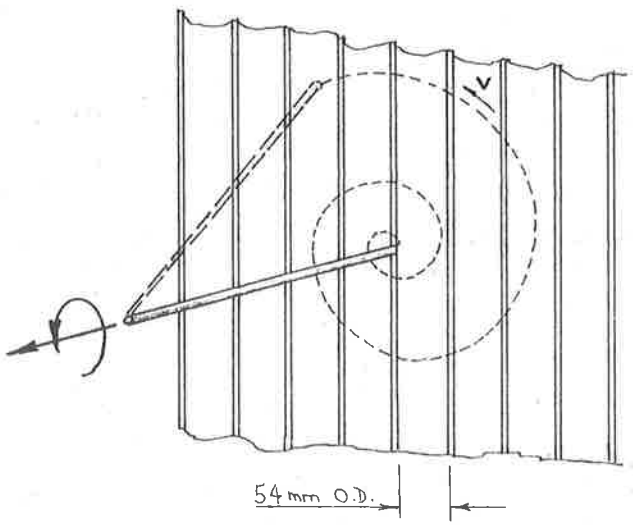

Jet flow rate = 0.4 l/s

FIGURE 1.1 : Water washing of tubes.

Regions of a furnace wall cleaned by this water washing operation have maintained a constant heat absorption rate for long periods whilst uncleaned parts of the wall suffered a 75 per cent reduction in flux density after 500 hours. Extension of the water washing process to superheater tubes is being examined and laboratory tests carried out by the State Electricity Commission of Victoria (SECV) have shown that repeated heating and quenching of tube samples leads to thermal fatigue cracking at the surface with the possibility of eventual tube failure. A number of experimental studies have been undertaken by the SECV[14] to determine the characteristics of crack depth and crack growth produced by cyclic heating and quenching of various tube steels at a number of different temperatures.

The on-load water washing process involves a number of parameters that can be controlled and which determine simultaneously the effectiveness of the cleaning operation and the severity of the quench. These parameters are being investigated experimentally by the SECV and they include jet size and velocity, probe entry velocity and speed of rotation, the requirement being to determine the optimum combination to produce maximum cleaning with minimum damage to the tubes. Thermal fatigue tests are time consuming and involve a large number of quench cycles and are therefore limited in the extent to which parameters can be varied. By carrying out a theoretical analysis of the initial effects of the quenching operation, to determine the variation of temperatures and stresses with time, certain guidelines for experimental investigation may be obtained.

Three-dimensional finite element analyses generally are expensive in terms of computer time because of the large number of equations to be solved and this is particularly so for transient analysis where the process is repeated for each time station. For this reason various ways of simplifying the problem were investigated in an attempt to obtain a more economical, if somewhat less rigorous solution.

2 HEAT CONDUCTION USING FINITE ELEMENTS

2.1 General Theory

The equation for transient heat conduction in substances with temperature dependent material properties may be written as:

$$\rho c \frac{\partial T}{\partial t} = \frac{\partial}{\partial x}\left(k \frac{\partial T}{\partial x}\right) + \frac{\partial}{\partial y}\left(k \frac{\partial T}{\partial y}\right) + \frac{\partial}{\partial z}\left(k \frac{\partial T}{\partial z}\right) + Q \qquad (1)$$

where ρc is the heat capacity, k the thermal conductivity and Q is the rate of internal heat generation.

The physical conditions of a particular problem will impose certain boundary conditions, the most common being:

a $T = T_b$ on a boundary where the temperature is specified;

b $$k\left(\frac{\partial T}{\partial x} l_x + \frac{\partial T}{\partial y} l_y + \frac{\partial T}{\partial z} l_z\right) + q_c = 0$$ for heat flow across a boundary

where l_x, l_y and l_z are the direction cosines of the normal to the boundary and q_c represents the rate of heat flow per unit area due to convection.

$$q_c = h(T-T_a)$$

where h is the surface conductance and T_a is the ambient fluid temperature.

The spacewise discretisation of equation (1) subjected to the boundary condition (a) and/or (b) can be accomplished using the steady-state variational form as shown by Zienkiewicz and Cheung[1] or by Galerkin's Method as described by Zienkiewicz et al[2,3].

Let the unknown temperature T throughout the solution domain be approximated by the relationship

$$T = \sum_{1}^{n} N_i(x,y,z)\ T_i(t) \tag{2}$$

where N_i are the usual shape functions, and T_i are the nodal temperatures. The simultaneous equations for the solution of n values of T_i are obtained by equating to zero for each node the weighted and integrated residual, resulting from the substitution of equation (2) into equation (1). Thus, for the i^{th} equation:

$$\int_R N_i \left\{ \left(\frac{\partial}{\partial x}\left(k_x \frac{\partial}{\partial x}\right) + \frac{\partial}{\partial y}\left(k_y \frac{\partial}{\partial y}\right) + \frac{\partial}{\partial z}\left(k_z \frac{\partial}{\partial z}\right) \right) \sum_{1}^{n} N_j T_j \right.$$

$$\left. + Q - \rho c \frac{\partial}{\partial t} \sum_{1}^{n} N_j T_j \right\} dxdydz = 0 \tag{3}$$

where the weighting function is made equal to the shape function

In this form second derivatives appear in the integral imposing unnecessary continuity conditions between elements and use can be made of Green's Theorem to modify equation (3) giving for a thermally isotropic material

$$-\int_R k \left(\frac{\partial N_i}{\partial x} \sum \frac{\partial N_j}{\partial x} T_j + \frac{\partial N_i}{\partial y} \sum \frac{\partial N_j}{\partial y} T_j + \frac{\partial N_i}{\partial z} \sum \frac{\partial N_j}{\partial z} T_j \right) dxdydz$$

$$+ \int_R N_i Q\ dxdydz - \int_R N_i\ \rho c \sum N_j \dot{T}_j\ dxdydz$$

$$+ \int_S N_i k \left(\sum \frac{\partial N_j}{\partial x} T_j\ l_x + \sum \frac{\partial N_j}{\partial y} T_j\ l_y + \sum \frac{\partial N_j}{\partial z} T_j\ l_z \right) dA = 0 \tag{4}$$

S is the external surface area

Only first order derivatives now have to be integrated and only continuity of shape functions have to be imposed.

Then equations (4) can be written in matrix form as:

$$[H]\{T\} + [P]\{\dot{T}\} + \{F\} = 0 \tag{5}$$

where

$$H_{ij} = \sum \int_E k\left[\frac{\partial N_i}{\partial x} \cdot \frac{\partial N_j}{\partial x} + \frac{\partial N_i}{\partial y} \cdot \frac{\partial N_j}{\partial y} + \frac{\partial N_i}{\partial z} \cdot \frac{\partial N_j}{\partial z}\right] dxdydz$$

$$+ \sum \int_{SE} N_i \, h \, N_j \, dA \tag{6}$$

where summation covers contribution of each element and E is the element region

$$P_{ij} = \sum \int_E \rho c \, N_i N_j \, dxdydz \tag{7}$$

Terms containing h are obtained by identifying the last term in equ (4) with the imposed boundary condition

$$F_i = -\sum \int_E N_i Q \, dxdydz - \sum \int_{SE} N_i \, h \, T_a \, dA \tag{8}$$

SE refers to elements with an external surface boundary condition specified

For the particular problem being considered there is no internal heat generation, i.e. Q = 0. The above equations are derived using Galerkin's Method but the same result is obtained using the variational form involving the minimisation of a functional.

2.2 Program Using Isoparametric Elements

The heat conduction analysis was carried out using computer programs with the parabolic type of isoparametric element which has 8 nodes and 20 nodes for the 2D and 3D elements respectively. It was necessary for the particular problem being considered to incorporate into the available programs the facility to cover heat flow across a boundary and also to add an iterative procedure to deal with temperature dependent material properties as described in Sections 2.3 and 2.4. The programs were also adapted to enable alternative time-stepping schemes to be used in the solution as described in Section 2.5.

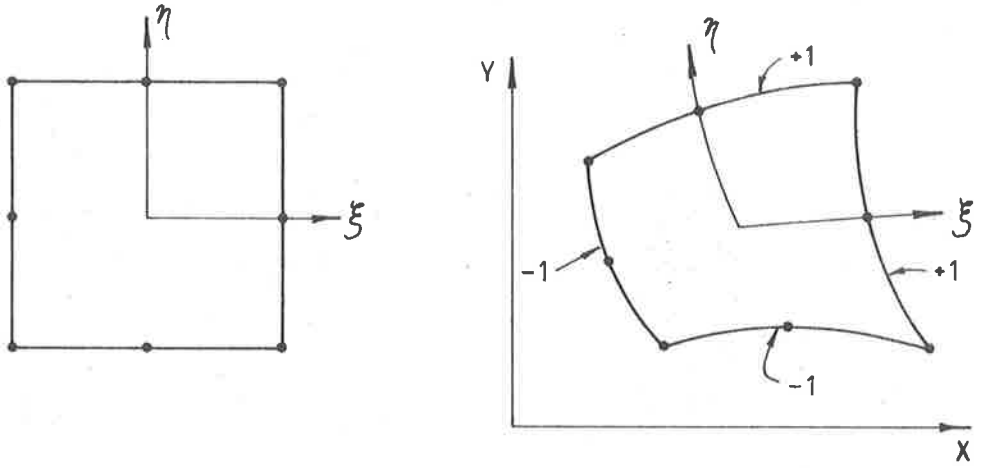

2D. ELEMENT

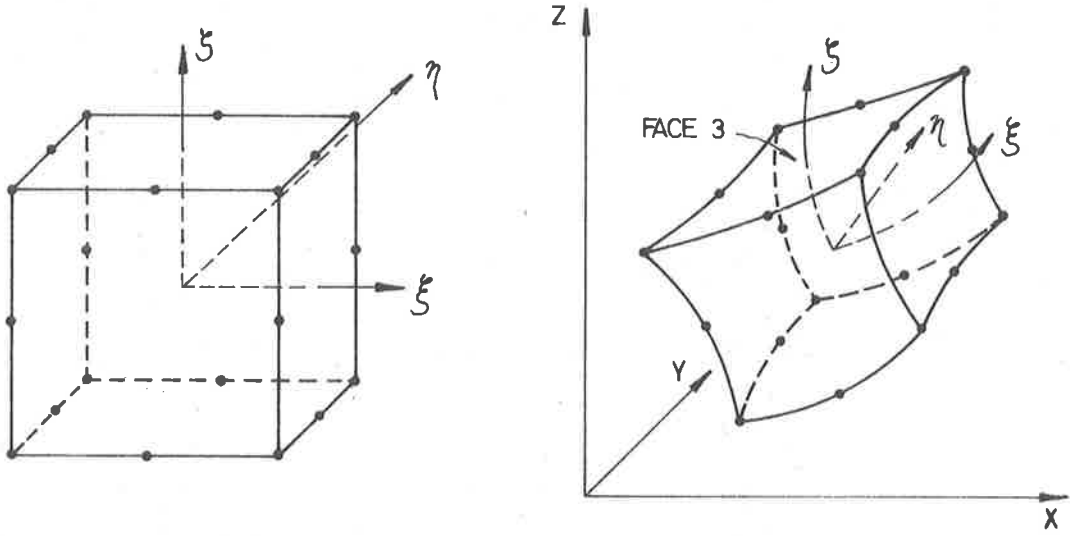

3D. ELEMENT

FIGURE 2.1 ISOPARAMETRIC ELEMENT
(PARABOLIC TYPE)

The isoparametric element[3] shown in Figure 2.1 is widely used and has a local system of curvilinear co-ordinates ξ, η and ζ with adjacent faces having values of ± 1. These co-ordinates are related to the cartesian global system by the shape functions N for the 3D element in the following manner:

$$x = [N_1, N_2, \ldots\ldots N_{20}] \begin{Bmatrix} x_1 \\ x_2 \\ \cdot \\ \cdot \\ \cdot \\ \cdot \\ x_{20} \end{Bmatrix}$$

where x_1 is the x co-ordinate of node 1 for the element etc.

This can be abbreviated to:

$$x = [N]\{x\}^e$$

and similarly,

$$y = [N]\{y\}^e$$

$$z = [N]\{z\}^e \qquad (9)$$

In the same way the temperature at any point within an element is prescribed in terms of the same shape function by

$$T = [N]\{T\}^e \qquad (10)$$

where $\{T\}^e$ is the nodal temperature vector.

The curvilinear system of local co-ordinates for an element allows the Gaussian Quadrature method of numerical integration to be used in forming the matrices H, P and F given in equations (6), (7) and (8). To derive these matrices some transformations are required to obtain the derivatives:

$$\begin{Bmatrix} \frac{\partial N_i}{\partial x} \\ \frac{\partial N_i}{\partial y} \\ \frac{\partial N_i}{\partial z} \end{Bmatrix} = [J]^{-1} \begin{Bmatrix} \frac{\partial N_i}{\partial \xi} \\ \frac{\partial N_i}{\partial \eta} \\ \frac{\partial N_i}{\partial \zeta} \end{Bmatrix} \quad \text{where } [J] \text{ is the Jacobian.} \tag{11}$$

$$[J] = \begin{bmatrix} \frac{\partial x}{\partial \xi} & \frac{\partial y}{\partial \xi} & \frac{\partial z}{\partial \xi} \\ \frac{\partial x}{\partial \eta} & \frac{\partial y}{\partial \eta} & \frac{\partial z}{\partial \eta} \\ \frac{\partial x}{\partial \zeta} & \frac{\partial y}{\partial \zeta} & \frac{\partial z}{\partial \zeta} \end{bmatrix} = \begin{bmatrix} \frac{\partial N}{\partial \xi} \\ \frac{\partial N}{\partial \eta} \\ \frac{\partial N}{\partial \zeta} \end{bmatrix} [\{x\}^e, \{y\}^e, \{z\}^e] \tag{12}$$

Elements of volume become

$$dxdydz = \det [J] \, d\xi d\eta d\zeta \tag{13}$$

The H, P and F matrices when determined are used in a time-stepping scheme to determine the nodal temperatures at the prescribed time increments. Assembly and solution of the equations was performed using the front solution technique[4].

2.3 Heat Flow Across a Boundary

This facility was incorporated for the 2D and 3D analysis and a description will be given for the latter case. If the heat flux across a boundary is proportional to the temperature difference

between the surface and the surrounding medium then it is given by $h(T-T_a)$, where T_a is the temperature of the medium and h is a constant known as the coefficient of surface heat transfer or the surface conductance. The boundary condition may then be written as:

$$k \frac{\partial T}{\partial n} + h(T-T_a) = 0 \tag{14}$$

When using finite elements for a heat-conduction analysis, iteration to satisfy this boundary condition is unnecessary even though the temperature gradient normal to the boundary and the temperature at the boundary are both unknown. As indicated in Section 2.1 appropriate additions to the H and F matrices for the element boundary in question, allows a solution to be obtained directly which will satisfy the required boundary flow condition. The additions to the H and F matrices obtained from equations (6) and (8) are respectively

$$\sum \int N_i \, h \, N_j \, dA \qquad \text{and} \qquad \sum \int N_i \, h \, T_a \, dA \tag{15}$$

For linear 2D elements these integrations may be performed explicitly as shown by Cheung and Medwell[5] but for the parabolic isoparametric elements used for this analysis, it was necessary to use the Gauss Quadrature method of numerical integration. The procedure used was to specify with input data the number and face of each element subjected to the boundary heat flux. The integrands in equation (15) were determined at nine Gauss points on the specified boundary surface of the 3D element, multiplied by a weighting function, and summed to complete the integration. This was then added to the appropriate coefficients in the H and F matrices. A transformation to obtain the element of surface area dA in local co-ordinates was

required for the integration and this depended on which face of the element formed the boundary. For example, if face 3 in Figure 2.1 was subjected to a boundary heat flux then the element of area in Equations (15) can be determined from the vector product in the following manner:

$$d\bar{A} = \bar{d\xi} \times \bar{d\eta}$$

$$= \hat{x} \begin{vmatrix} \frac{\partial y}{\partial \xi} & \frac{\partial z}{\partial \xi} \\ \frac{\partial y}{\partial \eta} & \frac{\partial z}{\partial \eta} \end{vmatrix} - \hat{y} \begin{vmatrix} \frac{\partial x}{\partial \xi} & \frac{\partial z}{\partial \xi} \\ \frac{\partial x}{\partial \eta} & \frac{\partial z}{\partial \eta} \end{vmatrix} + \hat{z} \begin{vmatrix} \frac{\partial x}{\partial \xi} & \frac{\partial y}{\partial \xi} \\ \frac{\partial x}{\partial \eta} & \frac{\partial y}{\partial \eta} \end{vmatrix} \qquad (16)$$

where $\hat{x}$, $\hat{y}$ and $\hat{z}$ are the cartesian unit vectors, and the derivatives can be obtained from equation (12).

2.4 Temperature Dependent Material Properties

The properties of two alloy steels used for superheater tubes are given in Table 3.1. To include, and investigate the sensitivity of solutions to the temperature dependence of material properties, an iterative procedure was incorporated into the programs in the following manner. For each time increment the properties at the known initial temperatures were used to form the H and P matrices of equation (5). Then using a time-stepping scheme the temperatures were determined at the end of the time increment. The mean temperatures for this increment were then found and the corresponding properties used to obtain a new solution which was then compared with the previous solution. If all the nodal temperatures were found to lie within a specified limit, then the procedure moved on to the next time step, otherwise the iteration was continued.

The Gauss method of numerical integration used for the isoparametric elements required that the functions to be integrated were determined at each of the Gauss points. The number of Gauss points used were 9 for the 2D elements and 27 for the 3D elements, enabling a good representation of material property variation to be included in the analysis. The temperatures at Gauss points were easily determined using equation (10) by substituting the local co-ordinates of the point into the shape function. Therefore the values of conductivity, density and specific heat contained in the functions to be integrated were taken at the temperature of each Gauss point as it was considered.

The iteration process described above was used for the two-level time-stepping schemes but it was found that this could be avoided by using an alternative three-level scheme. Details of the different schemes compared using the 2D analysis are given in the next section.

2.5 Time-Stepping Schemes

2.5.1 General

Solutions to the transient heat conduction equation (1) are governed by the system of first-order linear differential equations (5). Initial values of the temperature T at time t = 0 are generally specified and a numerical recurrence process or time-stepping scheme is required to determine the solution at subsequent times. A number of alternative schemes can be used, the requirement being a combination of efficiency and accuracy. The use of such schemes applied to the transient heat conduction equation has been examined by a number of researchers including DONEA[6], COMINI and DEL GUIDICE[7] and also WOOD and LEWIS[8].

The three schemes that were used for the 2D analysis will now be described.

2.5.2 Crank-Nicolson Scheme

If it is assumed that temperatures vary linearly with time during an arbitrary time interval Δt, the integration of equation (5) between times t and t + Δt gives:

$$[H]\left(\{T_t\} + \{T_{t+\Delta t}\}\right)/2 + [P]\left(\{T_{t+\Delta t}\} - \{T_t\}\right)/\Delta t = -\left(\{F_t\} + \{F_{t+\Delta t}\}\right)/2 \qquad (17)$$

which is the Crank-Nicolson algorithm. This equation can also be obtained by taking a central finite difference to approximate equation (5). It is of unconditional stability although requiring iteration within each time step for temperature dependent properties so that mid-interval values can be assigned to [H] and [P], i.e. $[H] = [H]_{(t+\frac{\Delta t}{2})}$

Equation (17) can be rewritten as:

$$\left(\tfrac{1}{2}[H] + \frac{1}{\Delta t}[P]\right)\{T_{t+\Delta t}\} = -\left(\tfrac{1}{2}[H] - \frac{1}{\Delta t}[P]\right)\{T_t\} - \tfrac{1}{2}\left(\{F_t\} + \{F_{t+\Delta t}\}\right) \qquad (18)$$

From this a solution for the nodal temperature vector $\{T_{t+\Delta t}\}$ can be obtained and used as the initial temperatures for the next time increment.

2.5.3 Galerkin Scheme

The Galerkin process can be applied to the matrix differential equation (5) and alternative integration schemes derived. This can be done by dividing the time dimension into 'finite elements' as described by ZIENKIEWICZ and PAREKH[2] to get

$$\{T\} = \sum_{s=0}^{k} N_s(t)\{T_s\} \quad \text{where s are time stations.}$$

Using the Galerkin process a weighted residual equation is obtained:

$$\int_0^t N_s\left([H] \sum N_s \{T_s\} + [P] \sum \frac{\partial N_s}{\partial t} \{T_s\} + \{F(t)\}\right)dt = 0 \qquad (19)$$

This on integration gives suitable recurrence relations.

If only initial and final states are considered in a time region with a linear variation of temperatures then,

$$T = [N_o, N_1] \begin{bmatrix}\{T_o\}\\ \{T_1\}\end{bmatrix} \qquad (20)$$

where $N_o = (\Delta t - t)/\Delta t$ and $N_1 = t/\Delta t$ (21)

The time derivative is,

$$\dot{T} = \left[\frac{\partial N_o}{\partial t}, \frac{\partial N_1}{\partial t}\right] \begin{bmatrix}\{T_o\}\\ \{T_1\}\end{bmatrix}$$

$$= \frac{1}{\Delta t}(-1, 1) \begin{bmatrix}\{T_o\}\\ \{T_1\}\end{bmatrix} \qquad (22)$$

$\{T_o\}$ is known so that only one weighted residual substitution is required. Substituting equations (21) and (22) into equation (5) multiplying by N_1 and integrating gives

$$\int_0^{\Delta t} N_1 \left([H] [N_o, N_1] \begin{bmatrix}\{T_o\}\\ \{T_1\}\end{bmatrix} + [P] \left[\frac{\partial N_o}{\partial t}, \frac{\partial N_1}{\partial t}\right] \begin{bmatrix}\{T_o\}\\ \{T_1\}\end{bmatrix} + \{F(t)\}\right)dt = 0$$

$$\int_0^{\Delta t} \frac{t}{\Delta t}\left([H] \left[\frac{\Delta t - t}{\Delta t}, \frac{t}{\Delta t}\right] \begin{bmatrix}\{T_o\}\\ \{T_1\}\end{bmatrix} + [P] \frac{1}{\Delta t}[-1, 1] \begin{bmatrix}\{T_o\}\\ \{T_1\}\end{bmatrix} + \{F(t)\}\right)dt = 0$$

$$[H]\left(\frac{1}{3}T_o + \frac{2}{3}T_1\right) + \frac{P}{\Delta t}(T_1 - T_o) + \frac{1}{3}(F_o + 2F_1) = 0$$

giving for $T_o = T_t$ and $T_1 = T_{t+\Delta t}$.

$$\left(\frac{2}{3}[H] + \frac{1}{\Delta t}[P]\right)\{T_{t+\Delta t}\} = -\left(\frac{1}{3}[H] - \frac{1}{\Delta t}[P]\right)T_{t-}\frac{1}{3}\left(\{F_t\} + 2\{F_{t+\Delta t}\}\right) \quad (23)$$

For temperature dependent properties [H] and [P] can be given their mid-interval values by carrying out an iteration at each time step.

2.5.4 Three-Level Scheme

To avoid an iteration within each time step an unconditionally stable three-level scheme proposed by LEES[9] can be used. Assuming the temperature varies linearly in the time interval between t-Δt and t+Δt equation (5) can be approximated as:

$$\frac{1}{3}[H_t]\left(\{T_{t+\Delta t}\} + \{T_t\} + \{T_{t-\Delta t}\}\right) + [P_t]\left(\{T_{t+\Delta t}\} - \{T_{t-\Delta t}\}\right)\frac{1}{2\Delta t} + F_t = 0$$

in which only central values of matrices H, P and F occur.

This equation can be written in the form

$$\left(\frac{1}{3}[H_t] + \frac{1}{2\Delta t}[P_t]\right)T_{t+\Delta t} = -\frac{1}{3}[H_t]T_t - \left(\frac{1}{3}[H_t] - \frac{1}{2\Delta t}[P_t]\right)T_{t-\Delta t} - F_t \quad \ldots (24)$$

If the temperature vector is known at two consecutive time steps then the prediction can be obtained explicitly without iteration. Normally the scheme is not self-starting because only the initial temperatures are known. This was overcome by using the Galerkin scheme with iteration for the first time step and then reverting to the three-level algorithm for subsequent intervals.

3 HEAT CONDUCTION ANALYSIS OF A SUPERHEATER TUBE

3.1 Boundary Conditions

The cross-section of the superheater tube under consideration is shown in Figure 3.1. To approximate the process of on-load water washing, which consists essentially of a localised impingement of a water jet on the tube outer surface, the following boundary conditions were used:

a A uniform initial temperature of 500°C was specified throughout the tube.

b The inner surface of the tube was assumed to remain at constant temperature and was therefore prescribed to be 500°C for all time stations in the analysis. This assumption was made on the basis of a continual steam flow in the tube and a short period of contact between the water jet and any one part on a tube.

c Influx of heat across the outer boundary adjacent to the quench region was neglected and assumed to be negligible for the period being considered.

d The area of the cooled region used was taken as being representative of the water jet impingement and the shape of this area was assumed to be of secondary importance provided the rapid localised cooling effect was achieved. For the axisymmetric analysis described in Section 3.3 the quench area was circular in shape whilst for the 3D analysis

of section 3.4 the quench area was square-shaped as shown in Figure 3.13. In practice the quench region would progress along a tube with each pass of the water jet as the rotating lance was advanced inwards as indicated in Figure 1.1.

TABLE 3.1 : MATERIAL PROPERTIES

	STEEL TYPE			
	2.25% Cr, 1% Mo		1% Cr, 0.5% Mo	
PROPERTY \ TEMPERATURE	100°C	500°C	100°C	500°C
Thermal Conductivity (w/m°C)	37.6	35.2	45.5	37.6
Density (t/m^3)	7.85	7.71	7.8	7.67
Specific Heat (kJ/kg°C)	0.490	0.678	0.490	0.678
Coefficient of Thermal Expansion ($°C \times 10^{-6}$)	11.9	15.7	12.3	15.2
Young's Modulus (GPa)	212	179	210	179

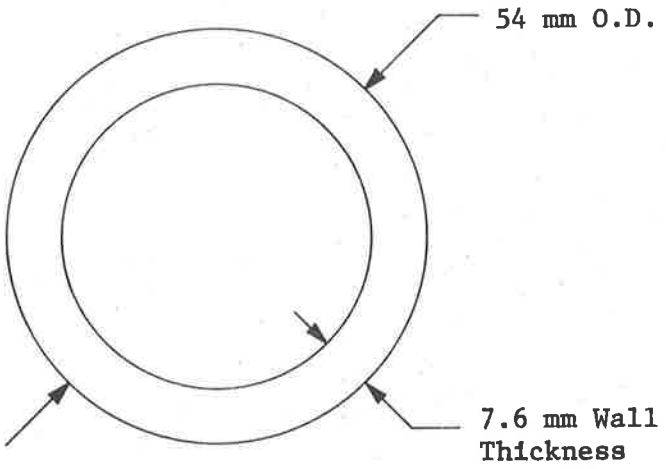

FIGURE 3.1 : Superheater tube section

e Symmetry was used to reduce the size of the problem by means of the non-conducting boundaries that exist in the finite element analysis unless otherwise specified.

f The value of Ta in equation (8) was taken as being 100°C. This represents the temperature of the water jet striking the tube surface and is assumed to remain constant for the quench duration and unaffected by the presence of any steam generated on contact.

3.2 Two-Dimensional Analysis

To examine the effects of a simplified approach and also to provide an economic means of investigating various points of interest, the initial analysis carried out was 2D. The finite element mesh used for this is shown in Figure 3.2 with the cooled region indicated. The 2D analysis represents the case of an infinite tube being quenched over a part of the outer surface extending along the entire length. Comparisons can be made later with results from a 3D analysis considering a finite quench length.

Three time-stepping schemes were directly assessed using the 2D analysis, also the effect of varying the surface conductance was investigated and finally an alternative superheater tube steel having different material properties was examined.

3.2.1 Comparison of Time-Stepping Schemes

The three time-stepping schemes described in Section 2.5 were used enabling comparisons of accuracy and solution times to be made. Exact analytical

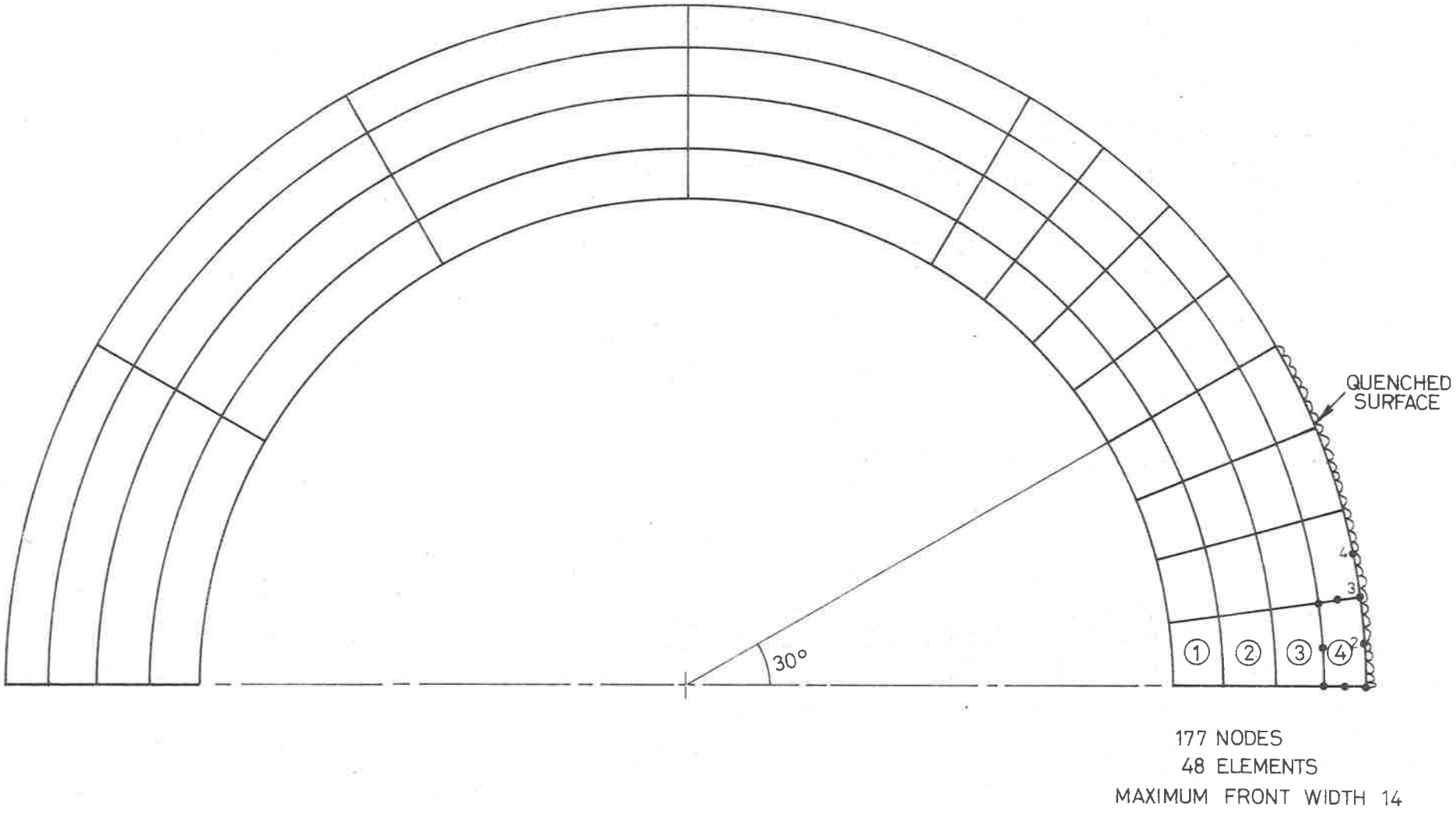

FIGURE 3.2 FINITE ELEMENT MESH FOR 2D HEAT CONDUCTION ANALYSIS.

solutions to the problem under consideration were not available but it was recognised that convergence to the true solution would occur with reduction in the time increment used in the time-stepping. Each of the schemes was, therefore, applied to the problem using 100 steps with intervals of 0.01 seconds and the temperatures obtained were found to agree within 1°C. This solution was taken as a reference when comparing results from the three schemes for larger time increments.

Results showing temperature variation through the thickness of the tube at the centre of the quench region are plotted in Figures 3.3 and 3.4 for the three schemes using time intervals of 0.1 and 0.2 seconds respectively. The solution times for 10 steps of 0.1 seconds were 90 seconds for both the Galerkin and the Crank-Nicolson schemes and 57 seconds for the three-level scheme. The allowable temperature difference specified in the iteration procedure was 1°C and this was found to require two iterations at the first time step and a single iteration at all subsequent steps for the Galerkin and Crank-Nicolson schemes. For the three-level scheme, two iterations were required for the first time step only with no further iteration at the following steps as described in Section 2.5.4.

The results showed little difference in accuracy between the Crank-Nicolson and Galerkin schemes, although a slight reduction in accuracy was apparent for the three-level scheme. For the subsequent 3D analysis, the Galerkin scheme with iteration was used in preference to the three-level scheme in order that improved accuracy could be obtained at the expense of extra solution time. The three-level scheme can be seen, however, to offer an economical means of taking temperature dependent properties into consideration and would be suitable for certain engineering problems where the slight reduction in accuracy would not be of great consequence.

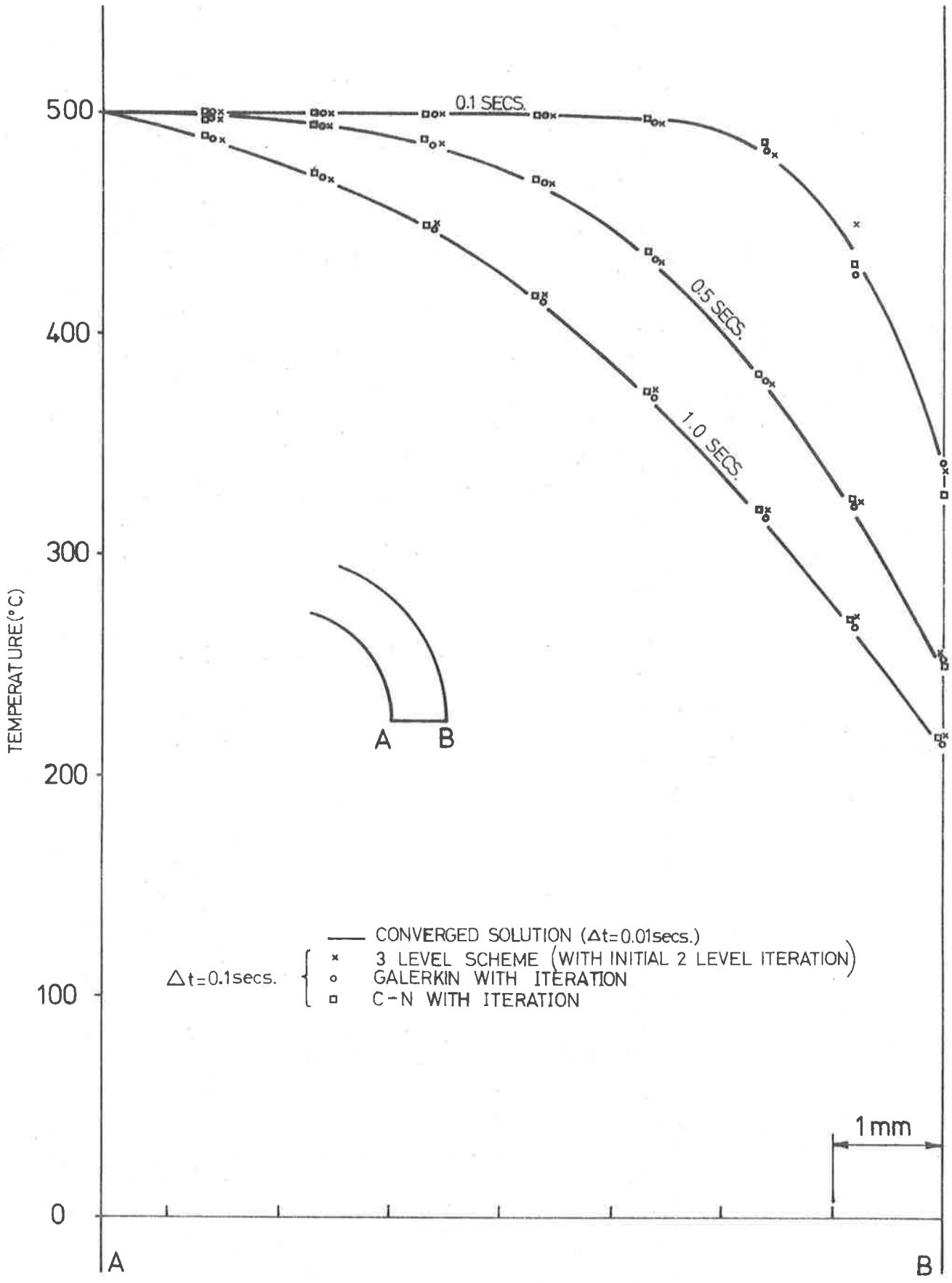

FIGURE 3.3 COMPARISON OF TIME-STEPPING SCHEME ($\Delta t = 0.1$secs.)

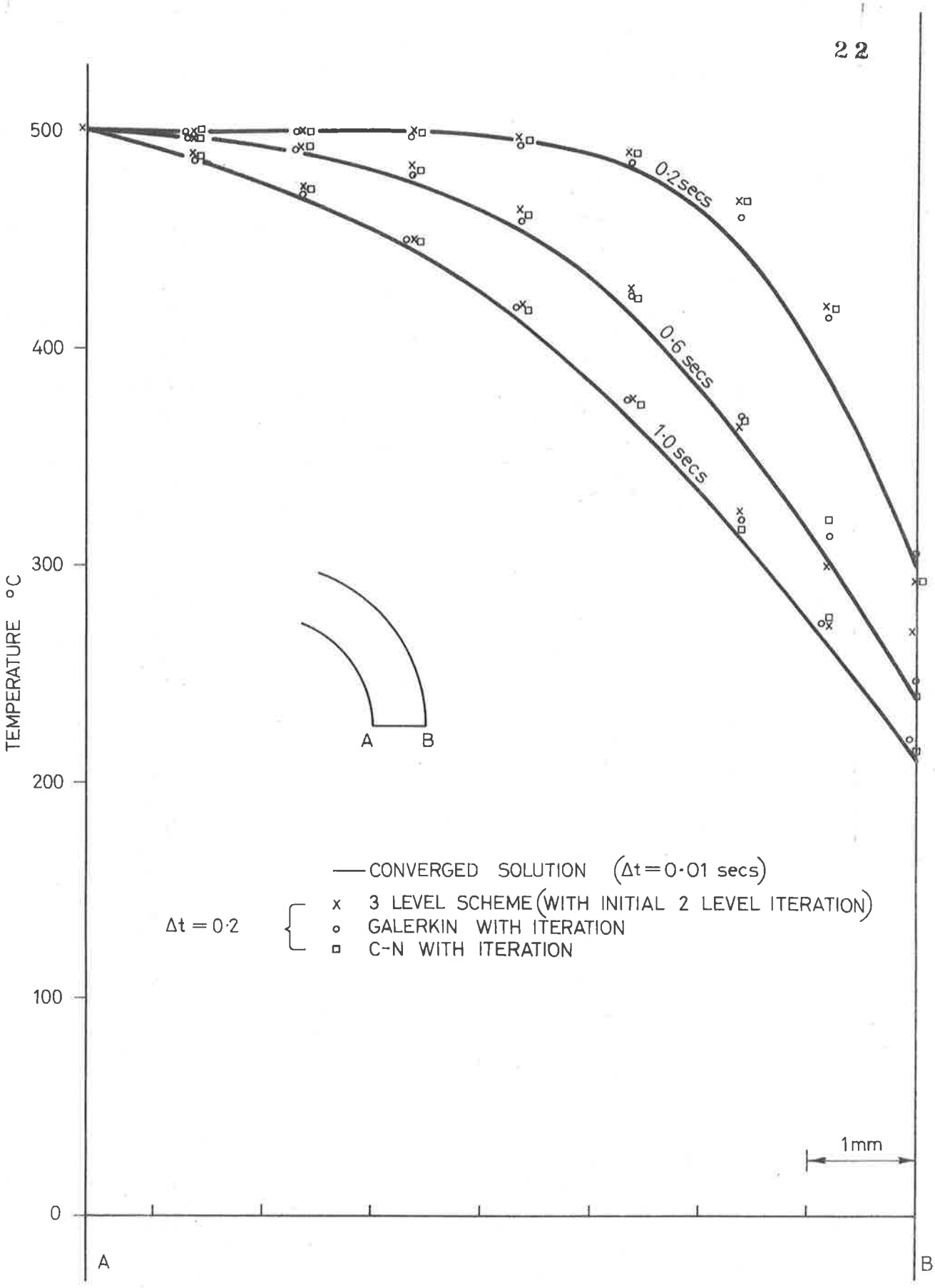

FIGURE 3.4 COMPARISON OF TIME STEPPING SCHEME ($\Delta t = 0 \cdot 2$ secs)

3.2.2 Temperature Dependent Material Properties

The necessity to take into account the variation of conductance, density and specific heat of a material with temperature depends on the extent to which these variations occur for the temperature range in the problem under consideration. Table 3.1 shows the variation of properties for two superheater tube steels. It can be seen that the variation in thermal conductivity is substantially less for the 2.25% Cr, 1% Mo steel than for the 1% Cr, 0.5% Mo steel. The penalty for including non-linearity effects into the analysis was the additional solution time required for iteration when using a two-level scheme or a loss in accuracy if the three-level scheme was used with the same time interval.

The extent to which the variation in properties affected the results was investigated using the Galerkin scheme by firstly carrying out the analysis using constant properties based on temperatures of 300°C and 500°C for both the superheater steels. Then the analysis was repeated using the iteration procedure at each time step in the manner described in Section 2.4. Results showing the temperature variation through the thickness at the centre of the quench region are plotted in Figures 3.5 and 3.6 for the two steels. Temperature differences of up to 4% were obtained from the constant property analyses using properties at the two reference temperatures. By taking into account the variation of the material properties it can be seen that for this case about 2% greater accuracy was obtained.

The analysis times for 10 steps of 0.1 seconds were 50 seconds for constant properties compared with 90 seconds for varying properties. All subsequent work carried out was for the 2.25% Cr, 1% Mo steel.

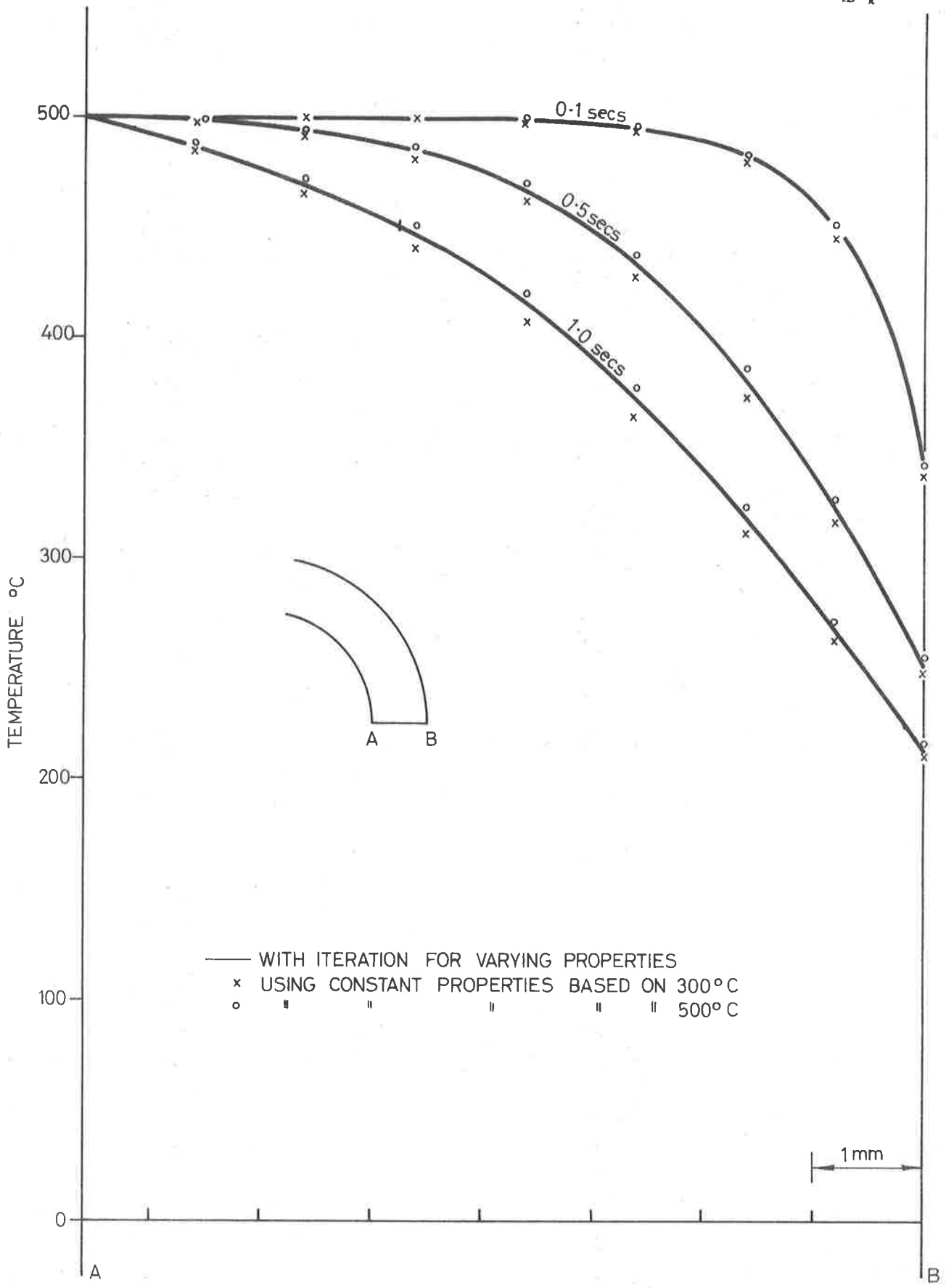

FIGURE 3.5 TEMPERATURE DEPENDENT MATERIAL PROPERTIES 2·25% Cr 1·0% Mo

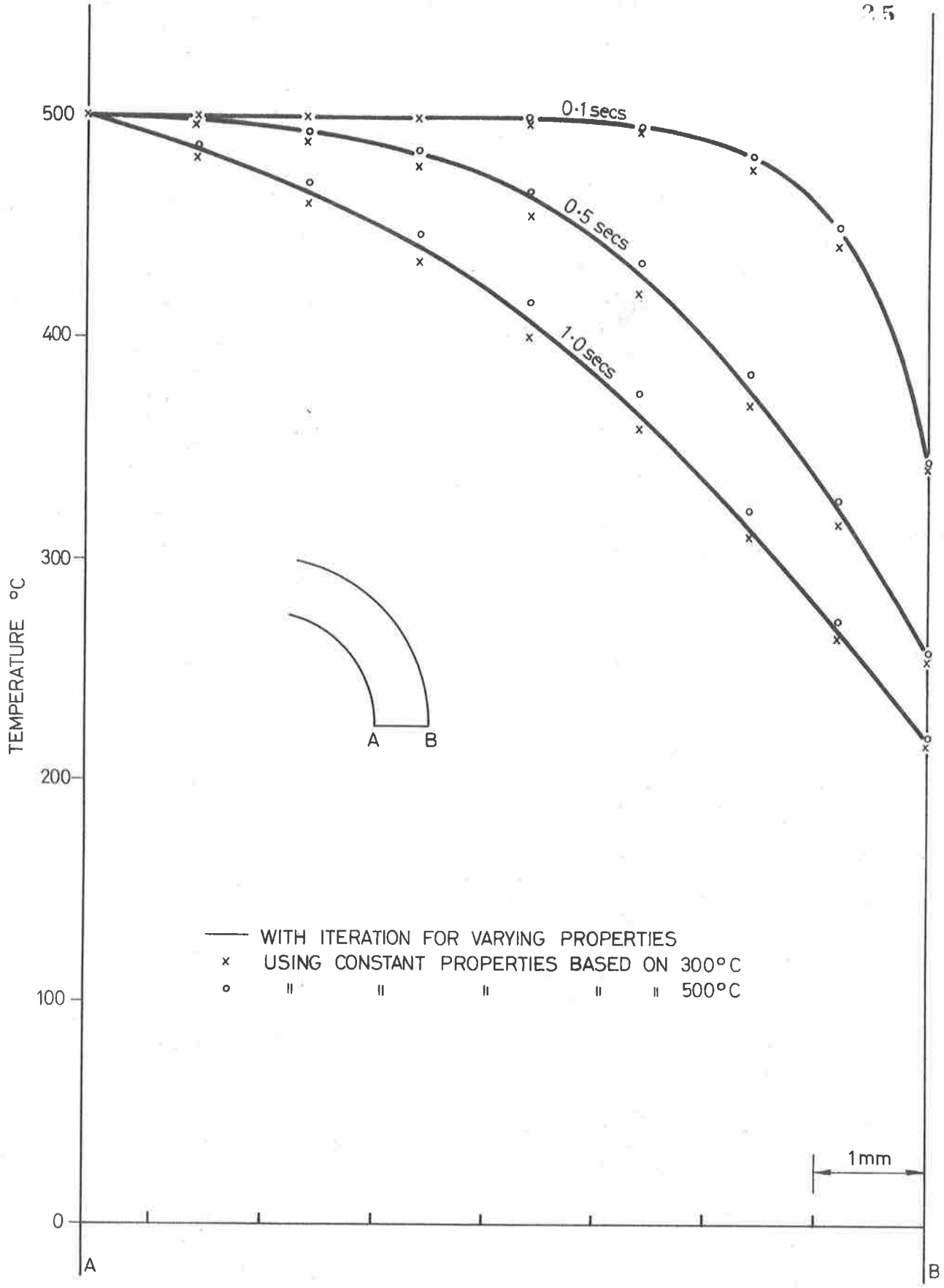

FIGURE 3.6 TEMPERATURE DEPENDENT MATERIAL
1% Cr 0·5% Mo

3.2.3 Surface Conductance

The magnitude of the surface conductance (h) in equation (14) is dependent on the cooling medium, the material of the hot body and the manner in which cooling is carried out. For this analysis the value of h used was 22 800 J/m^2 s deg K (4000 Btu/ft^2 h deg F) which is representative of steel being cooled by a strong water spray. The value of the surface conductance was assumed to remain constant and can be seen from equation (14) to govern the temperature gradient normal to the cooled boundary for a particular boundary temperature. It should be pointed out that a different or varying value of h can be easily implemented into a finite element solution, this being an advantage of the technique. The effect of using a higher value for the surface conductance can be seen in Figure 3.7 where results obtained for values of 22 800 and 45 600 J/m^2 s deg K are shown.

A simple analysis check was carried out by determining the temperature gradient on the boundary from Figure 3.7, at the time station of 0.1 seconds, and this was estimated to be 260°C/mm. Substituting this into equation (14) together with the boundary temperature of 340°C and the corresponding thermal conductivity of 20.86 gives:

$$h = (260 \times 10^3 \times 20.86)/(340-100) = 22\ 600\ J/m^2\ s\ deg\ K$$

3.2.4 Results

Two-dimensional analysis results are given for the 2.25% Cr, 1% Mo steel using the Galerkin scheme and a surface conductance of 22 800 J/m^2 s deg K. The variation of temperature through the thickness is plotted in Figure 3.14. Isothermals plotted from the results can be seen in Figures 3.15, 3.16 and 3.17 for times of 0.1, 0.5 and 1.0

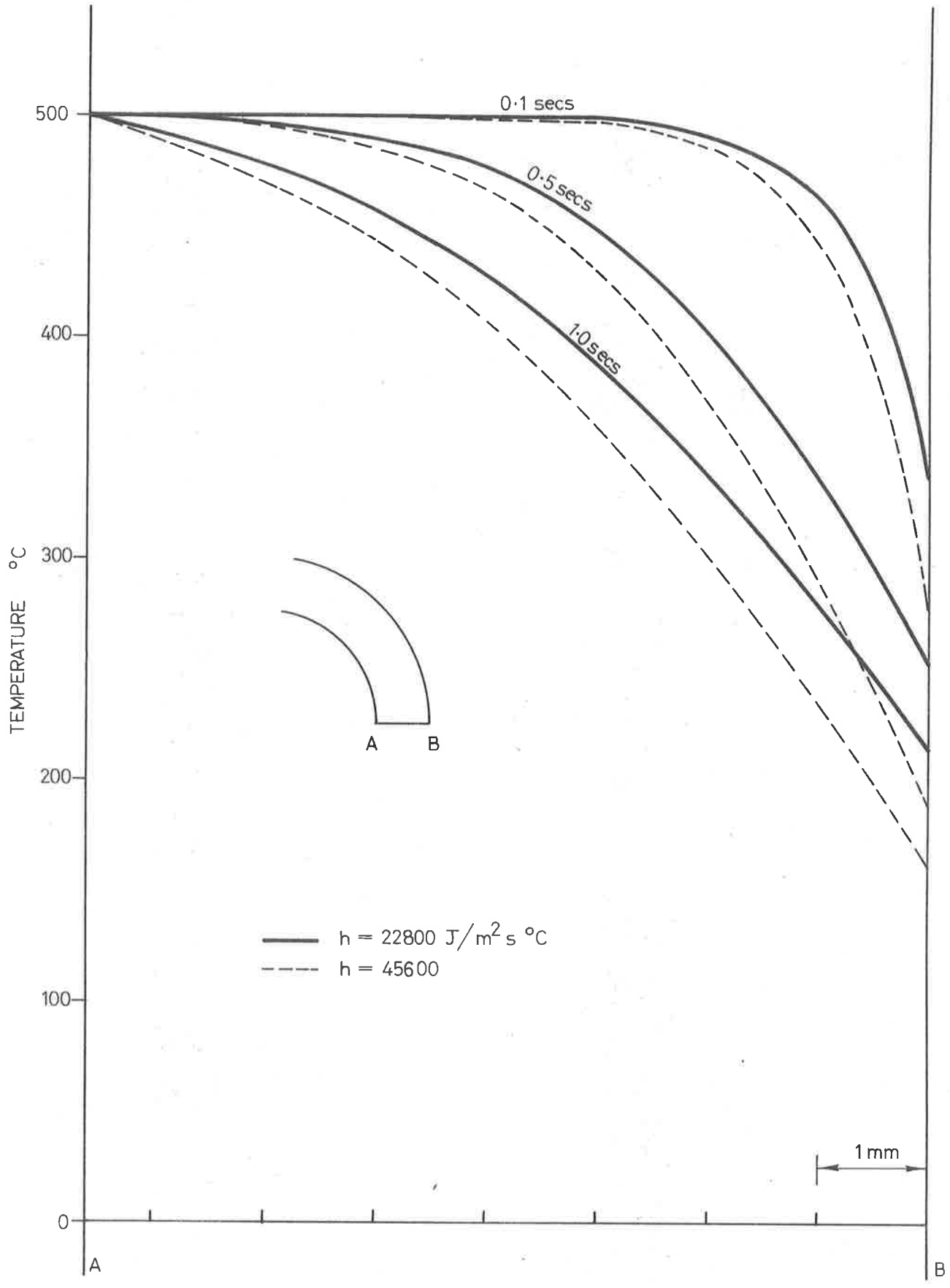

FIGURE 3.7 EFFECT OF CHANGING THE SURFACE CONDUCTANCE (h)

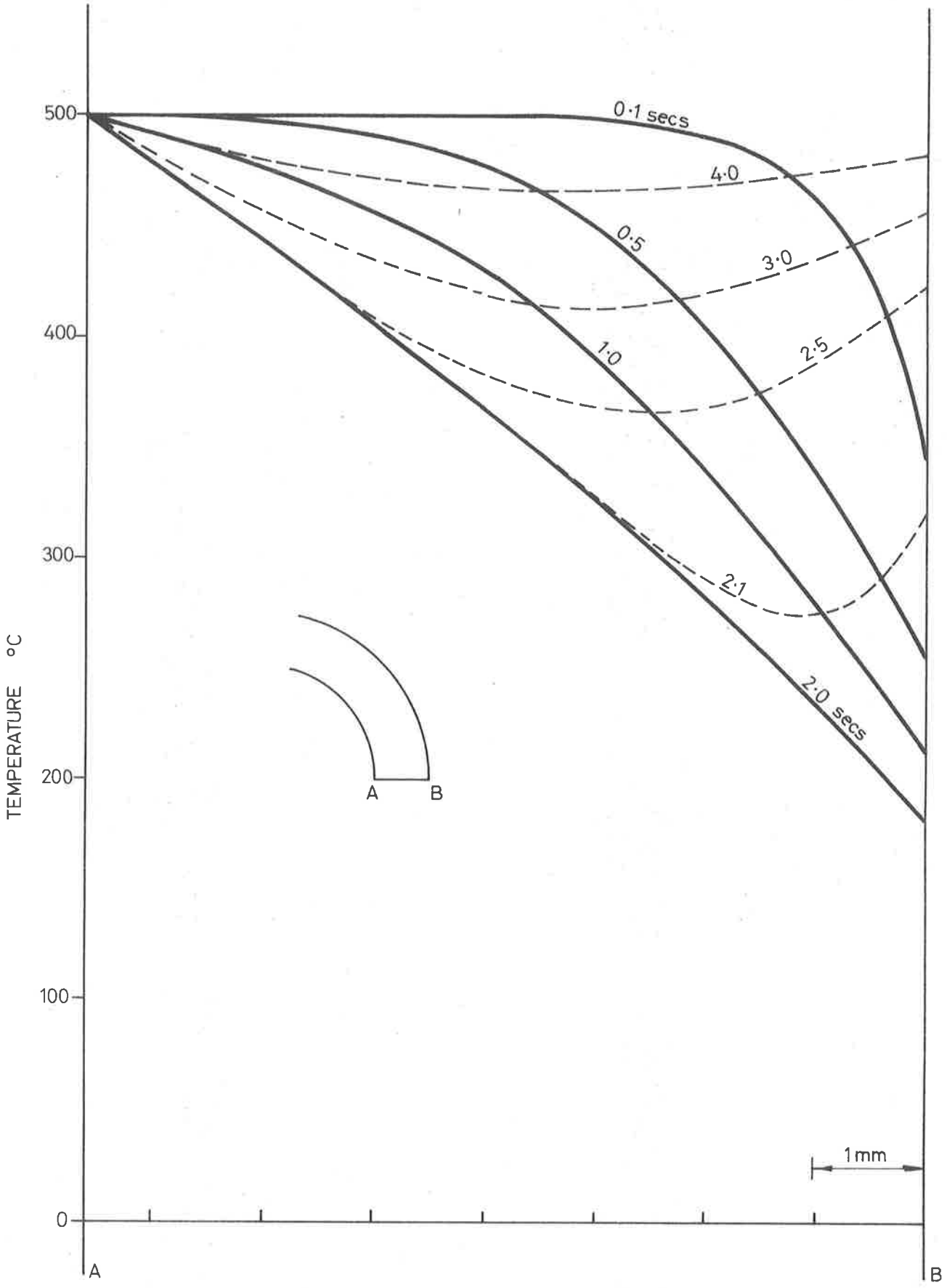

FIGURE 3.8 QUENCH DURATION OF 2 SECONDS.

seconds respectively after the initiation of the boundary quench. These results were obtained using 10 steps of 0.1 second intervals.

A further analysis using 40 steps of 0.1 second intervals was carried out where, after the initial two seconds of cooling, the boundary condition was changed to reheating. The results of this are shown in Figure 3.8. For the purposes of this investigation the primary concern was with the cooling condition which produces tensile stresses at the outside surface of the tube.

Further comments on the results are given in Section 3.4.3 in conjunction with the 3D results.

3.3 Axisymmetric Analysis

Another alternative to carrying out a full three-dimensional analysis would be to effectively 'open out' the tube and treat it as being a flat plate as shown in Figure 3.9. This approximation can then be treated as an axisymmetric problem about the centre of the quench region effectively reducing it to two dimensions and allowing a solution to be obtained more economically. The extent to which such an approximation would approach the true solution depends on the size of the quench area relative to the diameter D and thickness t of the tube, and also on the time period being considered. For a large D/t ratio a good approximation would be expected.

The 2D computer program was converted to cover axisymmetric heat flow. The equation for axisymmetric transient heat conduction can be written as:

$$\rho cr \frac{\partial T}{\partial t} = \frac{\partial}{\partial r}\left(rk \frac{\partial T}{\partial r}\right) + \frac{\partial}{\partial z}\left(rk \frac{\partial T}{\partial z}\right) + Q \qquad (25)$$

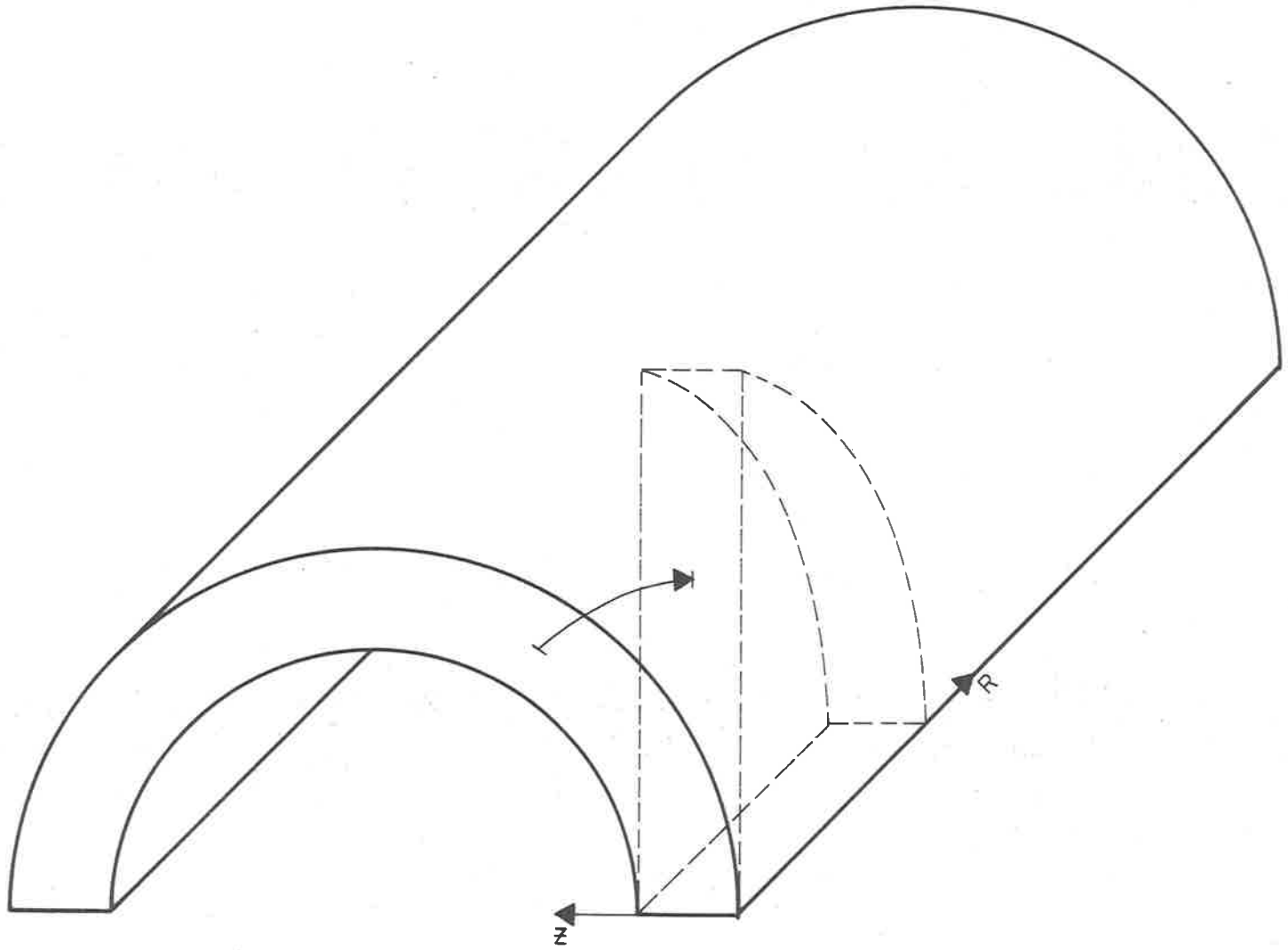

FIGURE 3.9. AXISYMMETRIC REPRESENTATION OF TUBE.

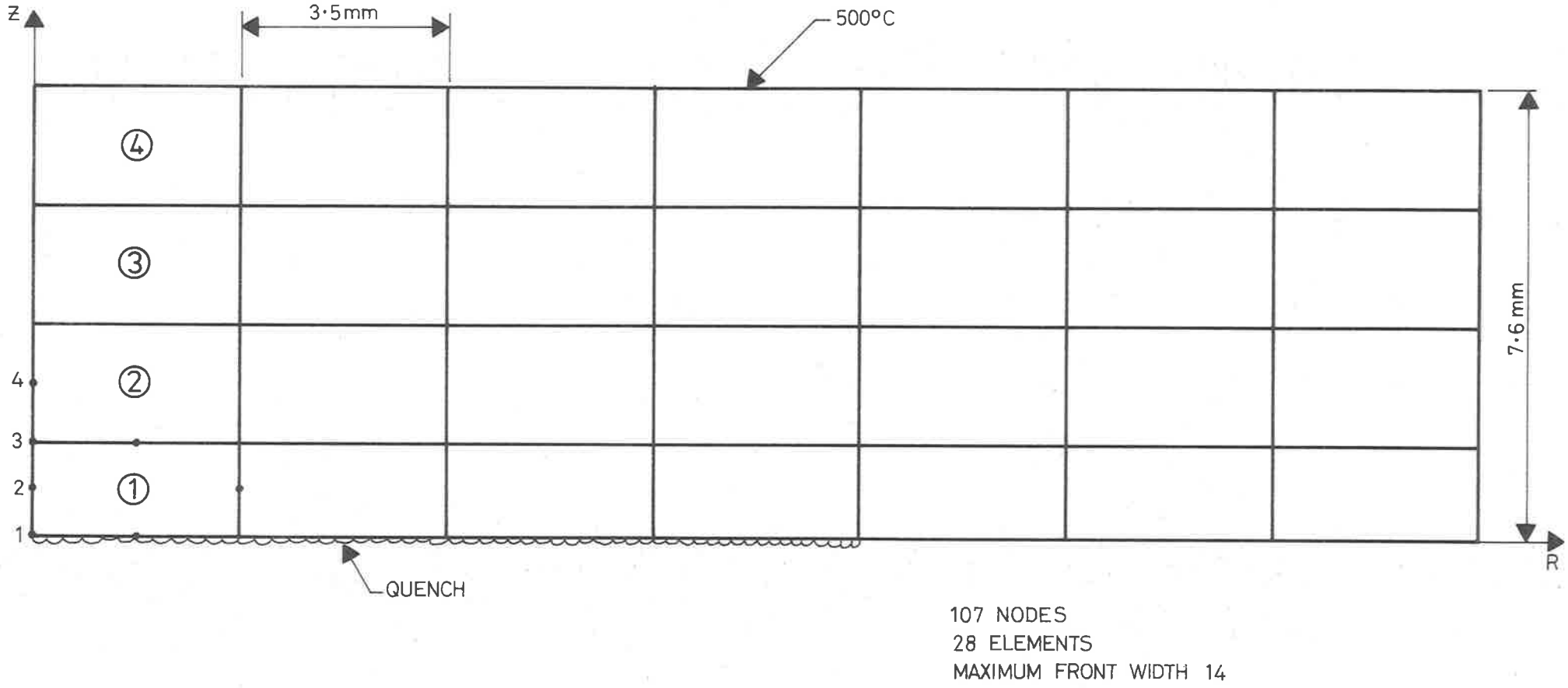

FIGURE 3.10. FINITE ELEMENT MESH FOR AXISYMMETRIC ANALYSIS.

where the 2D co-ordinates X and Y are replaced by r and z, the radial and axial distances. This equation can be dealt with in the same manner as equation (1) using elements of cross-sectional area instead of volume but with an additional radius term remaining from the $2\pi r$ necessary to give the swept volume. The integrals determined in the 2D program using the Gauss Method of numerical integration were easily modified to include the necessary radius term by obtaining the radius of the Gauss points as they were considered using the first equation (9). The integrals required for the boundary flow were modified in a similar manner.

The finite element mesh used for the axisymmetric analysis is shown in Figure 3.10, the maximum radius here being adequate for the time periods considered. Results obtained using 10 steps of 0.1 second increments are plotted in Figure 3.14 showing the transient variation of temperature through the thickness at the centre of the quench region. Also Figures 3.18, 3.19 and 3.20 show isothermals for the time stations 0.1, 0.5 and 1.0 seconds respectively. Comparisons are shown with results obtained subsequently from a full 3D analysis. The time for the axisymmetric analysis was 36 seconds.

3.4 Three-Dimensional Analysis

3.4.1 Preliminary 3D/Axisymmetric Check

Before proceeding with a full 3D analysis of the superheater tube it was decided to carry out a correlation of results obtained for an axisymmetric problem analysed using both the axisymmetric and the 3D programs. In this way it was hoped that any discrepancies existing in either of the programs, to which certain modifications and extensions had been made, would be revealed. Initial results did in fact lead to the detection of an error in the new boundary flow subroutine which was subsequently corrected.

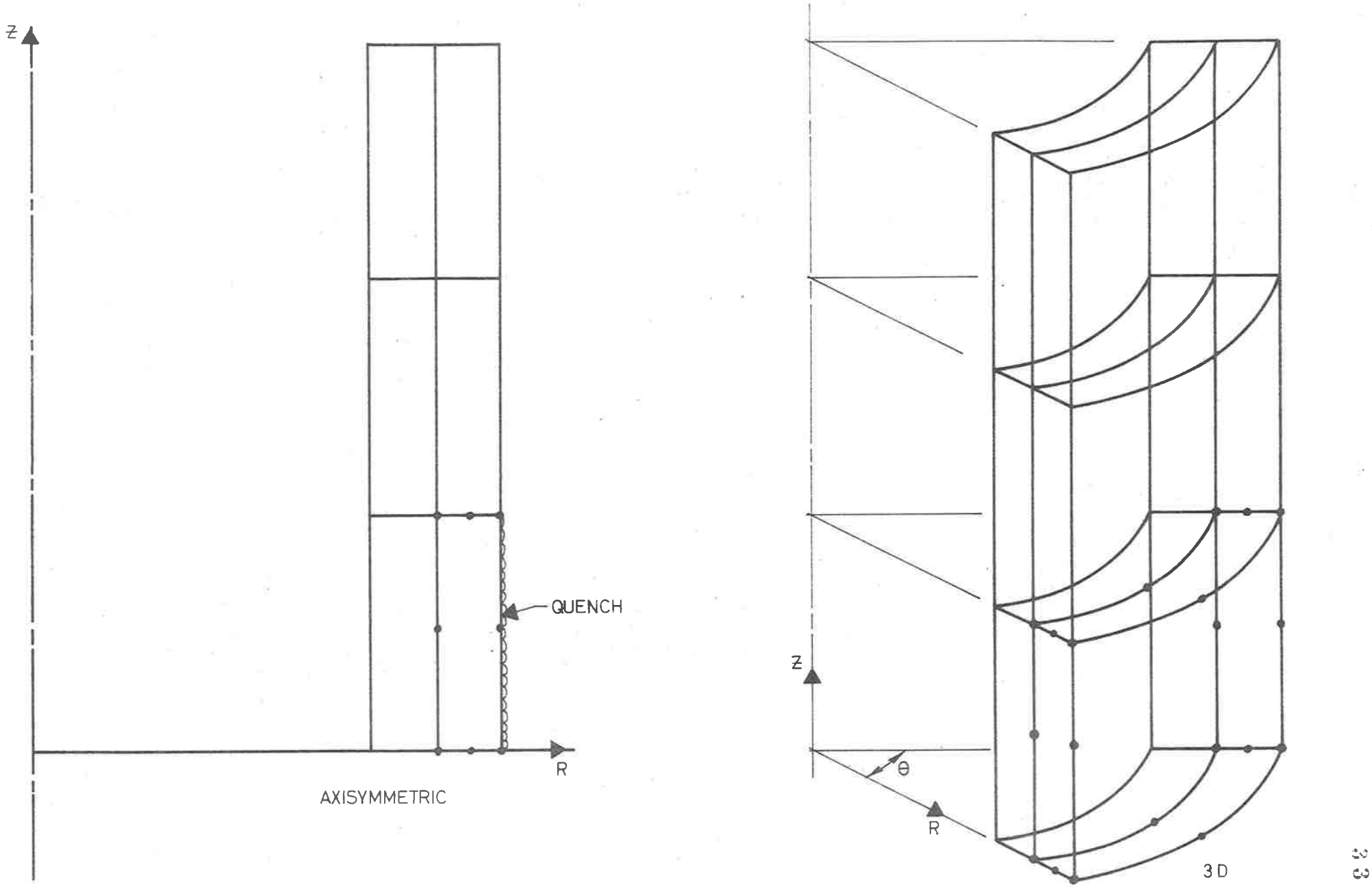

FIGURE 3.11. AXISYMMETRIC AND 3D TEST ANALYSIS.

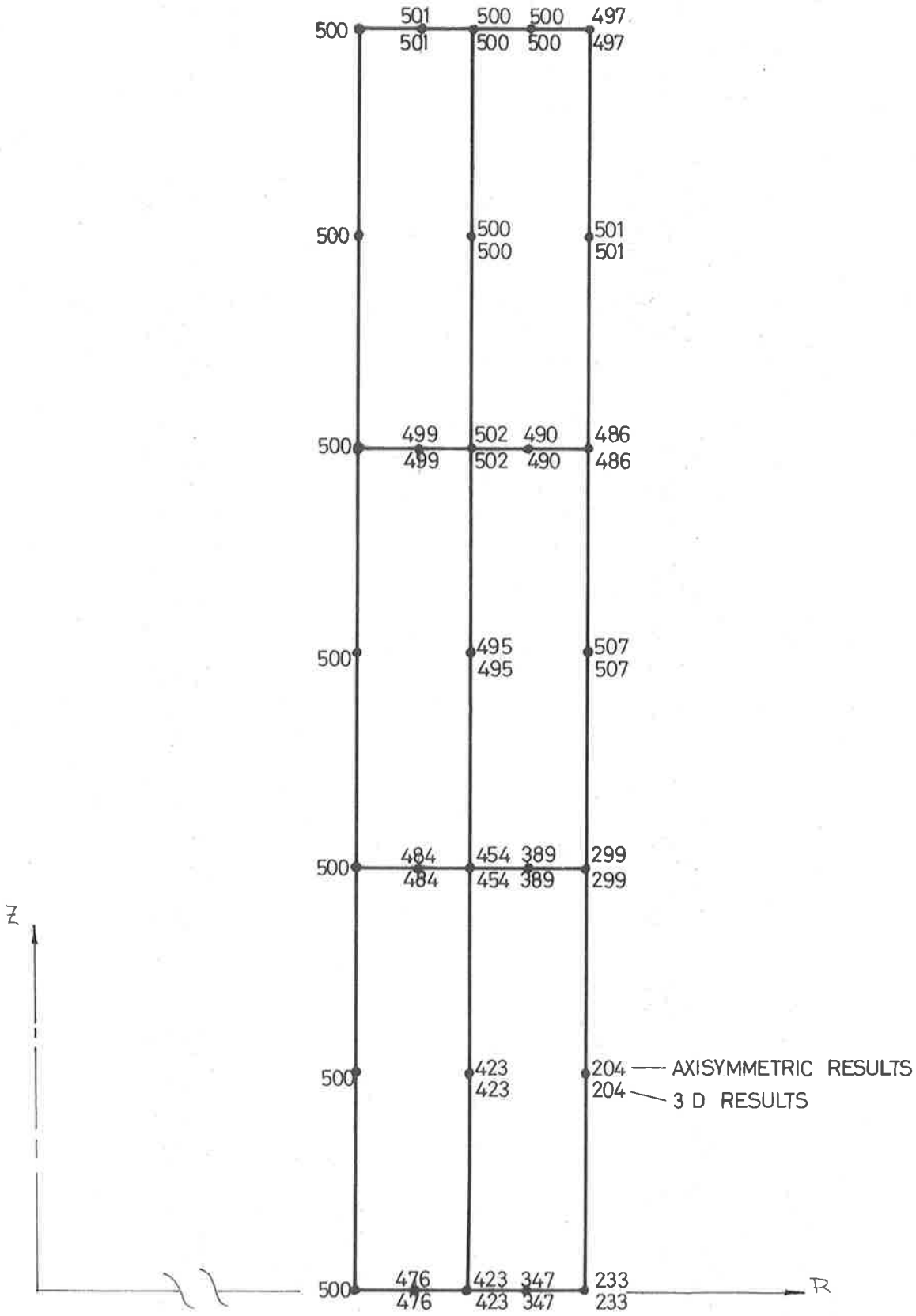

FIGURE 3.12. TEST ANALYSIS TEMPERATURES AFTER 1·0 SECOND.

The meshes used for the axisymmetric and 3D analysis of this test problem are shown in Figure 3.11. In this case the cooled section of the boundary was extended completely around the circumference in order to make the problem axisymmetric. The 3D analysis was made considering a sector of the tube having no heat flow across the flat side faces.

Results from the 3D and axisymmetric analyses, using 10 steps of 0.1 seconds, are shown in Figure 3.12 and were within 0.1% indicating compatibility for the two approaches.

3.4.2 Mesh Generation

An algorithm was written and added to the 3D program to generate the 3D finite element mesh shown in Figure 3.13. Firstly the cylindrical co-ordinates r, θ and z were generated for each of the nodes. Then the element topology, consisting of the 20 node numbers in accordance with the node numbering system adopted, was generated for each of the elements in turn. The ordering of the 20 nodes for each element was made consistent by starting with a corner node and working through the element in a clockwise direction. The method of solution used in the program for the simultaneous equations was the 'front solution'[4] and the order in which the elements were numbered governed the maximum front width. Care was taken to keep this to a minimum to optimise the solution in terms of time and storage requirements.

The procedure used in the solution is to consider each element in turn and determine its contribution to the equations currently being assembled in the storage area allocated for this purpose. The size of this area is governed by the maximum front width for the problem being considered. At any stage of the solution the front width is equal to the number of

'active' nodes, i.e. nodes for which equations have been partially assembled. When a node is encountered for the last time, during the sequential consideration of the elements, the corresponding completed equation is used to reduce the other equations being assembled and is then eliminated allowing another equation for a newly encountered node to be initiated. For this solution technique the node numbering sequence is arbitrary.

The mesh used contained 288 elements, 1629 nodes and the maximum front width was 114. An initial analysis was carried out using elements equally distributed around the circumference of the tube. The results from this were then used as a basis to redistribute the elements as shown in Figure 3.13 to obtain a finer mesh in the required area, leading to improved accuracy in the final solution.

3.4.3 Results and Observations

The transient temperature distributions through the wall of the tube at the centre of the quench region are shown in Figure 3.14. These were found to be the same for the 2D and 3D analysis, although this result is recognised to be dependent on the size of the quench area relative to the wall thickness and may not apply generally for a reduced quench area. The axisymmetric analysis can be seen to give results close to the 3D values for the first 0.2 seconds after which divergence occurs giving temperatures about 2.5% higher after 1.0 seconds. This can be explained by the reduction of the volume to inside surface area ratio caused by the 'opening out' required for the axisymmetric analysis, and also by the difference in the shape of the quench area which was circular for the axisymmetric analysis and square for the 3D analysis.

The 3D results showed the maximum temperature gradient through the tube wall to occur at the centre of the quench region A-B (Figure 3.13) and to reduce progressively towards the quench boundaries. This can be seen in Figures 3.21 and 3.22 for the time of 1.0 seconds and similar results were obtained for other time stations.

At circumferential and axial sections taken through the centre of the quench area (refer Figure 4.6), the temperatures obtained from the analysis were used to plot the isothermals shown in Figures 3.15 to 3.20. These figures show that the 2D results and the axisymmetric results were in good agreement with the 3D results remembering that direct comparisons could only be made at the sections shown.

Isothermals plotted from the 3D results for the outside surface of the tube are shown in Figures 3.23, 3.24 and 3.25 for the times of 0.1, 0.5 and 1.0 seconds respectively. Temperature gradients on the tube surface in the circumferential and axial directions from the centre of the quench are plotted in Figures 3.26 and 3.27. The maximum gradients can be seen to occur in the locality of the quench boundaries, and were approximately the same in both directions.

An examination of the typical temperature distributions shown in Figures 3.16, 3.19 and 3.24 for the 0.5 seconds time station shows that the isothermal surfaces produced by the surface cooling are 'dish shaped' following the contour of the curved wall.

A substantial central portion of the cooled region can be seen to have no temperature gradient in the circumferential or axial directions, such a gradient occurring only through the thickness of the tube. The variation of the surface temperature with time, at the centre of the quench, is shown in Figure 3.28.

The computer time for the 3D analysis using 10 steps of 0.1 seconds was 7994 seconds. Therefore, the axisymmetric analysis time of 36 seconds represents a considerable saving in computer time and gives a good general approximation to the heat conduction problem. A transfer of the axisymmetric results to the cylinder does, however, present certain difficulties, particularly if a subsequent stress analysis is to be carried out. The 2D analysis time of 90 seconds also represents a considerable saving but here the results are restricted to a single section through the tube.

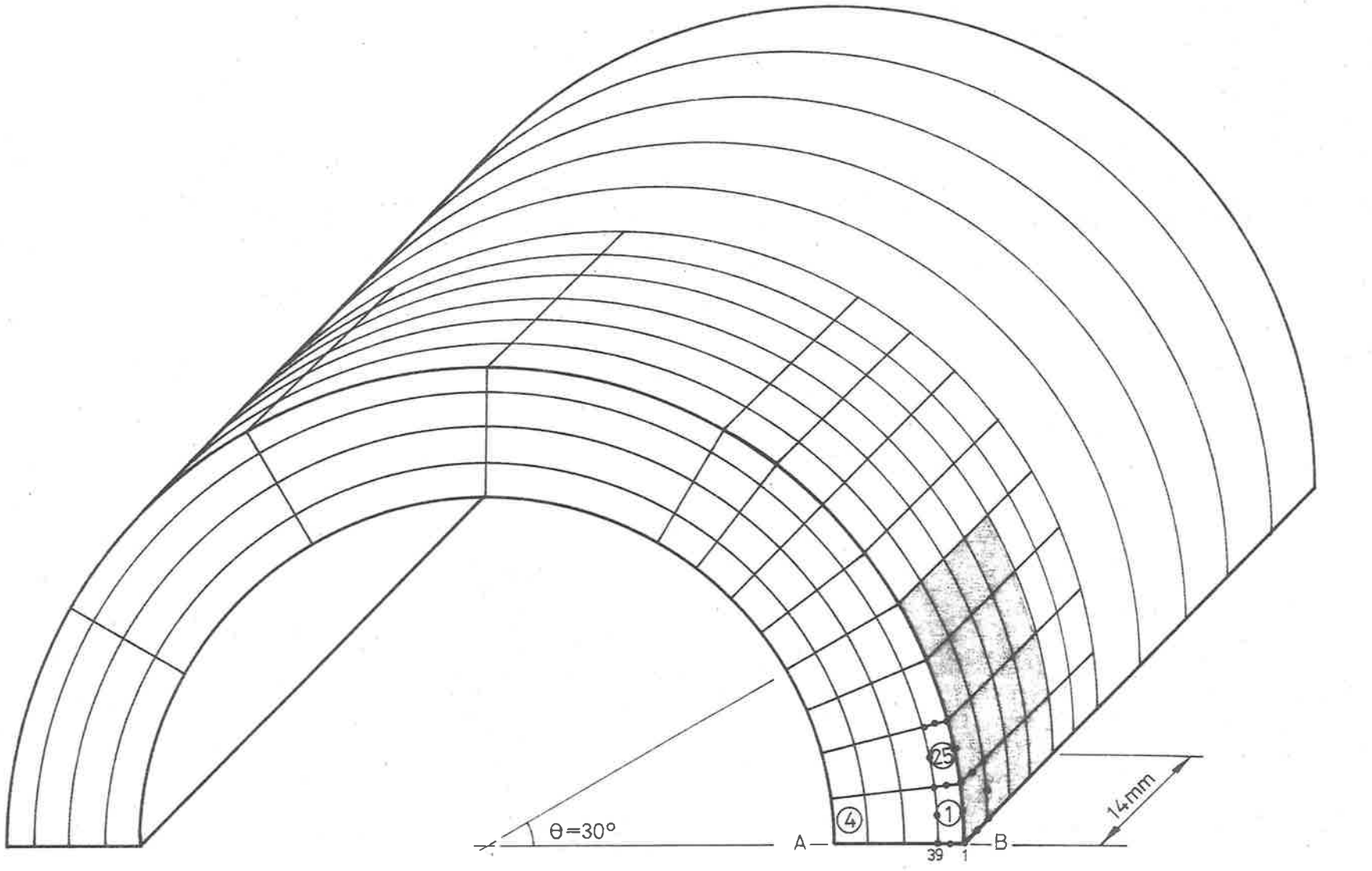

FIGURE 3.13. FINITE ELEMENT MESH FOR HEAT TRANSFER ANALYSIS.

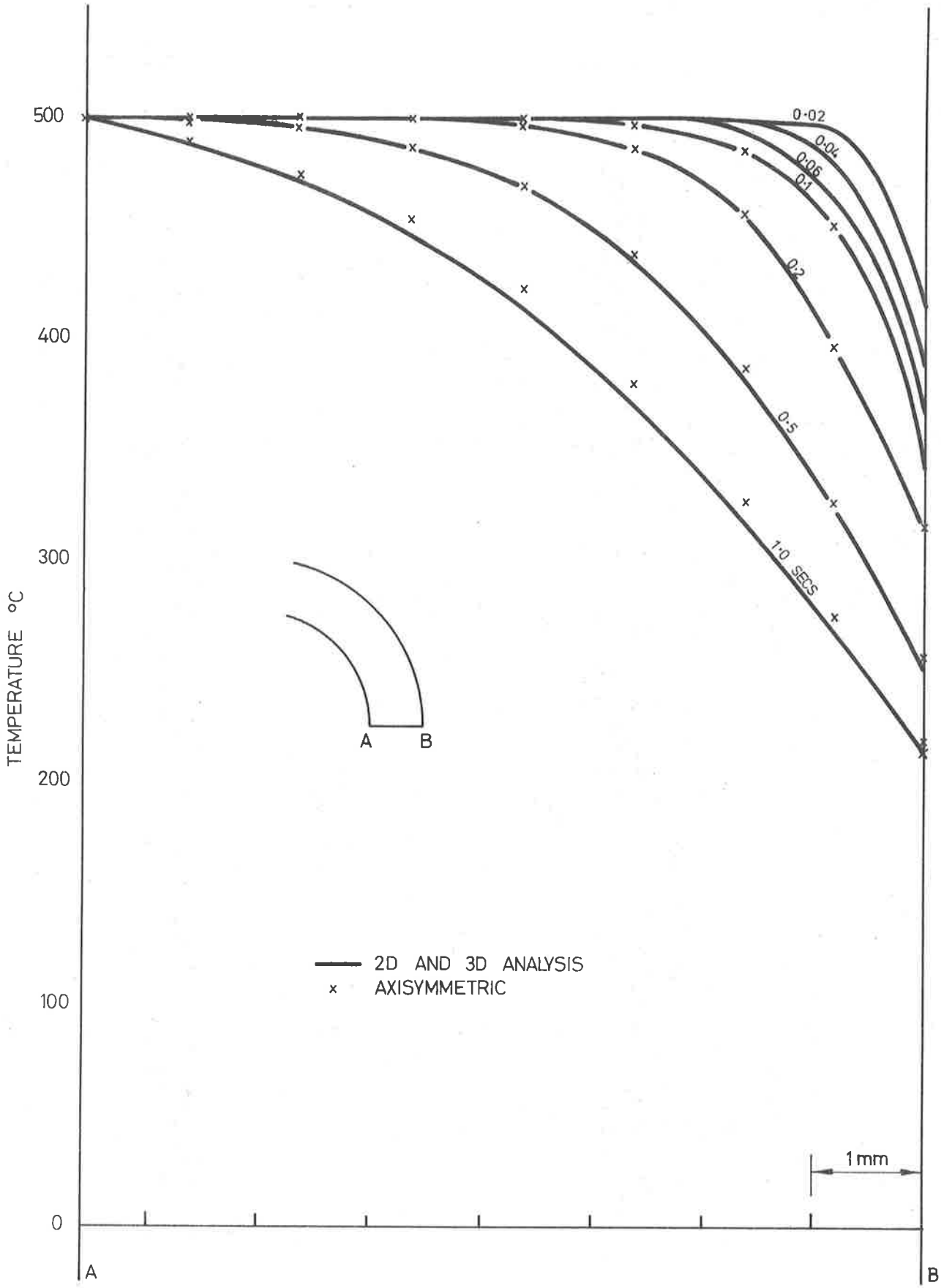

FIGURE 3.14. RADIAL TEMPERATURE DISTRIBUTION A-B

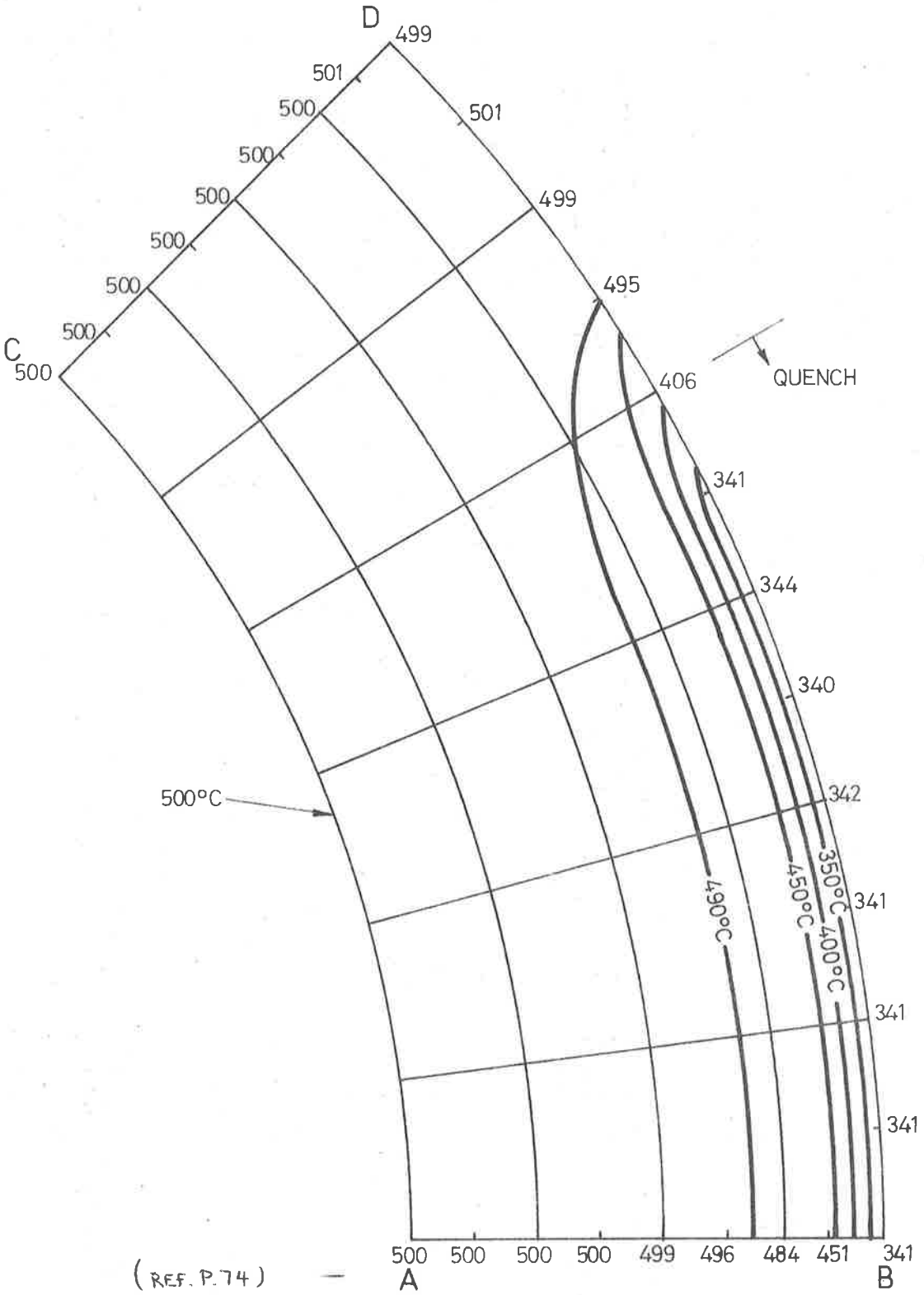

FIGURE 3.15. ISOTHERMALS AT 0·1 SECONDS. (2D AND 3D ANALYSIS)

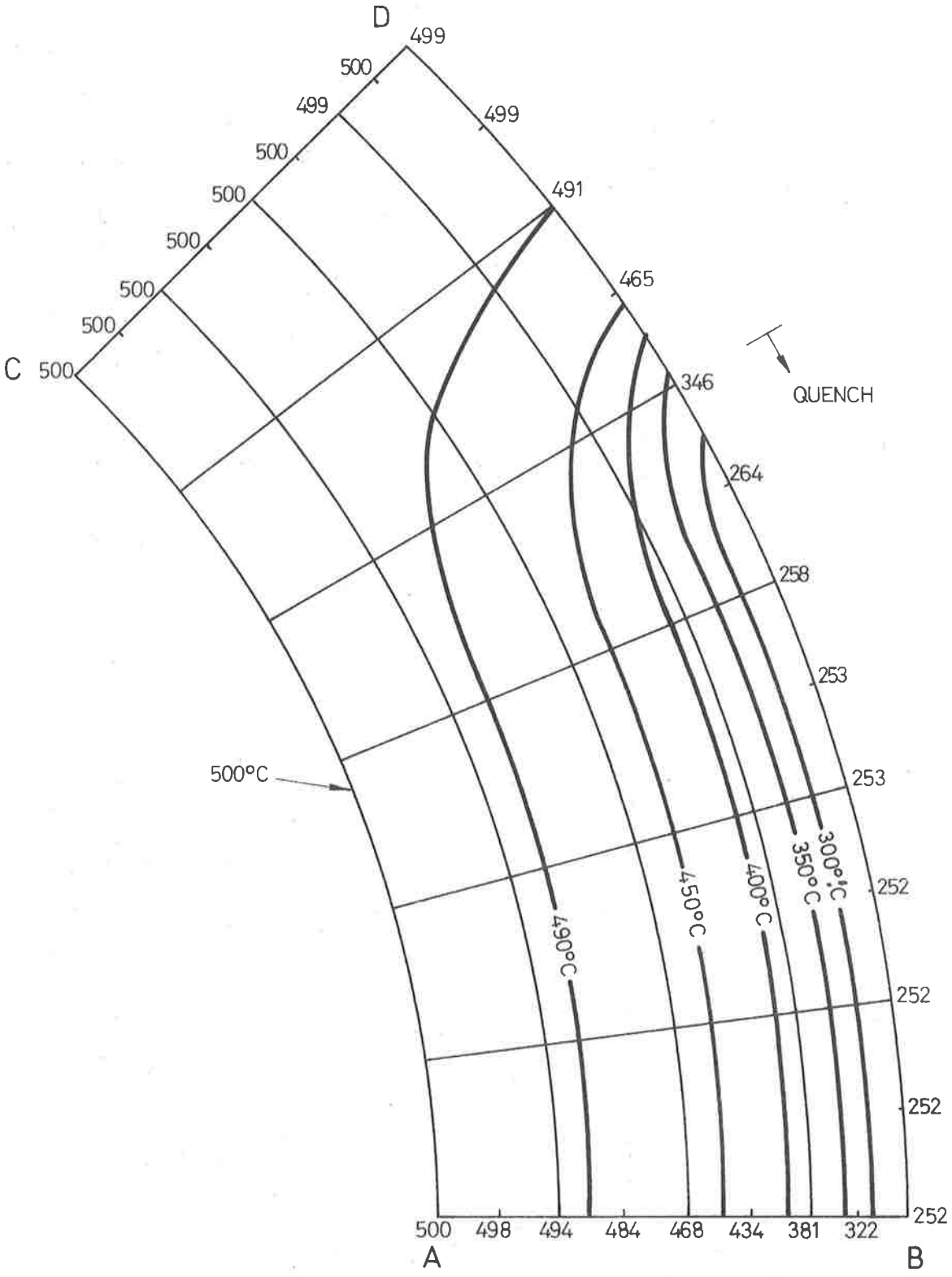

FIGURE 3.16. ISOTHERMALS AT 0·5 SECONDS. (2D AND 3D ANALYSIS.)

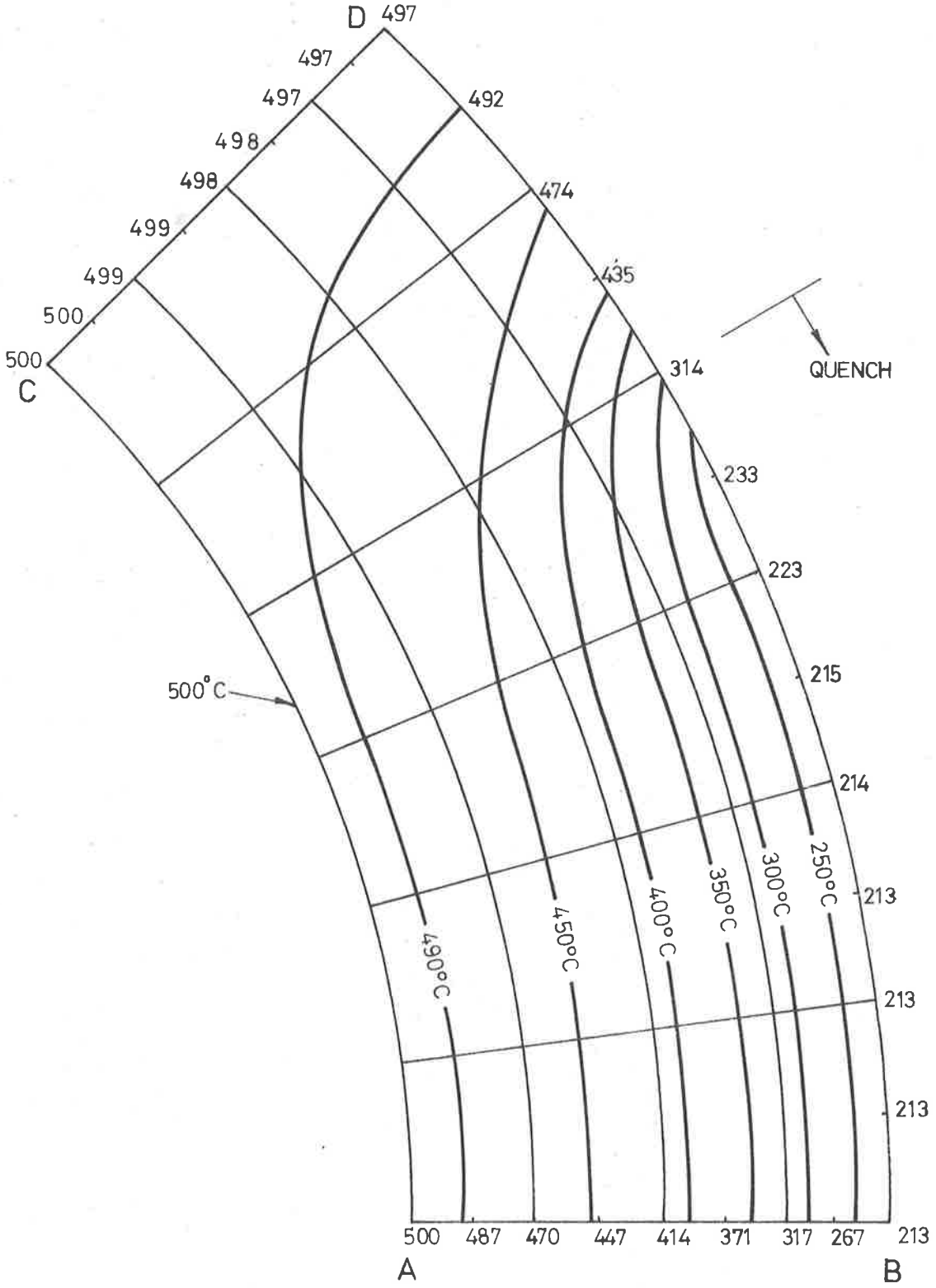

FIGURE 3.17 ISOTHERMALS AT 1.0 SECONDS (2D AND 3D ANALYSIS)

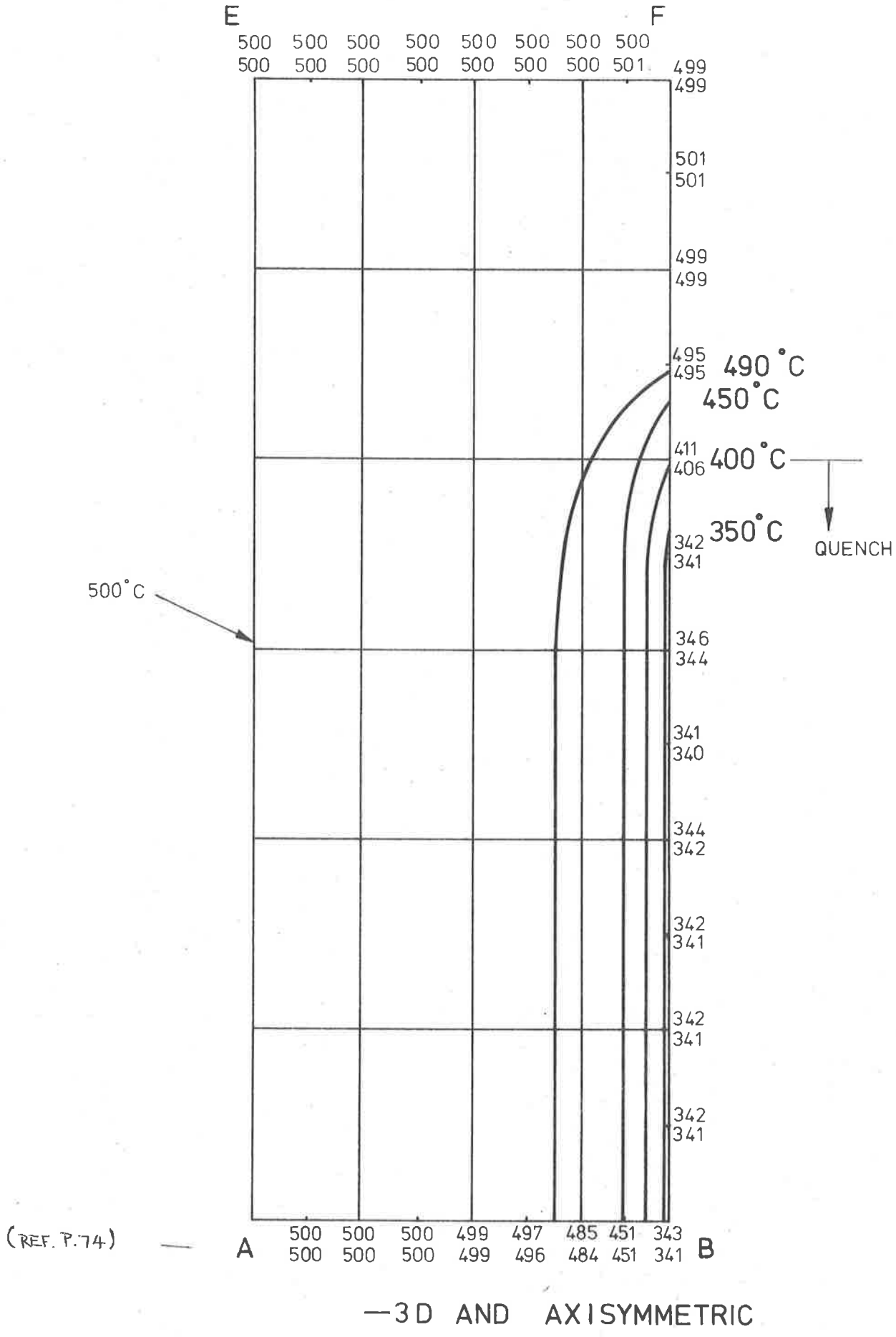

FIGURE 3·18 TEMPERATURE DISTRIBUTION AT 0·1 SECONDS.

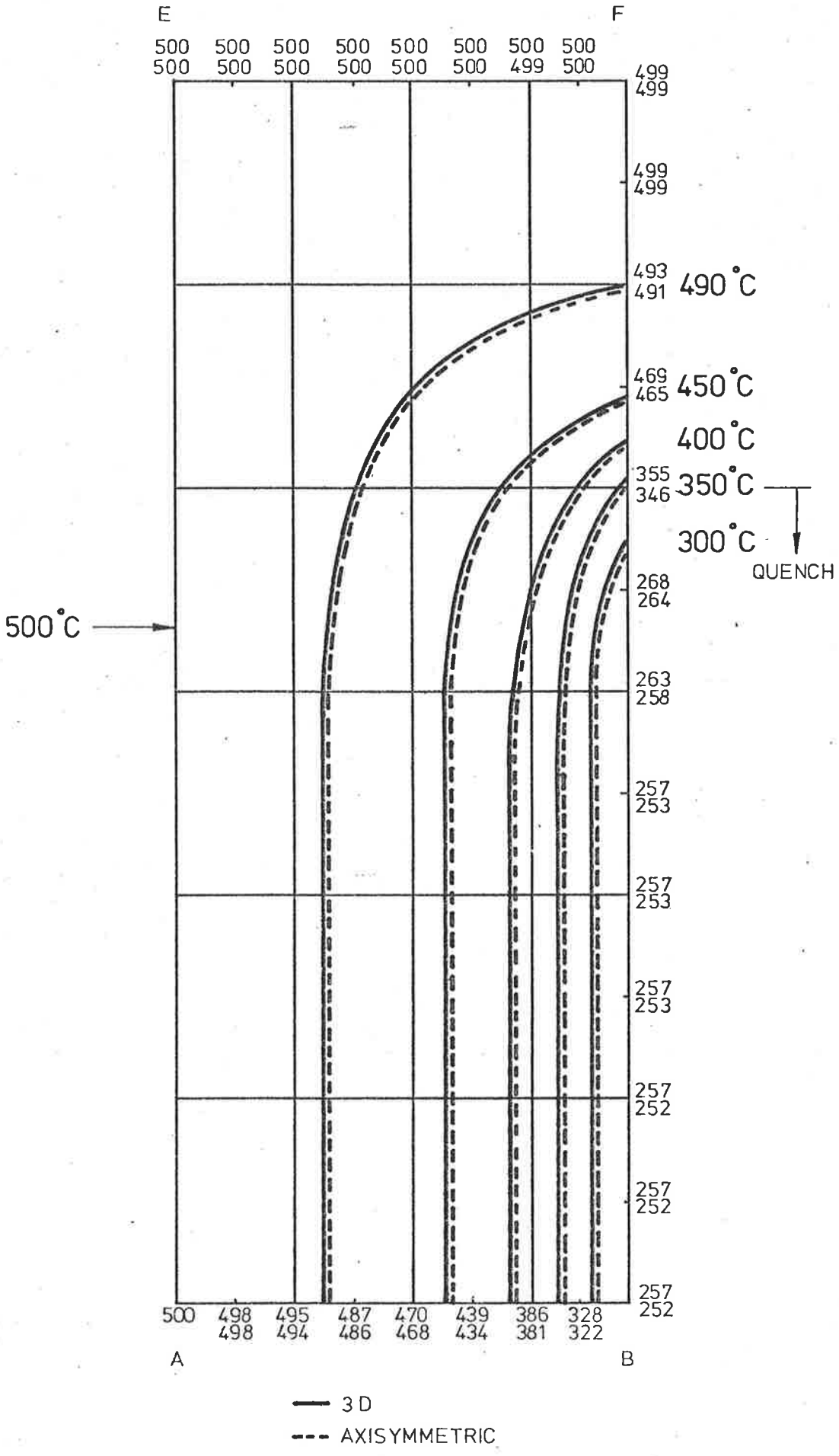

FIGURE 3·19 TEMPERATURE DISTRIBUTION AT 0·5 secs

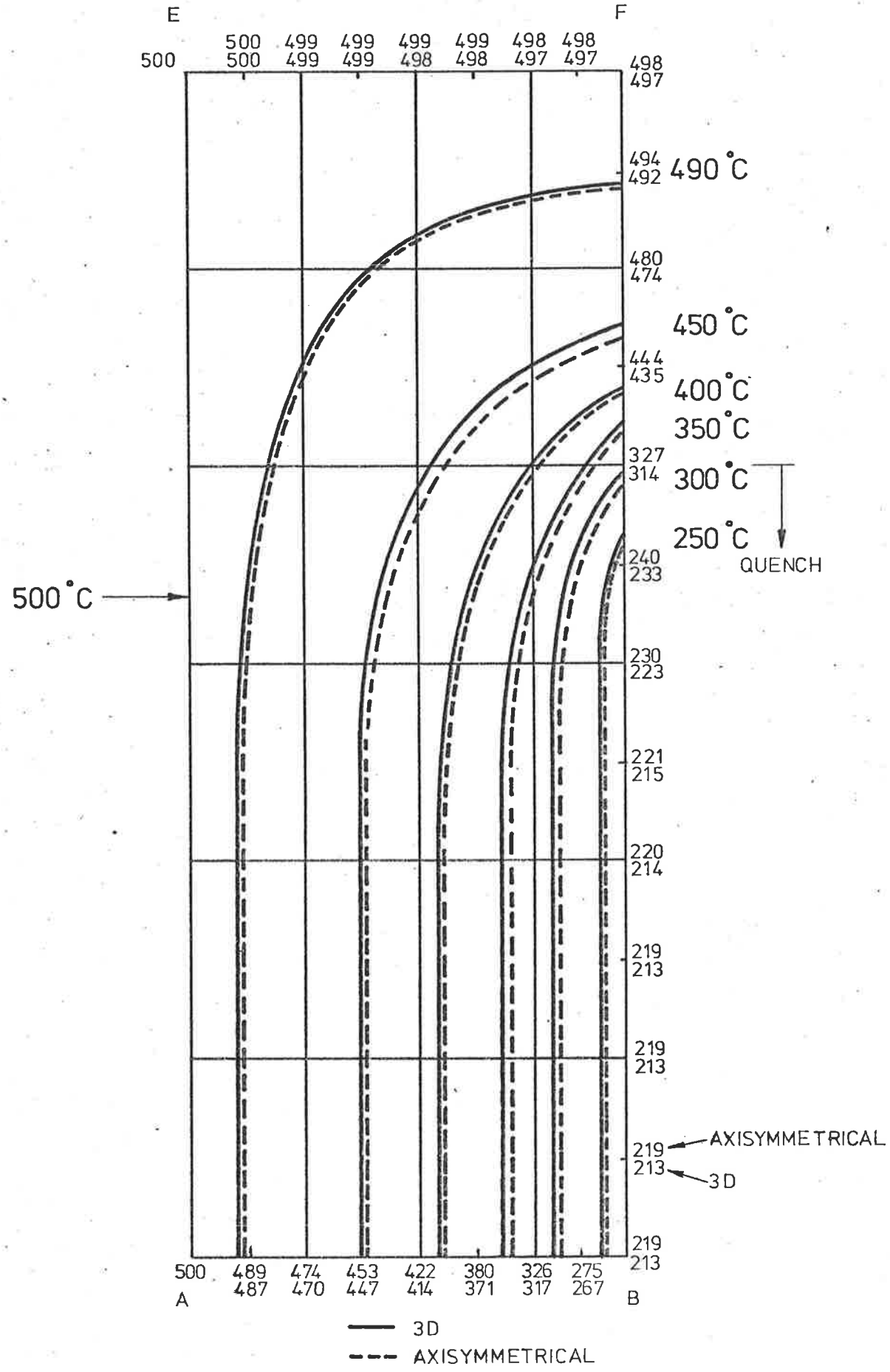

FIGURE 3·20 TEMPERATURE DISTRIBUTION AT 1·0 secs

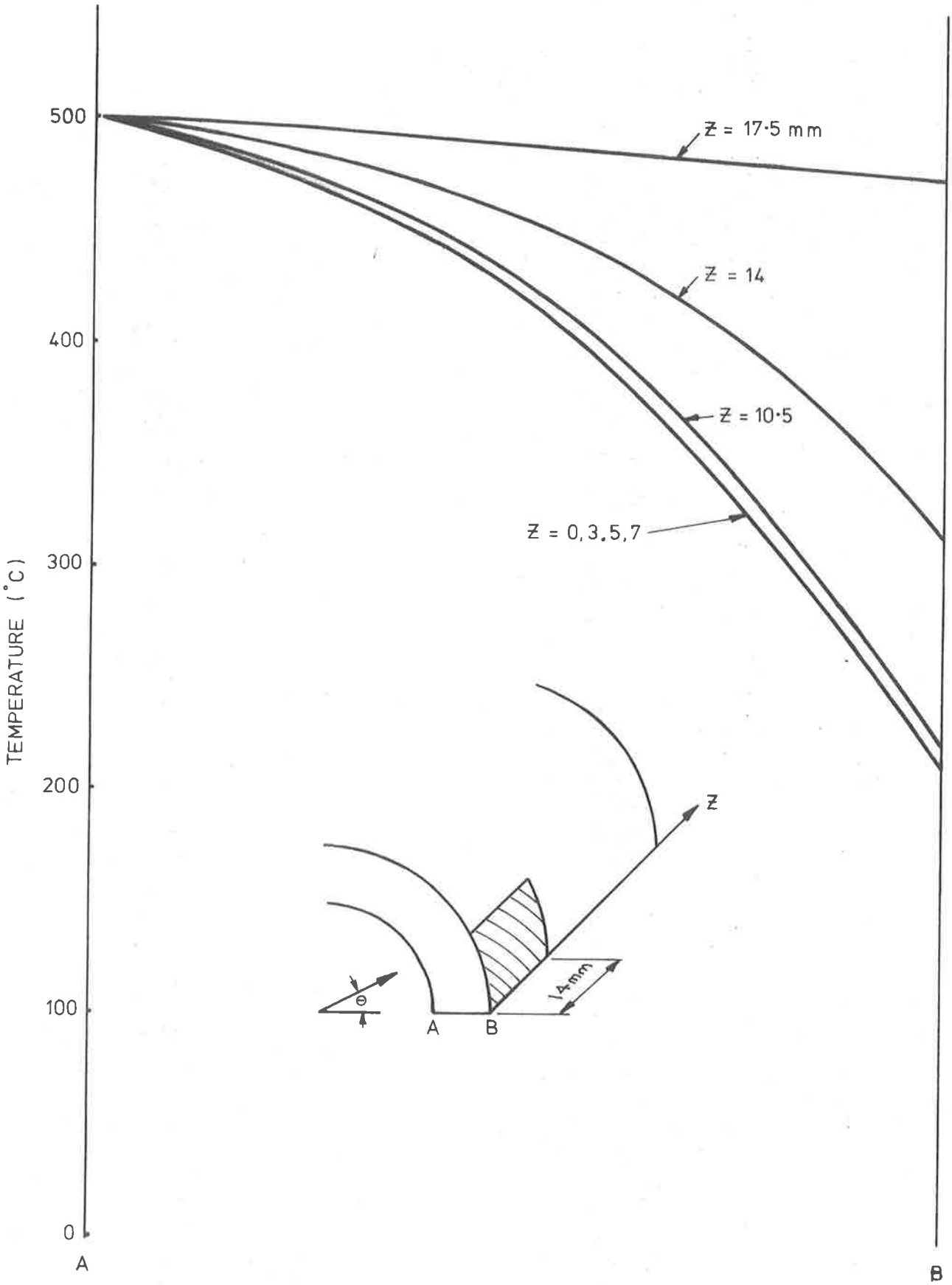

FIGURE 3·21 RADIAL DISTRIBUTION AT 1·0 SECONDS (θ = 0 DEG.)

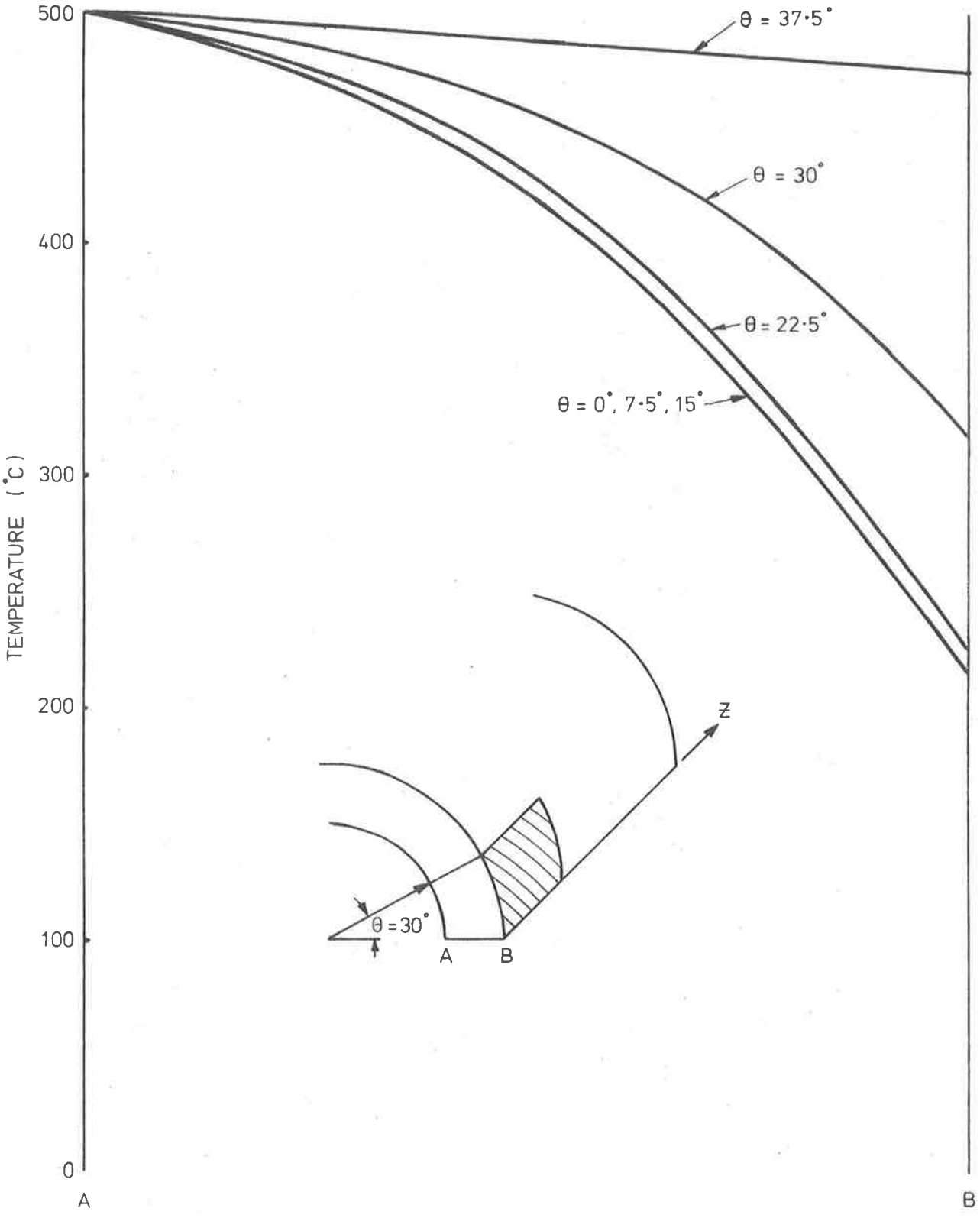

FIGURE 3·22 RADIAL TEMPERATURE DISTRIBUTION AT 1·0 SECS (Z = 0)

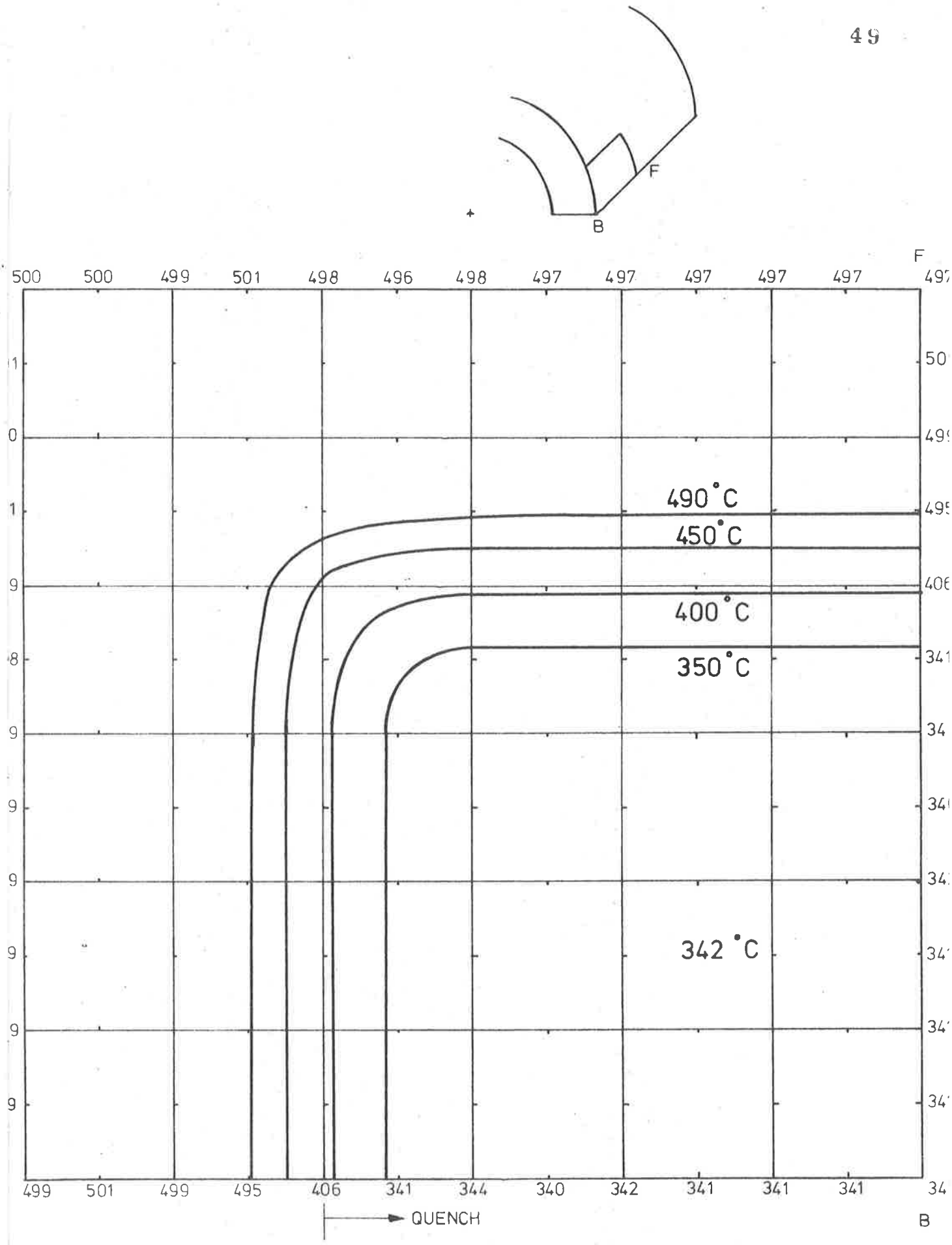

FIGURE 3·23 SURFACE TEMPERATURE DISTRIBUTION AT 0·1 SECS.

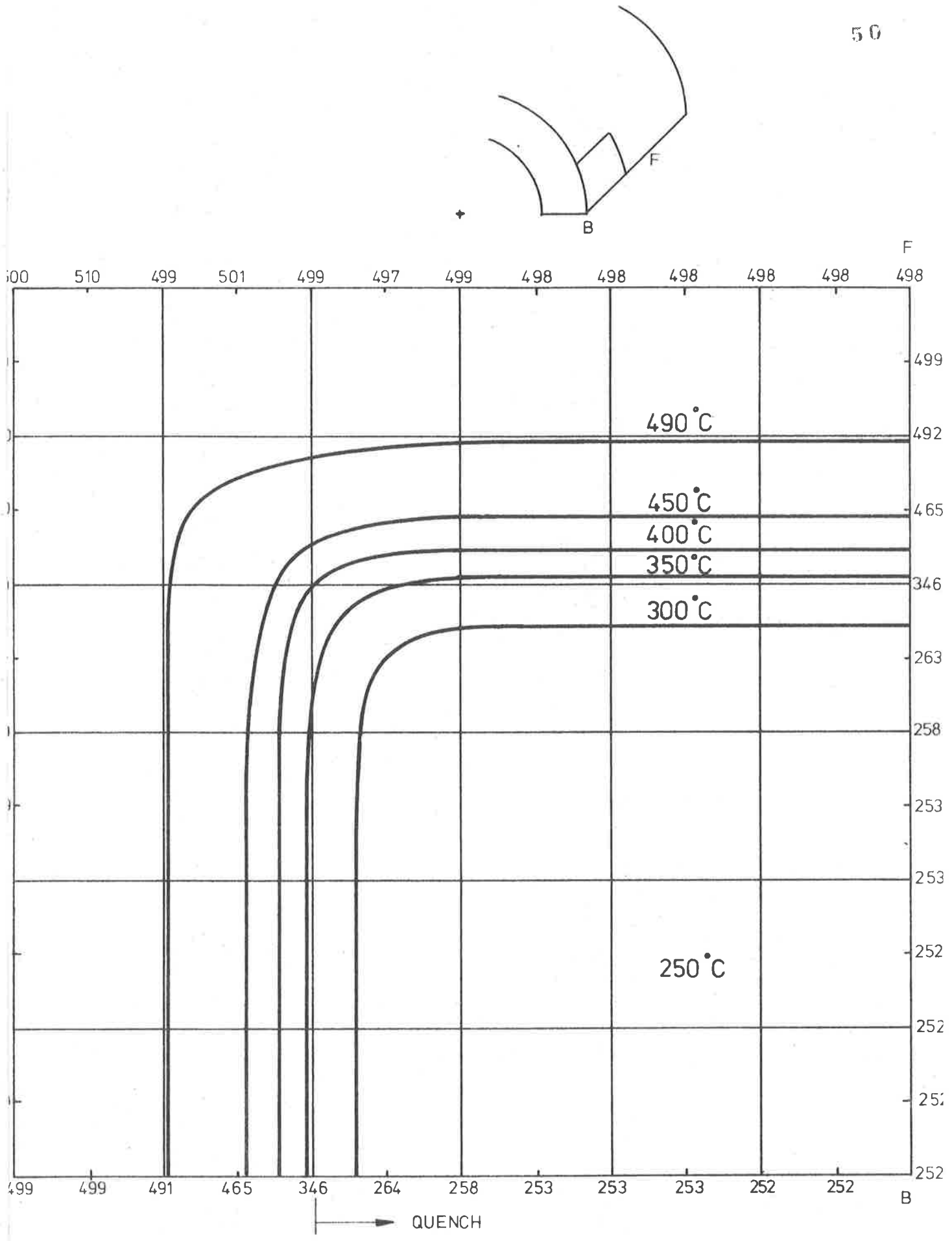

FIGURE 3·24 SURFACE TEMPERATURE DISTRIBUTION 0·5 secs

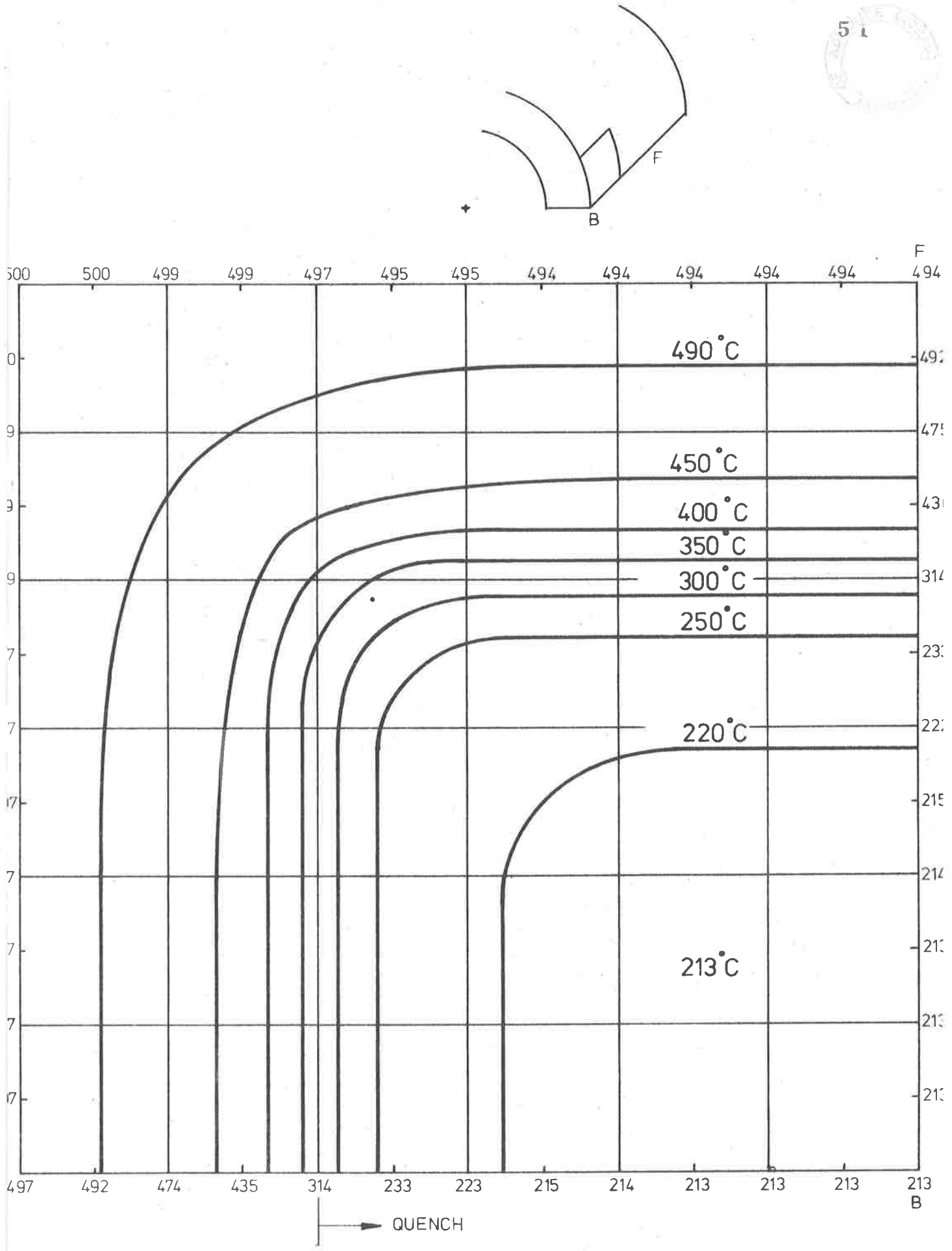

FIGURE 3·25 SURFACE TEMPERATURE DISTRIBUTION AT 1·0 secs

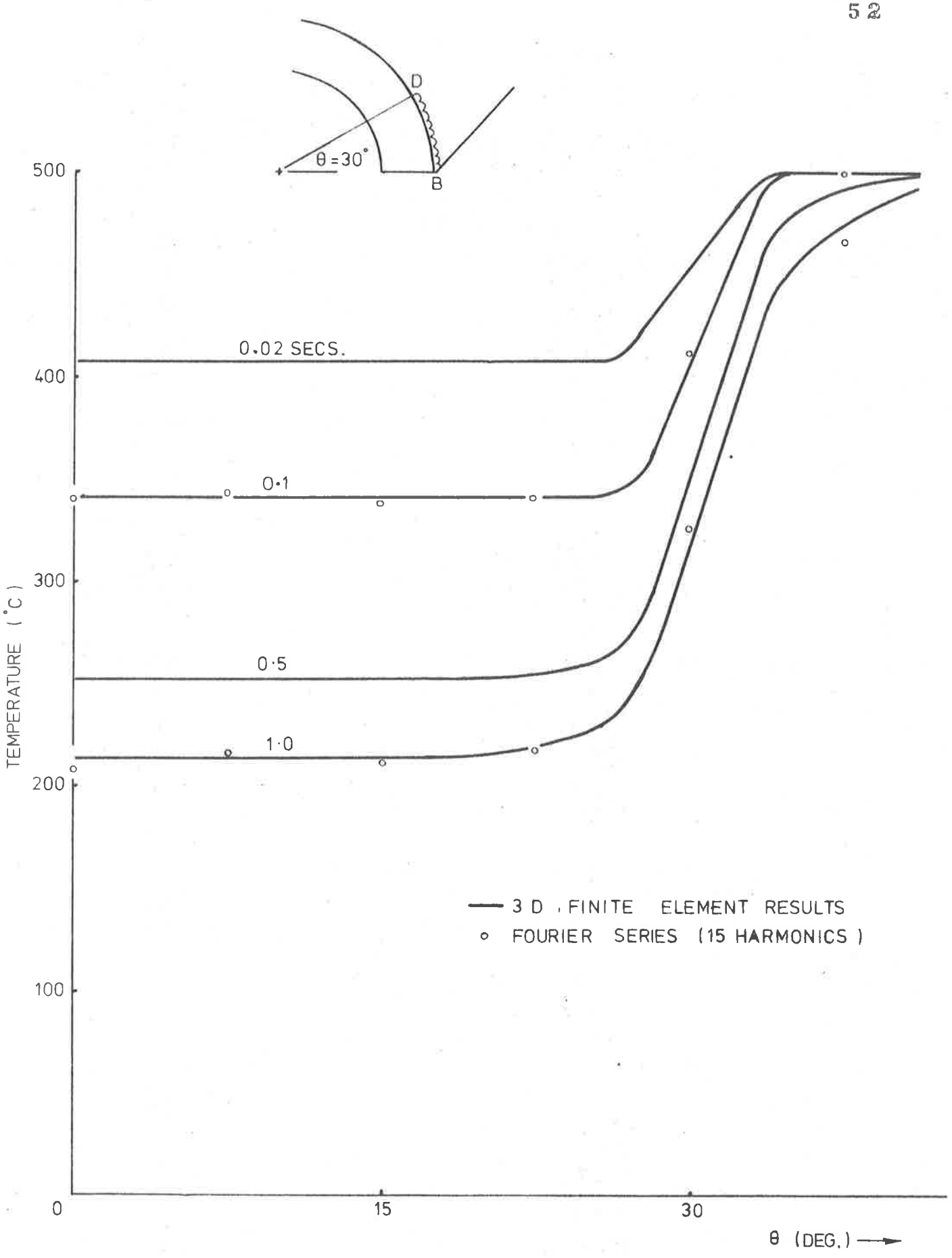

FIGURE 3·26 TEMPERATURE VARIATION (B–D)

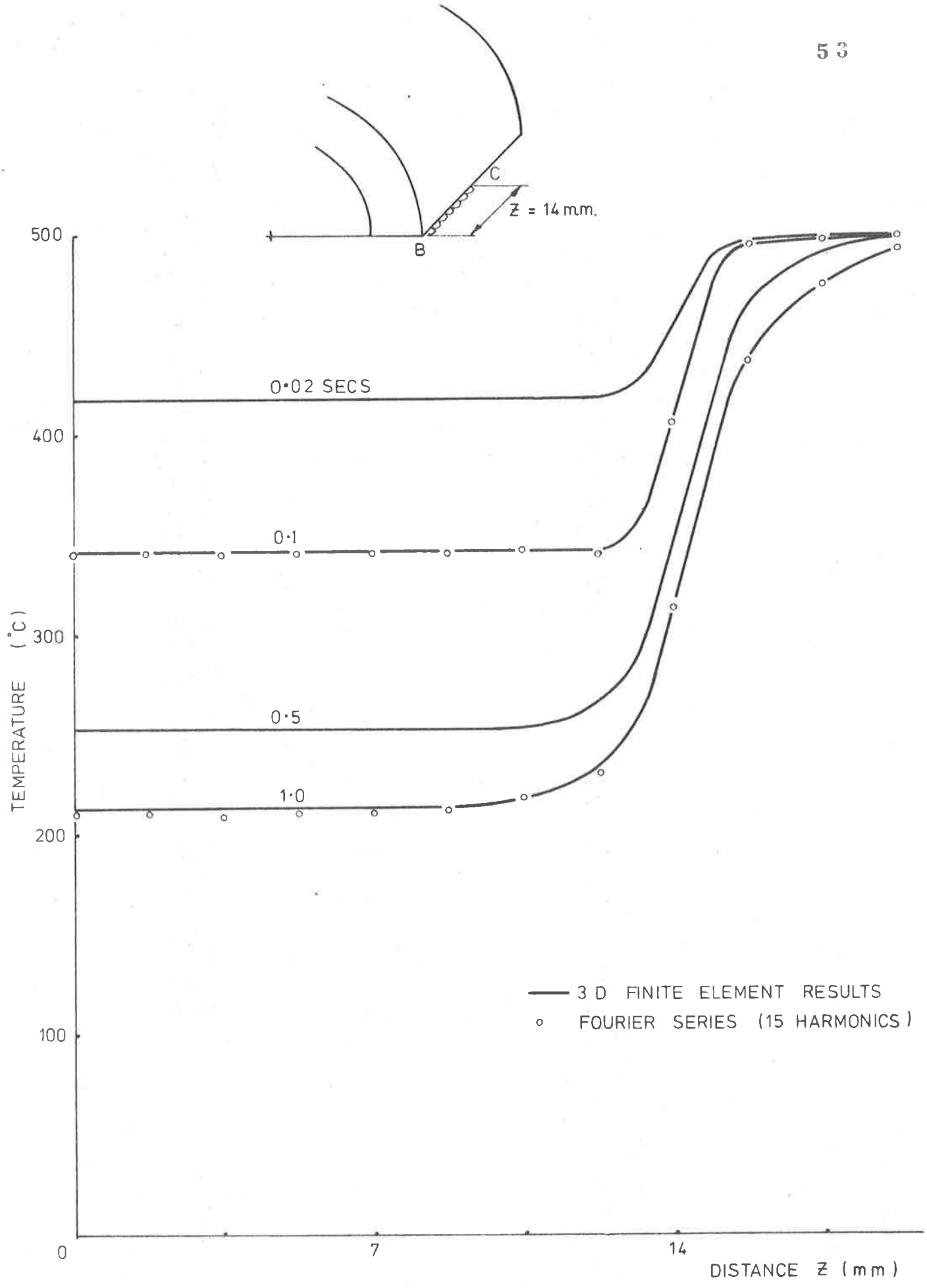

FIGURE 3·27 TEMPERATURE VARIATION (B — C)

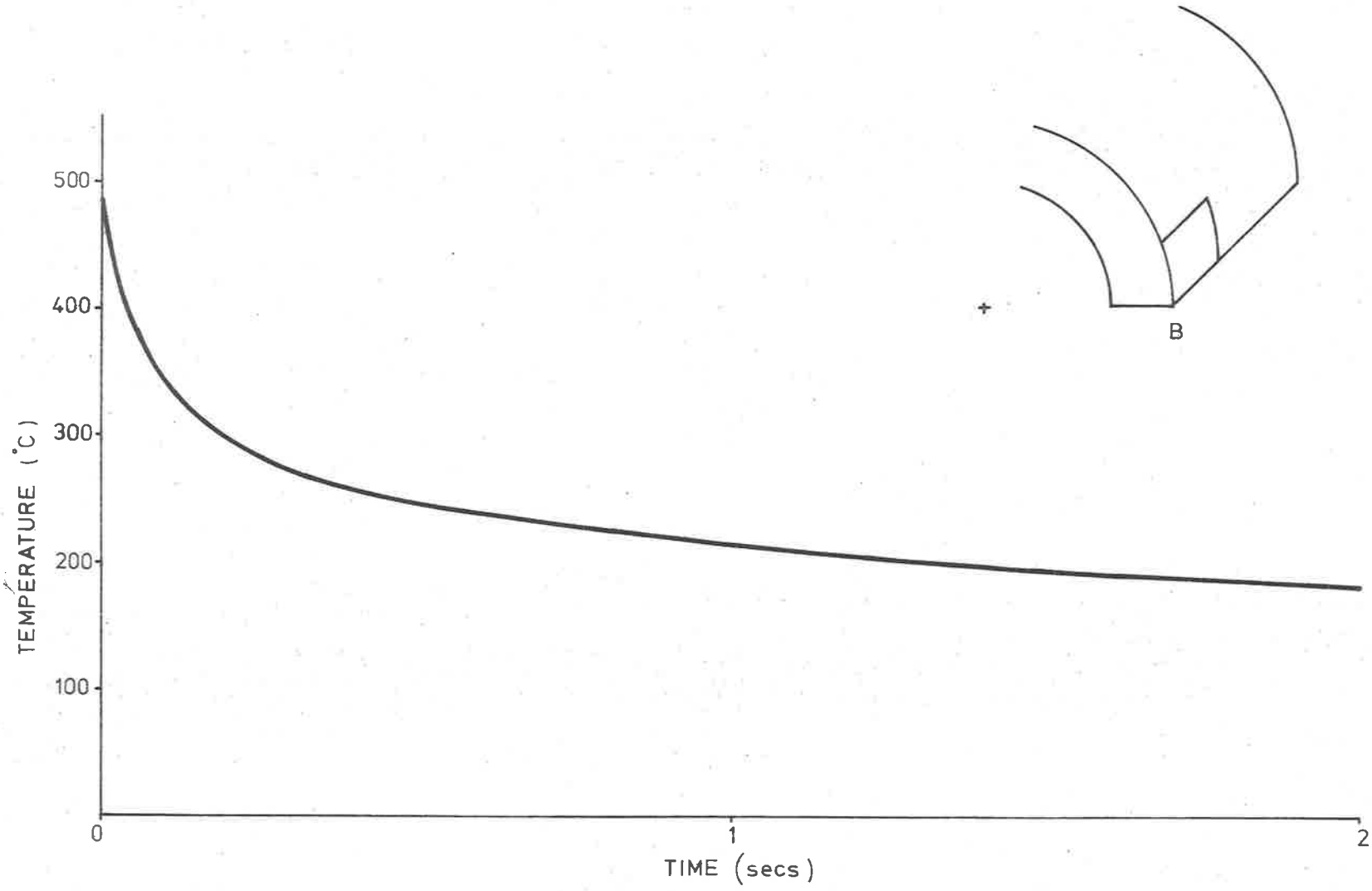

FIGURE 3·28 VARIATION WITH TIME OF TEMPERATURE AT B

4 LINEAR ELASTIC STRESS ANALYSIS

4.1 General

It was decided to limit the stress analysis to the determination of the linear elastic stresses corresponding to the temperatures obtained from the 3D transient heat conduction analysis. The primary objective of this analysis was to determine the distribution and time dependence of the stresses resulting from the surface quench. It was appreciated that the magnitudes of the linear elastic stresses obtained would not be true stresses in the vicinity of the quench surface after the elastic limit had been exceeded.

The conventional method of carrying out a 3D thermal stress analysis using finite elements would be to continue with the same mesh used for the temperature analysis and to determine a thermal load vector for the nodal temperatures at each time station.

The thermal load vector $\{P\}$ would then be used to derive the nodal displacements $\{\delta\}$ in the normal manner from the solution of the simultaneous equations

$$[K]\{\delta\} = \{P\} \tag{26}$$

where $[K]$ is the conventional stiffness matrix.

The stresses can then be obtained from the nodal displacements in the usual way. The estimated computer time required for such an analysis when applied to this problem would be 18 000 seconds. The extra time taken is because the stress analysis has three degrees of

freedom at each node compared with one variable for the temperature analysis which took 7994 seconds. This estimated time for the stress analysis assumed that multiple right-hand sides, which would reduce the solution time, could not be used because the temperature dependent properties of the elasticity matrix would require a recompilation of the stiffness matrix at each time step. It should be noted that for this particular problem the temperature variations caused by the surface quench were confined to a tube length of about 1½ times the quench length, for the time period considered. It does not necessarily follow that displacements and stresses would also be confined to this length, and therefore a stress analysis would need to consider a longer length of tube. This would be desirable also to allow reasonable displacement boundary conditions to be imposed. Consequently an extended finite element mesh would be required leading to a further increase in solution time.

In an attempt to obtain a more economical solution it was decided to investigate an alternative approach using a harmonic analysis. This technique makes use of Fourier Series and the superposition of a number of harmonic 2D finite element analyses to obtain a 3D solution.

4.2 Theory for Harmonic Analysis

The harmonic analysis of axisymmetric bodies with non-axisymmetric loading allows a two-dimensional treatment of the problem and was first used by WILSON[10]. The procedure of resolving displacements and loads into Fourier Series is used in the analysis of shells and also in the finite prism method introduced by CHEUNG[11]. A description of the application to axisymmetric bodies is given in the text by ZIENKIEWICZ[3].

The elements used for the analysis were the eight node parabolic isoparametric type and where necessary the theory will be related to this element. For an axisymmetric body the three components of displacement u, v and w are shown in Figure 4.2. These displacements can be described in a series form along the curved dimension of the body while maintaining a finite element representation in the cross-section. In this way a 3D problem can be reduced to a series of uncoupled 2D analyses. For each harmonic a 2D analysis is carried out with the nodal displacement amplitudes for the harmonic being the unknowns.

If the displacements are symmetric about $\theta = 0$ we can write

$$u = \sum_{n=0}^{\infty} u_n \cos n\theta$$

$$v = \sum_{n=0}^{\infty} v_n \cos n\theta \qquad (27)$$

$$w = \sum_{n=0}^{\infty} w_n \sin n\theta$$

where n is the harmonic number.

Similarly the temperature at any point on the nodal circle i shown in Figure 4.2 can be expressed as:

$$t = \sum_{n=0}^{\infty} t_{in} \cos n\theta \qquad (28)$$

where the temperature coefficients for node i can be determined from

$$t_{in} = \frac{2}{\pi}\int_0^{\pi} t \cos n\theta \, d\theta \qquad n > 0$$

and (29)

$$t_{io} = \frac{1}{\pi}\int_0^{\pi} t \, d\theta \qquad n = 0$$

The displacement amplitudes at any point within an element, for the n^{th} harmonic can be expressed in terms of the shape functions [N] as

$$\{f_n\} = \begin{Bmatrix} u_n \\ v_n \\ w_n \end{Bmatrix} = [N]\{\delta_n\} \tag{30}$$

where

$$[N] = [N_1 I_3, N_2 I_3, \ldots\ldots\ldots\ldots\ldots N_8 I_3]$$

$$\{\delta_n\}^T = \{u_{1n}, v_{1n}, w_{1n} \ldots\ldots\ldots u_{8n}, v_{8n}, w_{8n}\}$$

$[I_3]$ is a (3x3) unit matrix.

From equations (27) and (30) the total displacements at any point within an element can be written in terms of the nodal displacement amplitudes as

$$\{f\} = \begin{Bmatrix} u \\ v \\ w \end{Bmatrix} = \begin{Bmatrix} \sum_{n=0}^{\infty} \sum_{i=1}^{8} N_i \, u_{in} \cos n\theta \\ \sum_{n=0}^{\infty} \sum_{i=1}^{8} N_i \, v_{in} \cos n\theta \\ \sum_{n=0}^{\infty} \sum_{i=1}^{8} N_i \, w_{in} \sin n\theta \end{Bmatrix} \tag{31}$$

The six components of strain at a point are:

$$\{\varepsilon\} = \begin{Bmatrix} \varepsilon_{rr} \\ \varepsilon_{yy} \\ \varepsilon_{\theta\theta} \\ \varepsilon_{ry} \\ \varepsilon_{y\theta} \\ \varepsilon_{r\theta} \end{Bmatrix} = \begin{Bmatrix} \frac{\partial u}{\partial r} \\ \frac{\partial v}{\partial y} \\ \frac{u}{r} + \frac{1}{r}\frac{\partial w}{\partial \theta} \\ \frac{\partial u}{\partial y} + \frac{\partial v}{\partial r} \\ \frac{1}{r}\frac{\partial v}{\partial \theta} + \frac{\partial w}{\partial y} \\ \frac{1}{r}\frac{\partial u}{\partial \theta} + \frac{\partial w}{\partial r} - \frac{w}{r} \end{Bmatrix} \tag{32}$$

Differentiating equations (31) and substituting in (32) gives

$$\{\varepsilon_n\} = [B_n]\{\delta_n\}$$

where the submatrix $[B_{in}]$ for node i is

$$[B_{in}] = \begin{bmatrix} \frac{\partial N_i}{\partial r}\cos n\theta & 0 & 0 \\ 0 & \frac{\partial N_i}{\partial y}\cos n\theta & 0 \\ \frac{N_i}{r}\cos n\theta & 0 & \frac{nN_i}{r}\cos n\theta \\ \frac{\partial N_i}{\partial y}\cos n\theta & \frac{\partial N_i}{\partial r}\cos n\theta & 0 \\ 0 & -\frac{nN_i}{r}\sin n\theta & \frac{\partial N_i}{\partial y}\sin n\theta \\ -\frac{nN_i}{r}\sin n\theta & 0 & \left(\frac{\partial N_i}{\partial r} - \frac{N_i}{r}\right)\sin n\theta \end{bmatrix}$$

It is convenient to separate this as

$$[B_{in}] = [\bar{B}_{in}]\cos n\theta + [\bar{\bar{B}}_{in}]\sin n\theta \tag{33}$$

where

$$\bar{B}_{in} = \begin{bmatrix} \frac{\partial N_i}{\partial r} & 0 & 0 \\ 0 & \frac{\partial N_i}{\partial y} & 0 \\ \frac{N_i}{r} & 0 & \frac{nN_i}{r} \\ \frac{\partial N_i}{\partial y} & \frac{\partial N_i}{\partial r} & 0 \\ 0 & 0 & 0 \\ 0 & 0 & 0 \end{bmatrix} \quad (\bar{\bar{B}}_{in}) = \begin{bmatrix} 0 & 0 & 0 \\ 0 & 0 & 0 \\ 0 & 0 & 0 \\ 0 & 0 & 0 \\ 0 & -\frac{nN_i}{r} & \frac{\partial N_i}{\partial y} \\ -\frac{nN_i}{r} & 0 & \left(\frac{\partial N_i}{\partial r} - \frac{N_i}{r}\right) \end{bmatrix}$$

The linear elastic stress-strain relation can be written as

$$\{\sigma\} = [D]\,(\{\varepsilon\} - \{\varepsilon_o\}) \tag{34}$$

where [D] is the elasticity matrix which for an isotropic material takes the form

$$[D] = \frac{E}{(1-2\nu)(1+\nu)} \left[\begin{array}{cccc:cc} (1-\nu) & \nu & \nu & 0 & 0 & 0 \\ & (1-\nu) & \nu & 0 & 0 & 0 \\ & & (1-\nu) & 0 & 0 & 0 \\ & & & (\tfrac{1}{2}-\nu) & 0 & 0 \\ \hdashline & & & & (\tfrac{1}{2}-\nu) & 0 \\ \text{SYM} & & & & & (\tfrac{1}{2}-\nu) \end{array}\right] = \left[\begin{array}{c:c} D_{11} & \\ \hdashline & D_{22} \end{array}\right] \tag{35}$$

$\{\varepsilon_o\}$ is the initial strain vector and for thermal strains at node i

$$\{\varepsilon_o\} = \sum_{n=0}^{\infty} t_{in} \cos n\theta \, \{\alpha\} \tag{36}$$

where

$$\{\alpha\} = \begin{Bmatrix} \alpha \\ \alpha \\ \alpha \\ 0 \\ 0 \\ 0 \end{Bmatrix} \quad \alpha \text{ - coefficient thermal expansion}$$

By the minimisation of the total potential energy in the normal manner and considering thermal loads only we can write

$$[K] \begin{Bmatrix} \{\delta^1\} \\ \{\delta^2\} \\ \vdots \\ \{\delta^n\} \end{Bmatrix} = \begin{Bmatrix} \{P^1\} \\ \{P^2\} \\ \vdots \\ \{P^n\} \end{Bmatrix} \tag{37}$$

where

$$\{\delta^n\} = \begin{Bmatrix} u_{1n} \\ v_{1n} \\ w_{1n} \\ u_{2n} \\ v_{2n} \\ w_{2n} \\ \vdots \end{Bmatrix}$$

A typical submatrix of the stiffness [K] is

$$[K_{ij}{}^{n,m}] = \int_V [B_{in}]^T [D] [B_{jm}] \, dV \tag{38}$$

and a typical term of the thermal load vector becomes

$$\{P_{in}\} = \int_V [B_{in}]^T [D] \, t_{in} \, \{\alpha\} \, dV$$

$$= 2\pi \int_A [B_{in}]^T [D] \, t_{in} \, \{\alpha\} \, r \, dA \tag{39}$$

substituting equations (33) and (35) into (38)

$$[K_{ij}{}^{n,m}] = \int_V \left([\bar{B}_{in}]^T \cos n\theta + [\bar{\bar{B}}_{in}]^T \sin n\theta \right) [D]$$

$$\left([\bar{B}_{jm}] \cos m\theta + [\bar{\bar{B}}_{jm}] \sin m\theta \right) dV$$

because of the zero off-diagonal submatrices in [D]

$$[\bar{B}_{in}]^T\,[D]\,[\bar{\bar{B}}_{jm}] \;=\; 0 \;=\; [\bar{\bar{B}}_{in}]^T\,[D]\,[\bar{B}_{jm}]$$

so that the products of sine and cosine terms are eliminated leaving

$$[K_{ij}{}^{n,m}] \;=\; \int_V [\tilde{B}_{in}]^T\,[D]\,[\tilde{B}_{jm}]\,\cos n\theta\,\cos m\theta\,dV$$

$$+\int_V [\bar{\bar{B}}_{in}]^T\,[D]\,[\bar{\bar{B}}_{jm}]\,\sin n\theta\,\sin m\theta\,dV$$

further simplification follows from the orthogonal properties

$$\int_0^{\pi}\cos n\theta\,\cos m\theta\,d\theta \;=\; \begin{cases} 0 & \text{if } n \neq m \\ \frac{\pi}{2} & \text{if } n = m \neq 0 \\ \pi & \text{if } n = m = 0 \end{cases}$$

$$\int_0^{\pi}\sin n\theta\,\sin m\theta\,d\theta \;=\; \begin{cases} 0 & \text{if } n \neq m \\ \frac{\pi}{2} & \text{if } n = m \neq 0 \\ 0 & \text{if } n = m = 0 \end{cases}$$

therefore

$$[K_{ij}{}^{n,m}] \;=\; 0 \quad \text{for} \quad n \neq m$$

this means that the matrix [K] becomes a diagonal one and the final assembled equations of the system have the form

$$\begin{bmatrix} [K^{11}] & & & \\ & [K^{22}] & & \\ & & \ddots & \\ & & & [K^{nn}] \end{bmatrix} \begin{Bmatrix} \{\delta^1\} \\ \{\delta^2\} \\ \vdots \\ \{\delta^n\} \end{Bmatrix} = \begin{Bmatrix} \{P^1\} \\ \{P^2\} \\ \vdots \\ \{P^n\} \end{Bmatrix} \tag{40}$$

and the large system of equations reduces to n separate problems

$$[K^{nn}]\ \{\delta^n\} = \{p^n\} \tag{41}$$

where

$$[K_{ij}^{n,n}] = \frac{\pi}{2} \int_A [\bar{B}_{in}]^T\ [D]\ [\bar{B}_{jn}] + [\bar{\bar{B}}_{in}]^T\ [D]\ [\bar{\bar{B}}_{jn}]\ .\ r\ dA$$

which can be simplified to

$$[K_{ij}^{n,n}] = \frac{\pi}{2} \int_A \left([\bar{B}_{in}] + [\bar{\bar{B}}_{in}]\right)^T\ [D]\ \left([\bar{B}_{jn}] + [\bar{\bar{B}}_{jn}]\right)\ .\ r\ dA$$

because the zero off-diagonal matrices in [D] give

$$[\bar{B}_{in}]^T\ [D]\ [\bar{\bar{B}}_{jn}] = 0 = [\bar{\bar{B}}_{in}]^T\ [D]\ [\bar{B}_{jn}]$$

For the zero harmonic

$$[K_{ij}^{0,0}] = \pi \int_A [\bar{B}_{i0}]^T\ [D]\ [\bar{B}_{j0}]\ r\ dA$$

The displacement amplitudes at each node for harmonic n can be determined from equation (41), and the stress amplitudes obtained from

$$\{\sigma_i^n\} = [D]\ \left([B_n]\ \{\delta_n\} - t_{in}\ \{\alpha\}\right)$$

Knowing the amplitudes, the displacements and stresses at any point on the nodal circles can be obtained for each harmonic and summed to give the total values.

4.3 Numerical Integration for Temperature Coefficients

To determine the thermal load vector $\{P_n\}$ for the n^{th} harmonic, the Fourier temperature coefficients for each nodal circle must be obtained from equations (29). The nodal temperatures at each time station are known from the heat-conduction analysis and a numerical integration becomes necessary to determine the required temperature coefficients. The finite element mesh used for the harmonic stress analysis is shown in Figure 4.1 and is compatible with the mesh used for the 3D temperature analysis except that it has been extended to cover a greater tube length for the reasons mentioned in Section 4.1. The temperature of the additional length of tube taken into consideration would be unaffected by the surface quench and therefore numerical integration was unnecessary for this constant temperature section. A typical variation of temperature around the circumference for a surface node in the quench region is shown diagramatically in Figure 4.2. Results from the heat-conduction analysis show that at angles of θ greater than 60 degrees the nodal temperatures remained constant at 500°C for the time period considered. This enabled contributions to the integrals in equations (29) for the range $\pi/3$ to π to be determined explicitly and added to the numerical integration carried out over the range 0 to $\pi/3$.

A subroutine was written to perform the numerical integration and determine the temperature coefficients for each node. The coefficients computed for each harmonic in turn were progressively substituted into equation (28) to obtain a running total of the temperatures after each harmonic at points around the nodal circle which correspond to nodes in the previous 3D mesh. This allowed the temperature convergence at

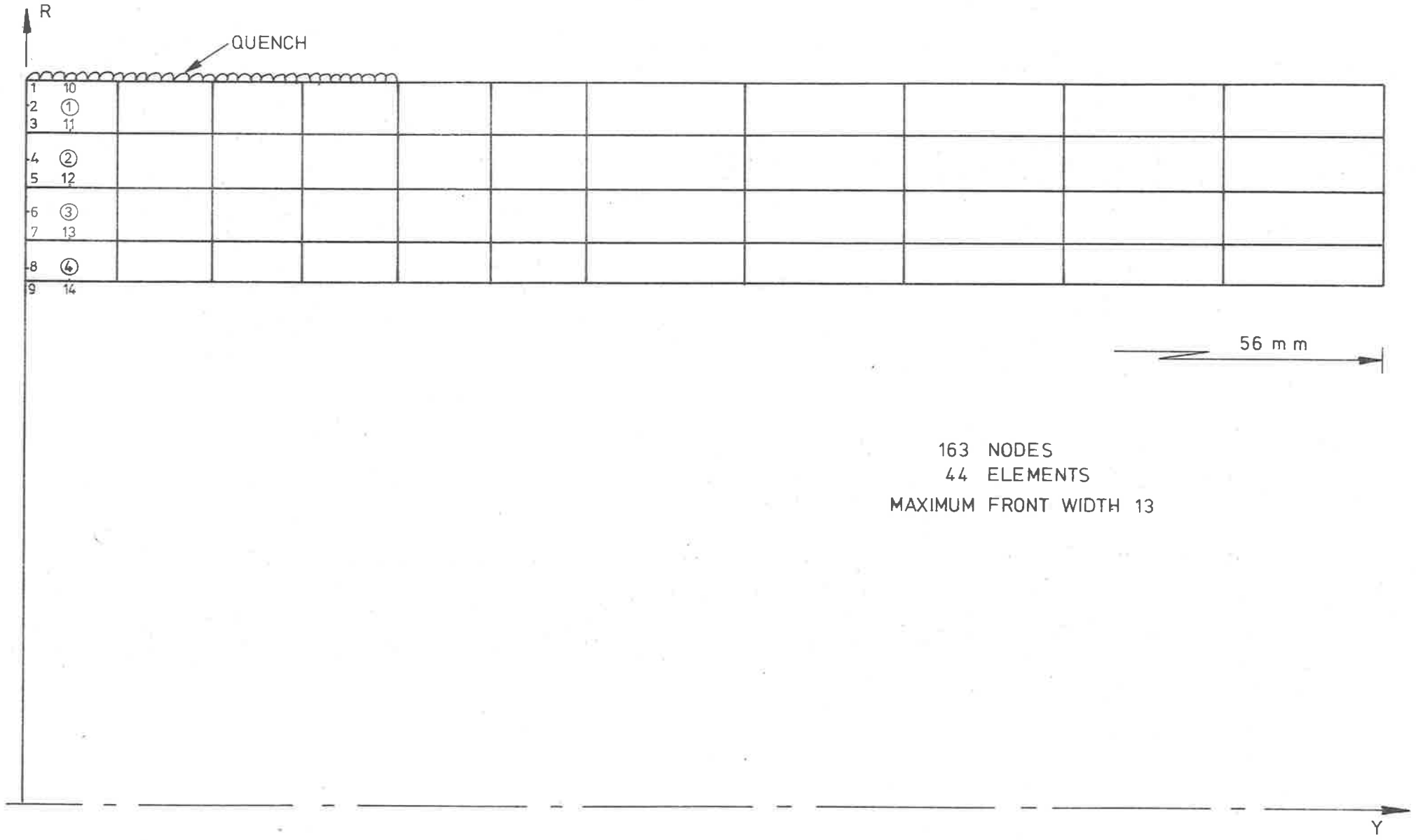

FIGURE 4·1 FINITE ELEMENT MESH FOR HARMONIC ANALYSIS

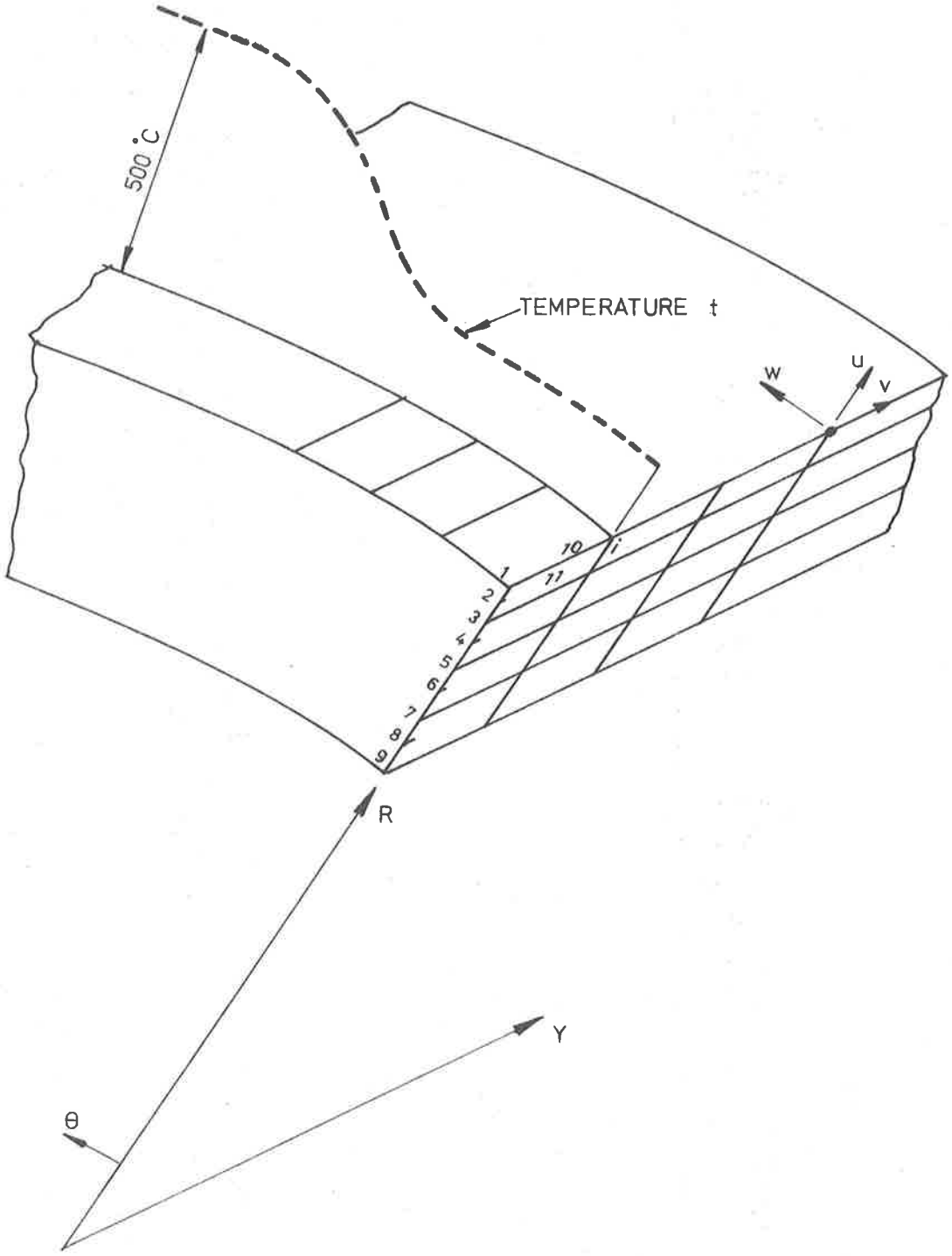

FIGURE 4·2 DIAGRAMMATIC VARIATION OF TEMPERATURE FOR NODE i

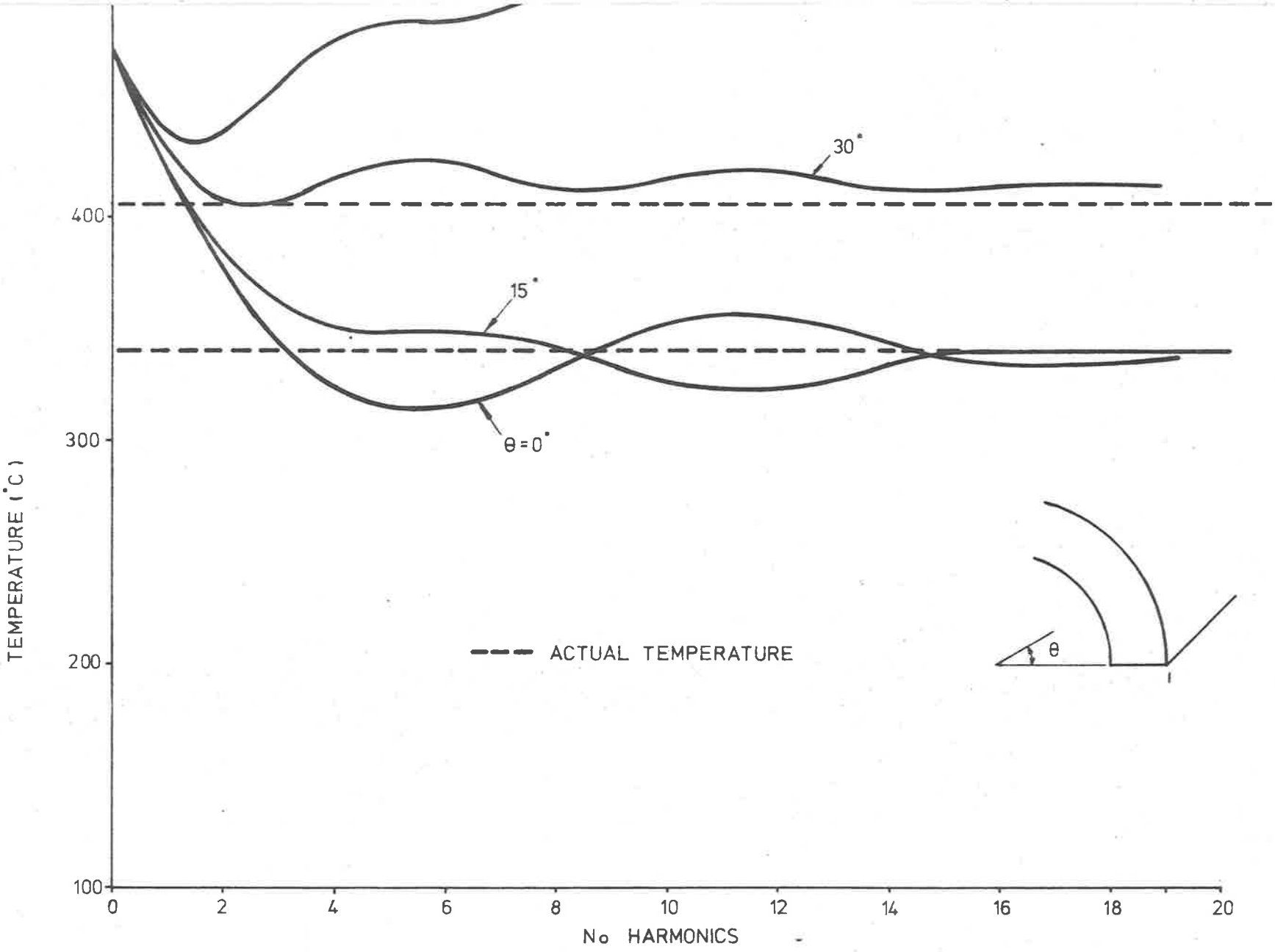

FIGURE 4·3 TEMPERATURE CONVERGENCE NODE CIRCLE 1.
(t = 0·1 secs)

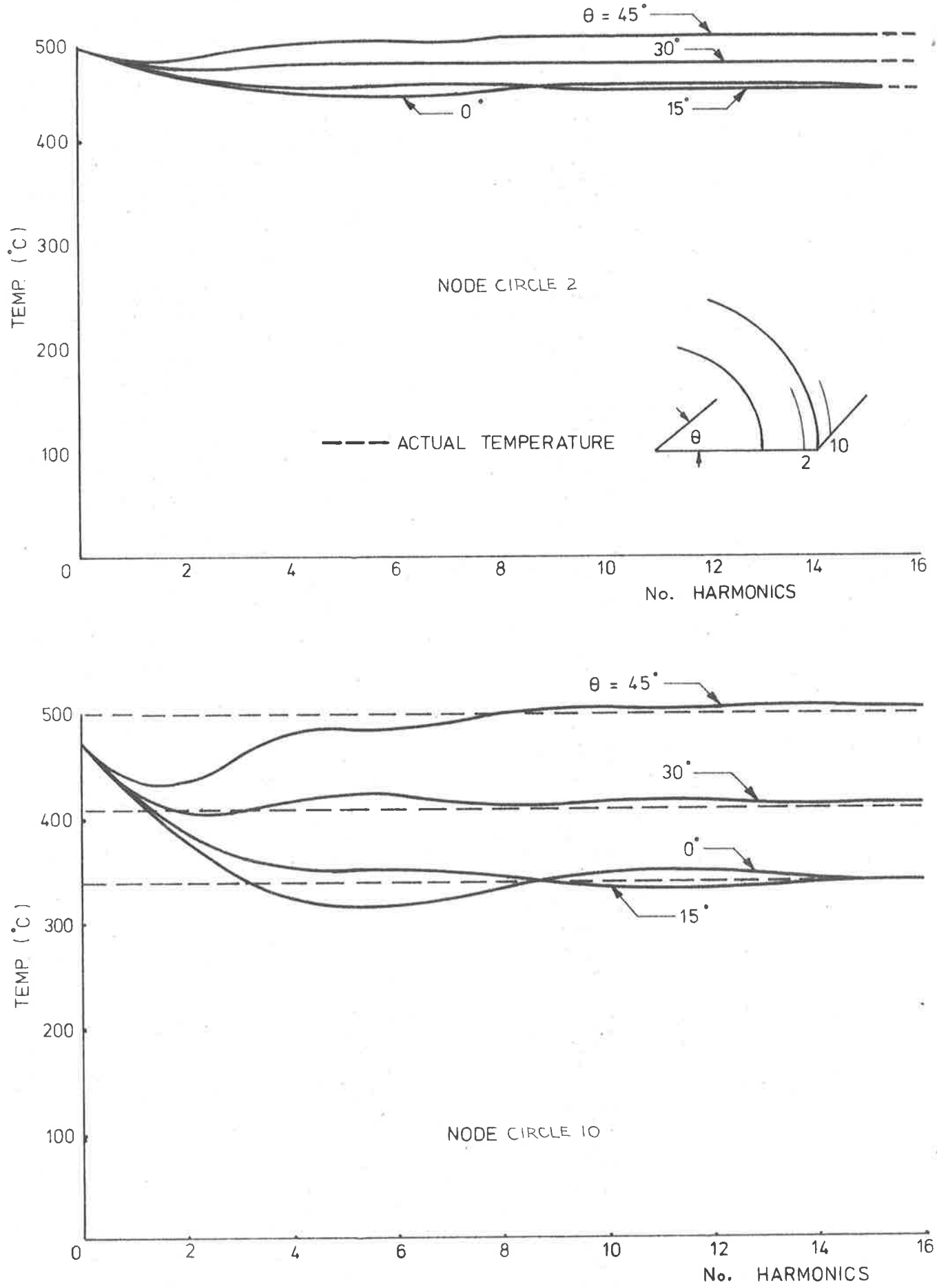

FIGURE 4·4 TEMPERATURE CONVERGENCE
(t = 0·1 SECS)

all points to be examined. In this way results obtained using the Trapezoidal Rule and also Simpson's Rule for the numerical integration were compared. It was found that temperatures at some nodes converged more rapidly than others, and for the mid-side nodes in particular a satisfactory convergence was initially obtained but the addition of higher harmonics led to a subsequent divergence. This unacceptable occurrence was a result of the limited number of integration points around the nodal circles corresponding to the previous 3D nodal positions used for the temperature analysis. These integration points, spaced at 3.75 degree intervals for the corner nodes and at 7.5 degree intervals for the mid-side nodes, were adequate for the lower harmonics but produced spurious results for higher harmonics when the half-cycle angles became equal to or less than the intervals stated. Results obtained using the Trapezoidal Rule and Simpson's Rule were almost identical, both methods being affected by the anomaly described. A way of overcoming this problem was found by assuming a linear variation of temperature between adjacent integration points around the circumference and by carrying out an exact integration between each pair of points in the following manner:

Temperature at angle θ between two points may be written as

$$t = t_1 + \frac{(t_2 - t_1)}{(\theta_2 - \theta_1)} (\theta - \theta_1) \qquad \theta_1 < \theta < \theta_2$$

therefore

$$\int_{\theta_1}^{\theta_2} t \cos n\theta \, d\theta = \int_{\theta_1}^{\theta_2} \left(t_1 + \frac{(t_2 - t_1)}{(\theta_2 - \theta_1)} (\theta - \theta_1)\right) \cos n\theta \, d\theta$$

$$= \frac{t_1}{n} (\sin n\theta_2 - \sin n\theta_1)$$

$$+ \frac{(t_2 - t_1)}{(\theta_2 - \theta_1)} \left[\frac{1}{n^2} (\cos n\theta_2 - \cos n\theta_1) + \frac{1}{n} (\theta_2 \sin n\theta_2 - \theta_1 \sin n\theta_1) \right]$$

$$- \frac{(t_2 - t_1)}{(\theta_2 - \theta_1)} \cdot \frac{\theta_1}{n} (\sin n\theta_2 - \sin n\theta_1)$$

Using this approach convergence was found to continue when including higher harmonics to an acceptable level for all nodes. The number of harmonics required before the convergence oscillations 'damped out' depended on the temperature of the particular point relative to the mean temperature of the nodal circle, but 15 harmonics was sufficient to cover all points satisfactorily. Typical convergence curves are shown in Figures 4.3 and 4.4 for the corner node 1 and for the mid-side nodes 2 and 10 at various points around the circumference. Using 15 harmonics the temperatures obtained in the circumferential and axial directions passing through the centre of the quench region are plotted in Figures 3.26 and 3.27 together with results from the 3D heat-conduction analysis.

4.4 Programming Procedure

An existing 'finite prism' computer program using parabolic iso-parametric elements was adapted to carry out the harmonic linear elastic analysis for this problem. A number of basic changes and modifications were found to be necessary which will be briefly described.

a The Fourier series displacement functions for a straight simply-supported prism required modification to give the even, even and odd functions necessary for the u, v and w displacements of an axisymmetric body subjected to a temperature loading symmetric about $\theta = 0$.

b A zero harmonic term was added which represented an axisymmetric temperature loading corresponding to the mean nodal circle temperatures.

c Compilation of the thermal load vectors given by equation (39) was included for each harmonic. The required temperature coefficients were obtained using the subroutine mentioned in Section 4.3 which was added to the program.

d The stress and strain formulations were changed to the cylindrical co-ordinate system required for the analysis of axisymmetric bodies.

e An allowance for the temperature dependence of the material properties in the elasticity matrix was incorporated by using for each element, properties corresponding to its centroidal mean circumferential temperature.

The general procedure followed by the program was to read in a complete set of nodal temperatures, obtained from the 3D temperature analysis, corresponding to a particular time station. Then considering the first harmonic, nodal temperature coefficients were determined and used to obtain the thermal load vector. The element stiffness matrices for the harmonic were generated and assembled into the equations which were solved using the frontal solution giving the displacement amplitudes for each nodal circle. Stress amplitudes were then obtained

and used to determine stresses at angles corresponding to the 3D node positions. This procedure was repeated for each harmonic in turn and the stresses were progressively summed at each point. In this way the linear elastic stresses were obtained for each time station. The specification of displacements was necessary only for the v direction on the end plane of symmetry.

4.5 Axisymmetric Temperature Test

A preliminary test of the converted computer program was carried out by analysing a cylinder subjected to an axisymmetric temperature distribution. The inner surface temperature was taken as 500°C and the outer surface as 0°C. For this case the analytical solution for the temperature at any radius r is given by:

$$t = \frac{500}{\log (b/a)} \log (b/r)$$

a and b being the inner and outer radii.

Using this expression the nodal temperatures for the mesh shown in Figure 4.1 were generated and the resulting stresses computed and compared with the analytical solution given by Timoshenko and Goodier[12]. The stresses are plotted in Figure 4.5 and acceptable agreement was obtained taking into account that the finite element solution converges with increasing mesh fineness.

For this special case where the temperatures were axisymmetric the zero harmonic only was used and numerical integration was unnecessary to determine the mean nodal circle temperatures normally obtained for this harmonic. Nevertheless the case was felt to be sufficient to test the basic workings of the program, considering that the numerical integration procedure had been tested independently.

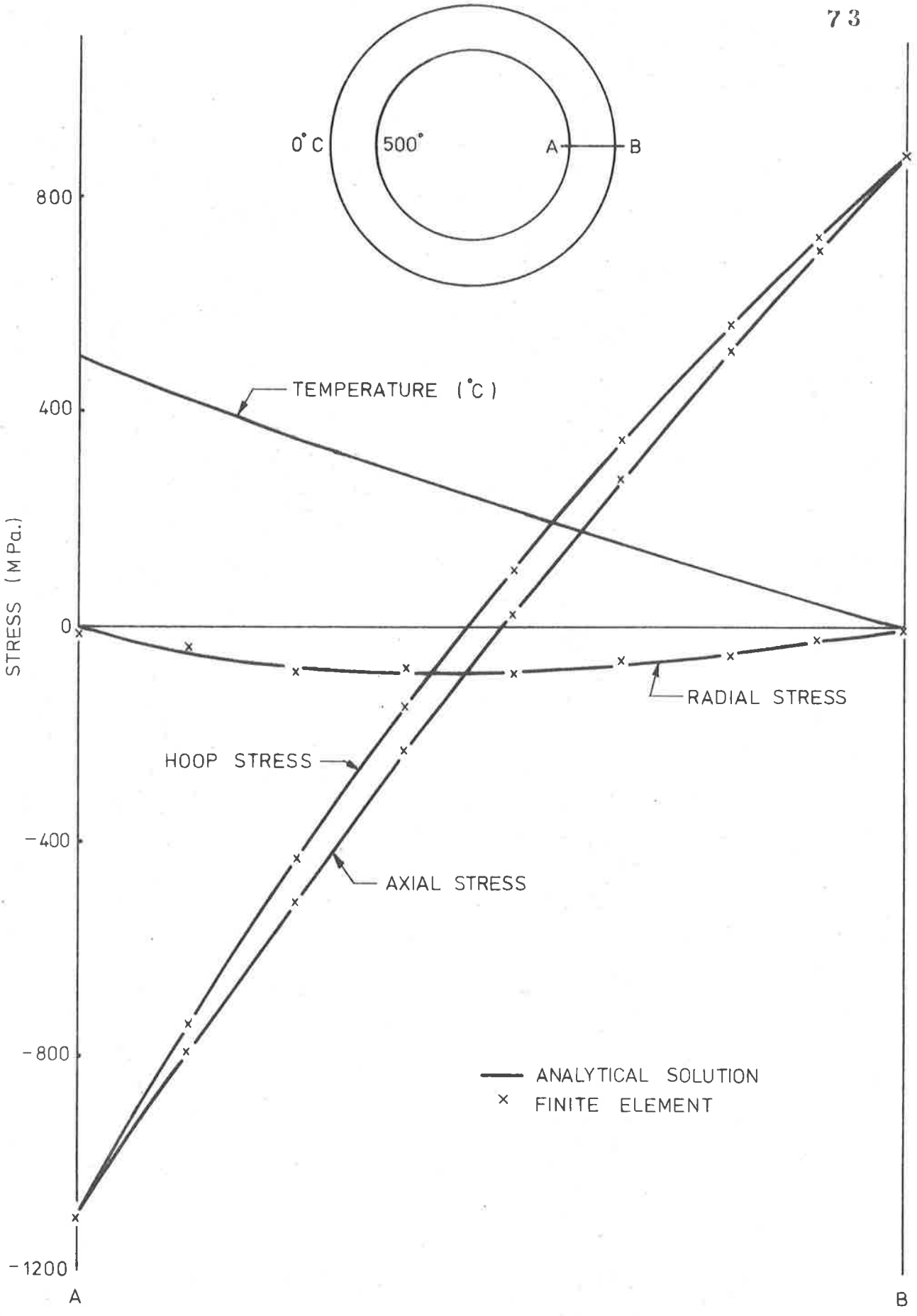

FIGURE 4·5 AXISYMMETRIC THERMAL STRESSES IN CYLINDER

4.6 Results and Observations

The stresses given in the results are due to the quenching operation only and do not include the relatively small normal working stresses. Results will be referred to the positions shown in Figure 4.6 where the point B is at the centre of the quench region.

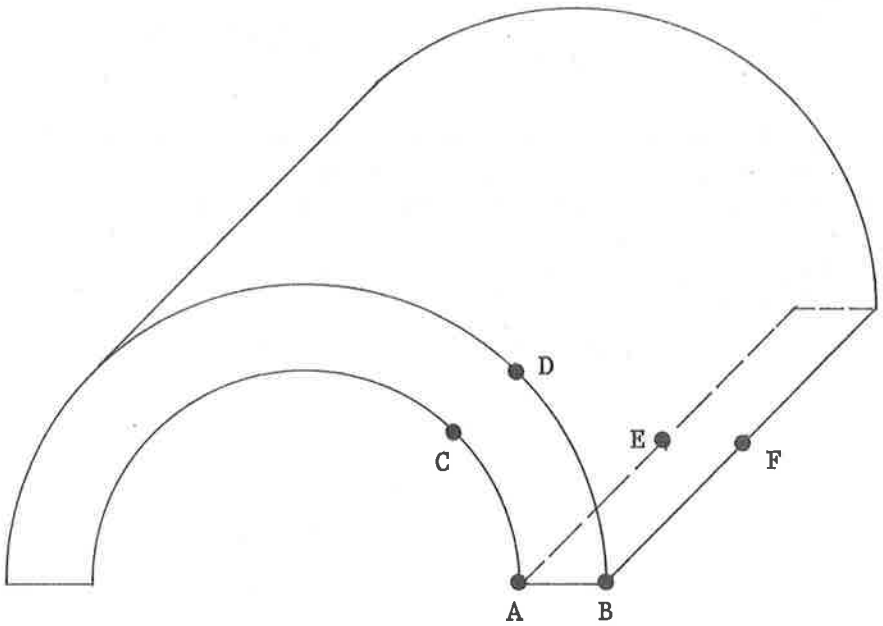

FIGURE 4.6

Convergence of the hoop stress at specified points around the circumference B-D is shown in Figure 4.7 for the time station t = 0.1 seconds. Harmonic number 15 was taken as being a suitable cut-off point and was used for the remainder of the analysis. A further indication of the convergence is shown in Figure 4.8 for the hoop stress from B-D.

Variation with time of stresses resulting from the surface quench initiated at t = 0 seconds is shown in Figure 4.9. The hoop stress and the axial stress at B can be seen to increase rapidly, reaching maximum values at about t = 0.1 seconds with little subsequent change over the remainder of the quench period. The hoop and axial stresses around the circumference B-D are shown in Figures 4.10 and 4.11, for selected time stations, and also the variation of these stresses along the axial line B-F can be seen in Figures 4.12 and 4.13. These results show that at any point in time during the quenching operation, the surface hoop and axial stresses remain fairly constant over the central portion of the cooled region but reduce steeply towards the quench boundaries. These stresses are the principal stresses at the surface, the radial stress being zero. It can be seen from typical heat-conduction results shown in Figures 3.15 and 3.18 that the only temperature gradient at the central portion of the quench region was through the thickness. Considering a flat plate with the same temperature variation through the thickness, the corresponding surface stresses[13] are shown in Figure 4.9 and can be seen to be somewhat lower than the tube stresses. The difference can be attributed to the contraction restraints arising at the boundaries of the quench area.

The variation of stresses through the thickness A-B of the tube are plotted in Figures 4.14 and 4.15 and the maximum tensile peaks can be seen to occur at the outside. A sharp reduction of stress with depth is evident until compression occurs over the inner part of the wall. The maximum axial stress at the surface is seen to be slightly greater than the hoop stress, both being in excess of the elastic limit of the

steel. For the 2.25% Cr 1% Mo steel the 0.2% proof stress is equal to 262 MPa at ambient temperature reducing to 187 MPa at 500°C. Radial stresses produced by the surface cooling were zero at the inner and outer surfaces and were of relatively small magnitude at points within the tube wall.

The maximum lateral displacement, at the end of the length of tube considered, resulting from axial bending was equal to 0.0019 mm showing that the localised quench effects produced little interaction with the overall bending stiffness of the tube. The horizontal diametral displacement at the quench section however was equal to -0.0192 mm indicating a greater degree of interaction with the sectional ring stiffness. See sketch below.

This explains why the maximum surface axial stress was marginally greater than the corresponding hoop stress and is in accordance with the circumferential cracking produced by on-load deslagging tests carried out by the State Electricity Commission of Victoria[14].

The computer time for the stress analysis was 880 seconds for each time increment.

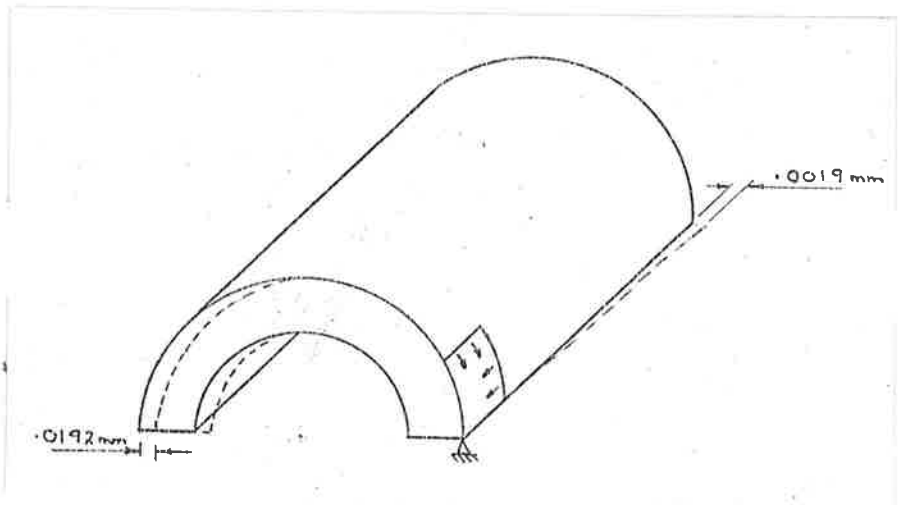

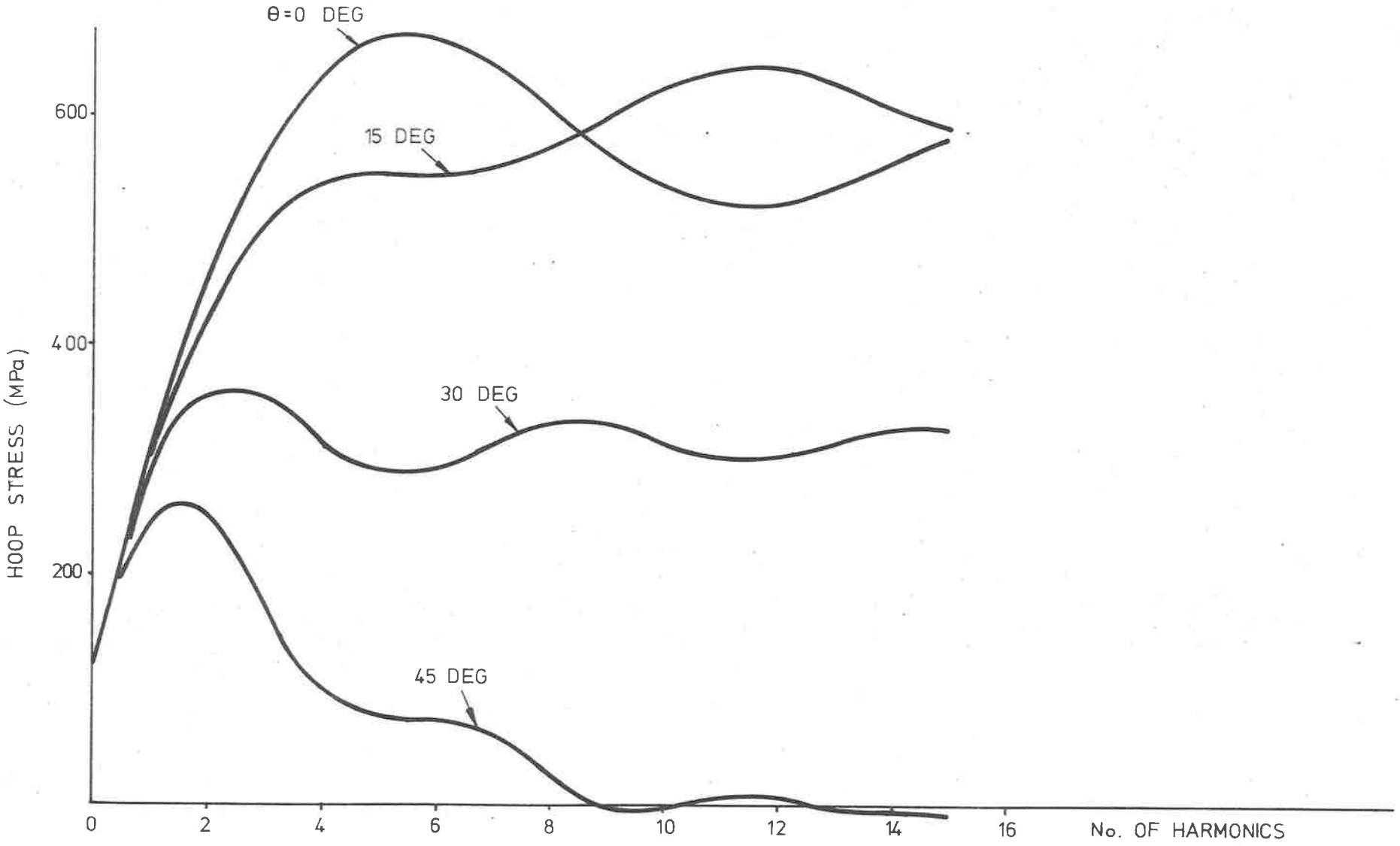

FIGURE 4·7 CONVERGENCE OF HOOP STRESS B-D (t = 0·1 secs)

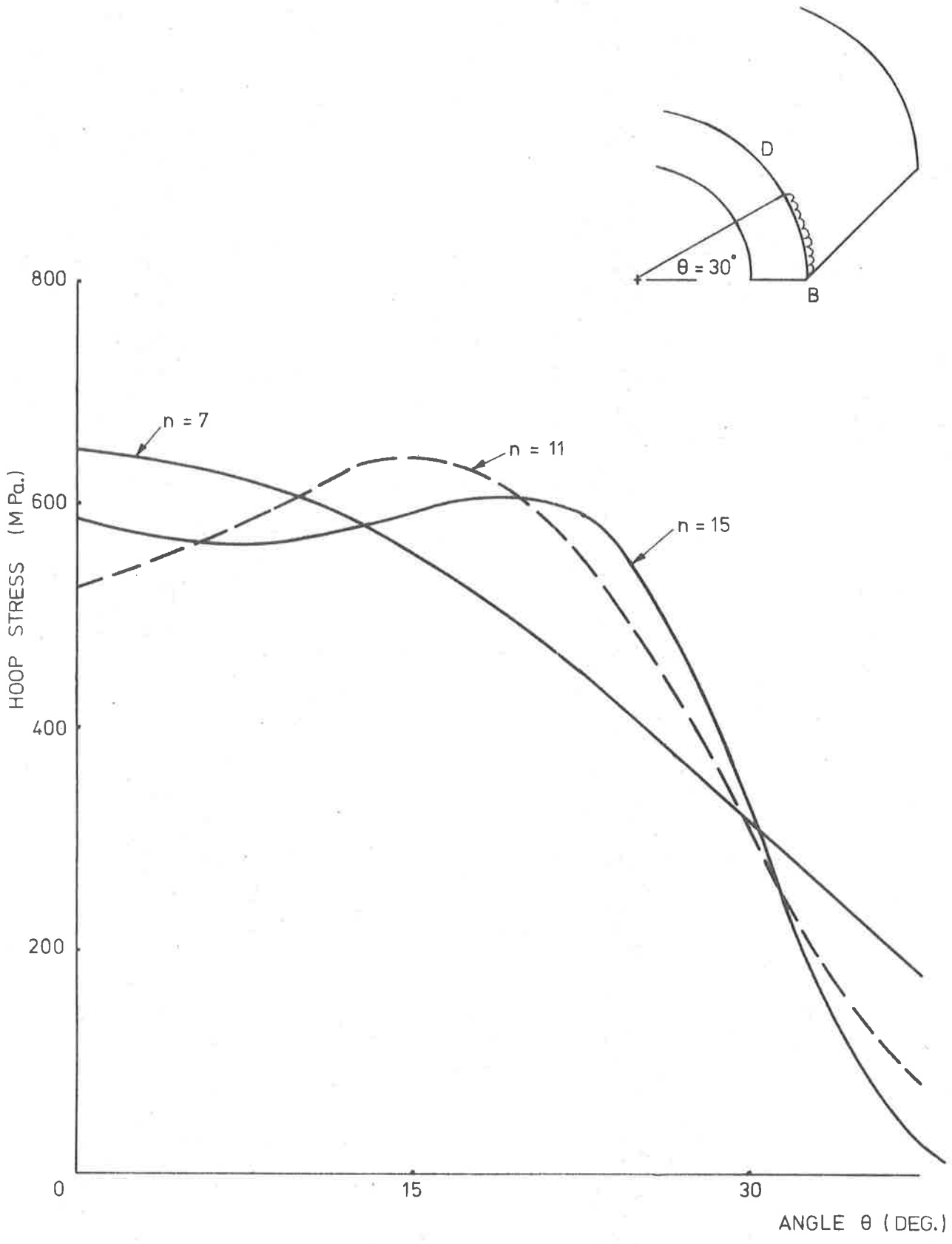

FIGURE 4·8 HOOP STRESS AT B — D
AFTER n HARMONICS
(t = 0·1 SECS.)

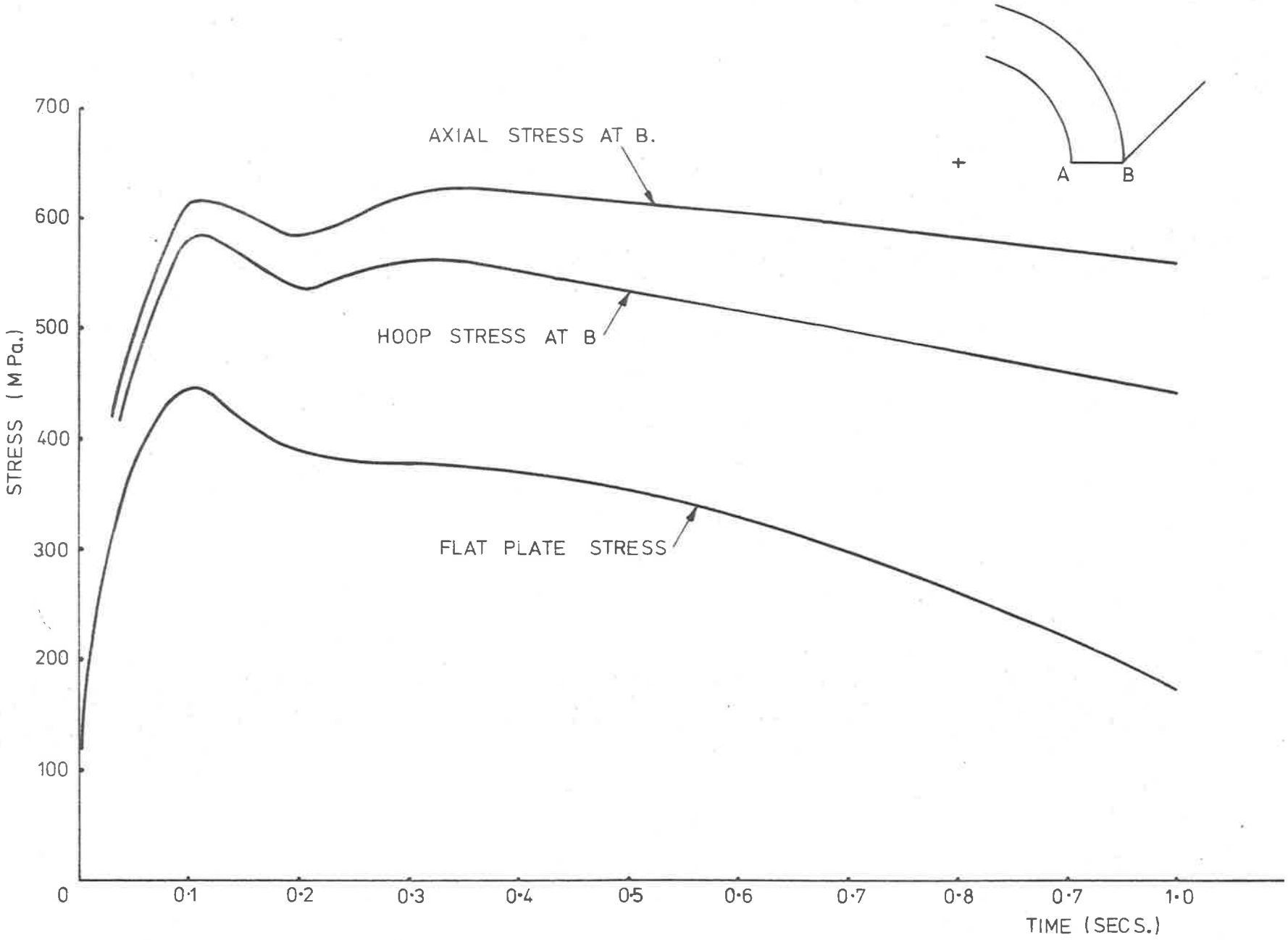

FIGURE 4·9 VARIATION OF STRESS WITH TIME.

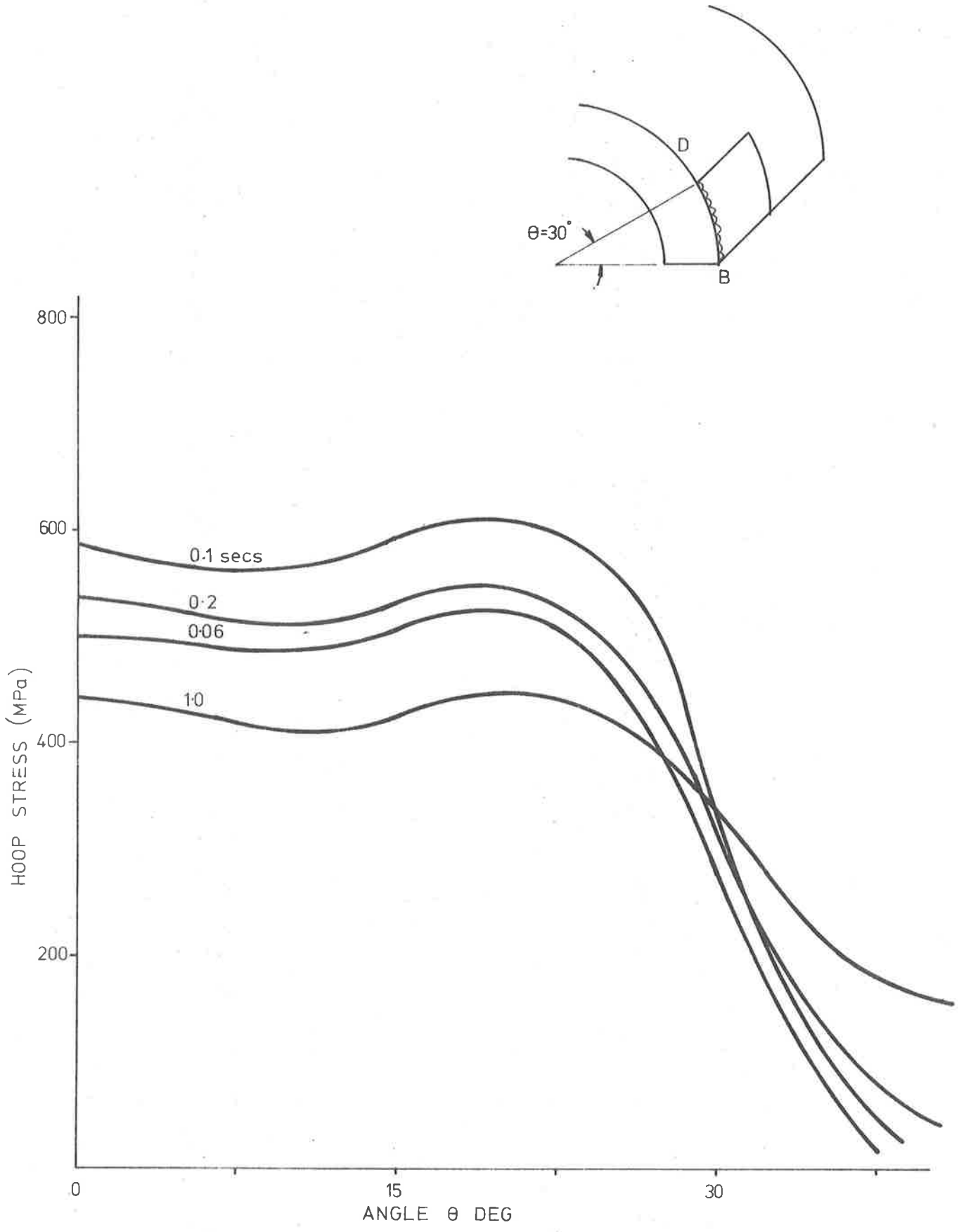

FIGURE 4·10 HOOP STRESS AT B-D

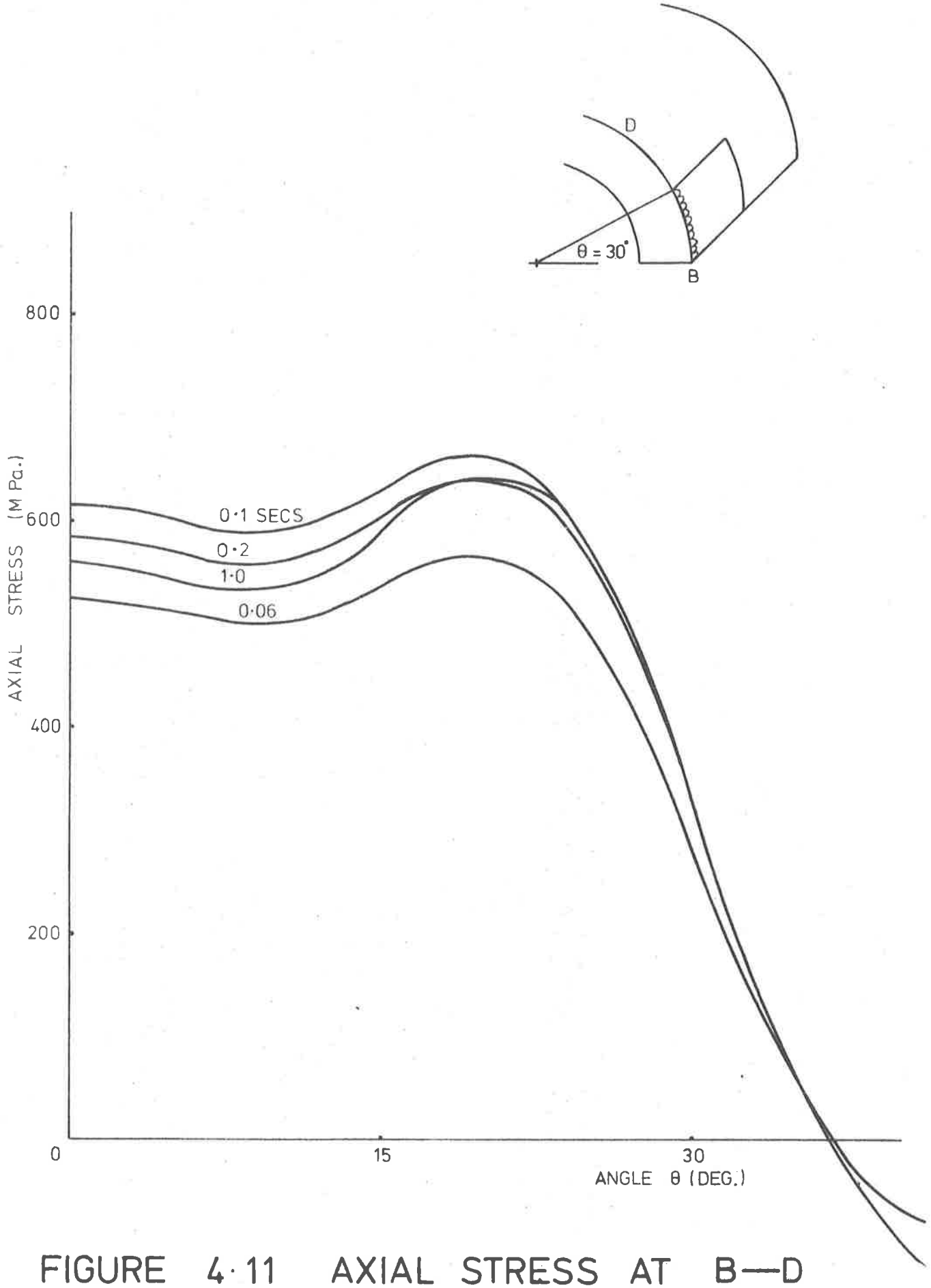

FIGURE 4·11 AXIAL STRESS AT B—D

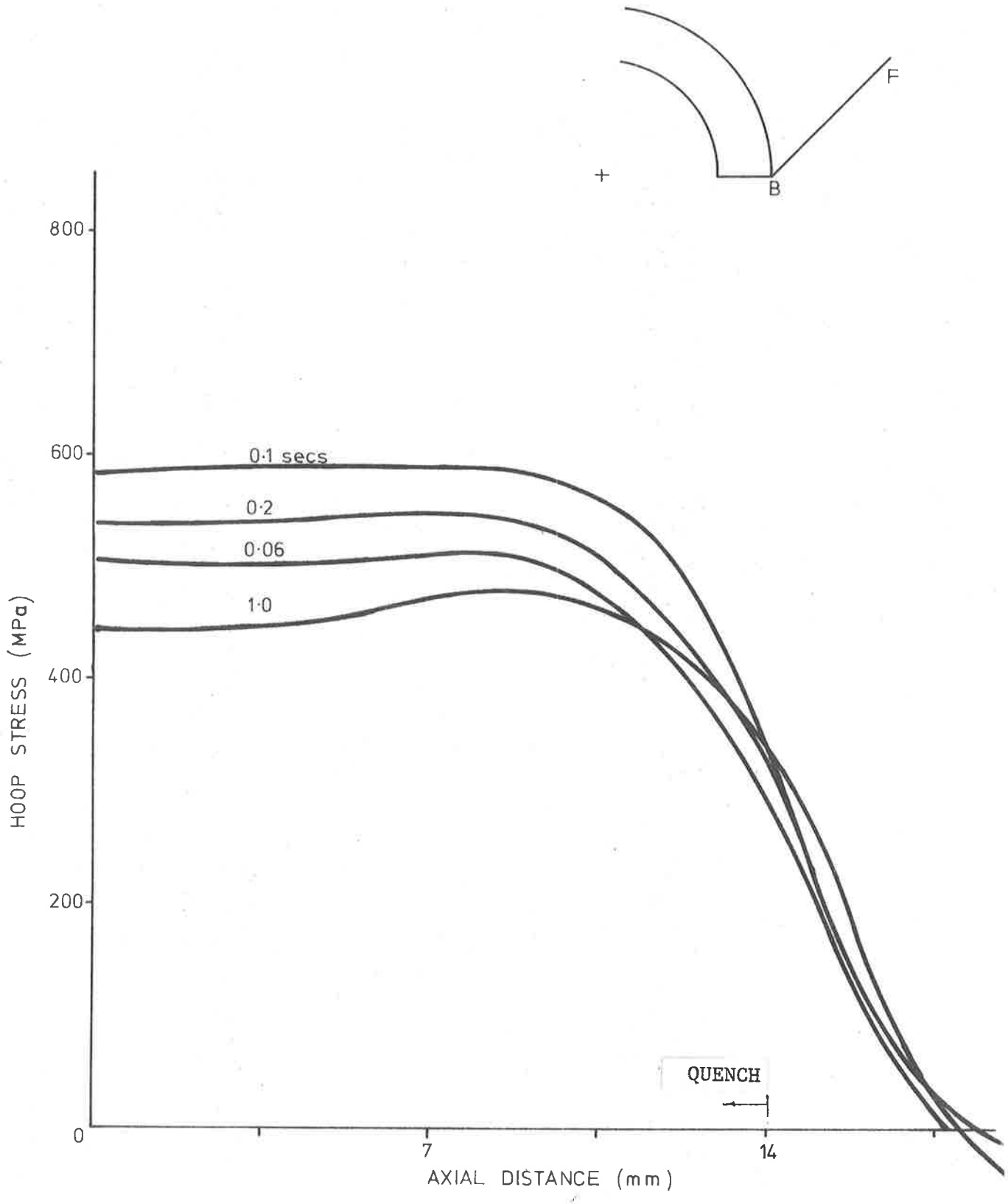

FIGURE 4·12 HOOP STRESS B – F

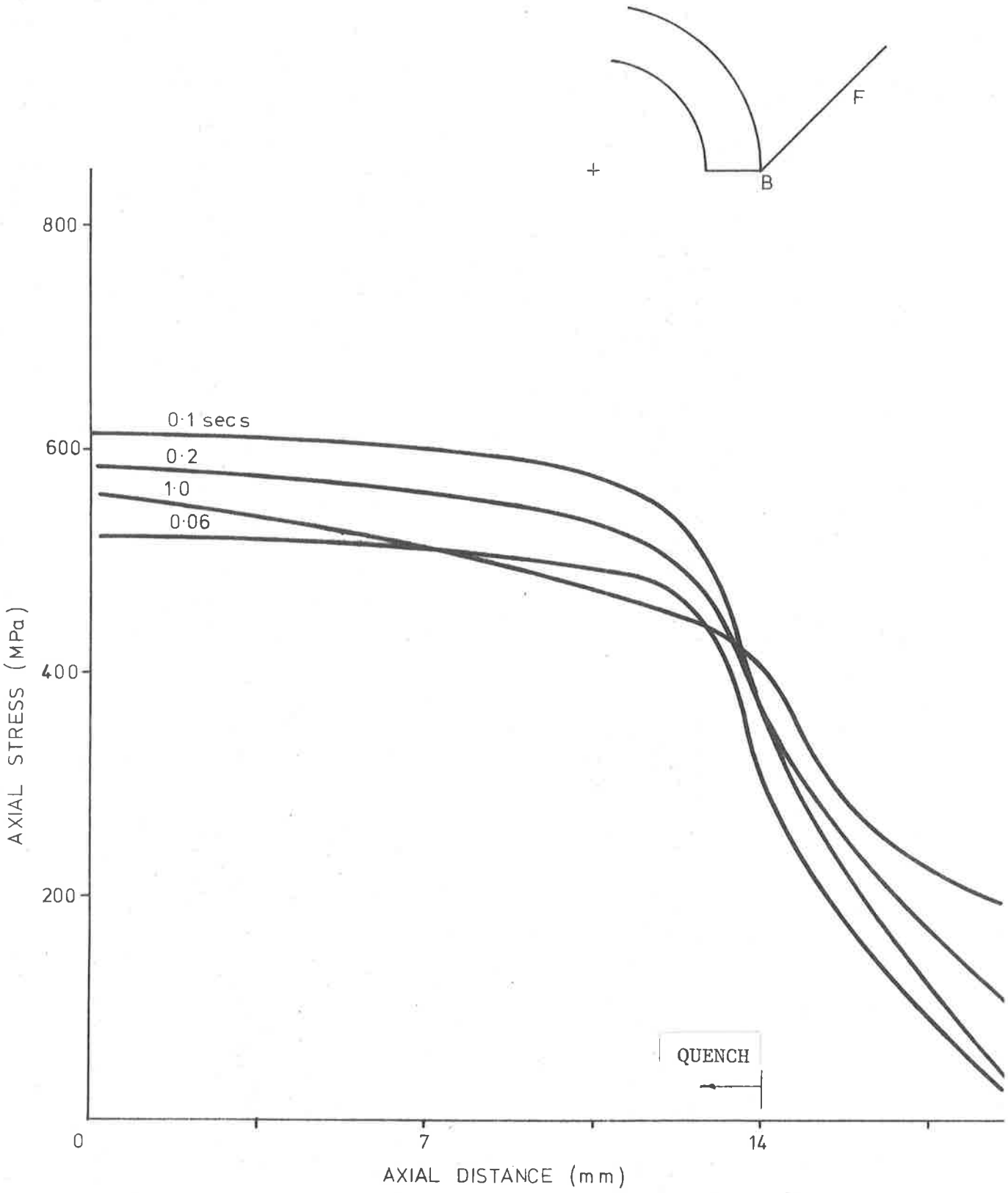

FIGURE 4·13 AXIAL STRESS AT B-F

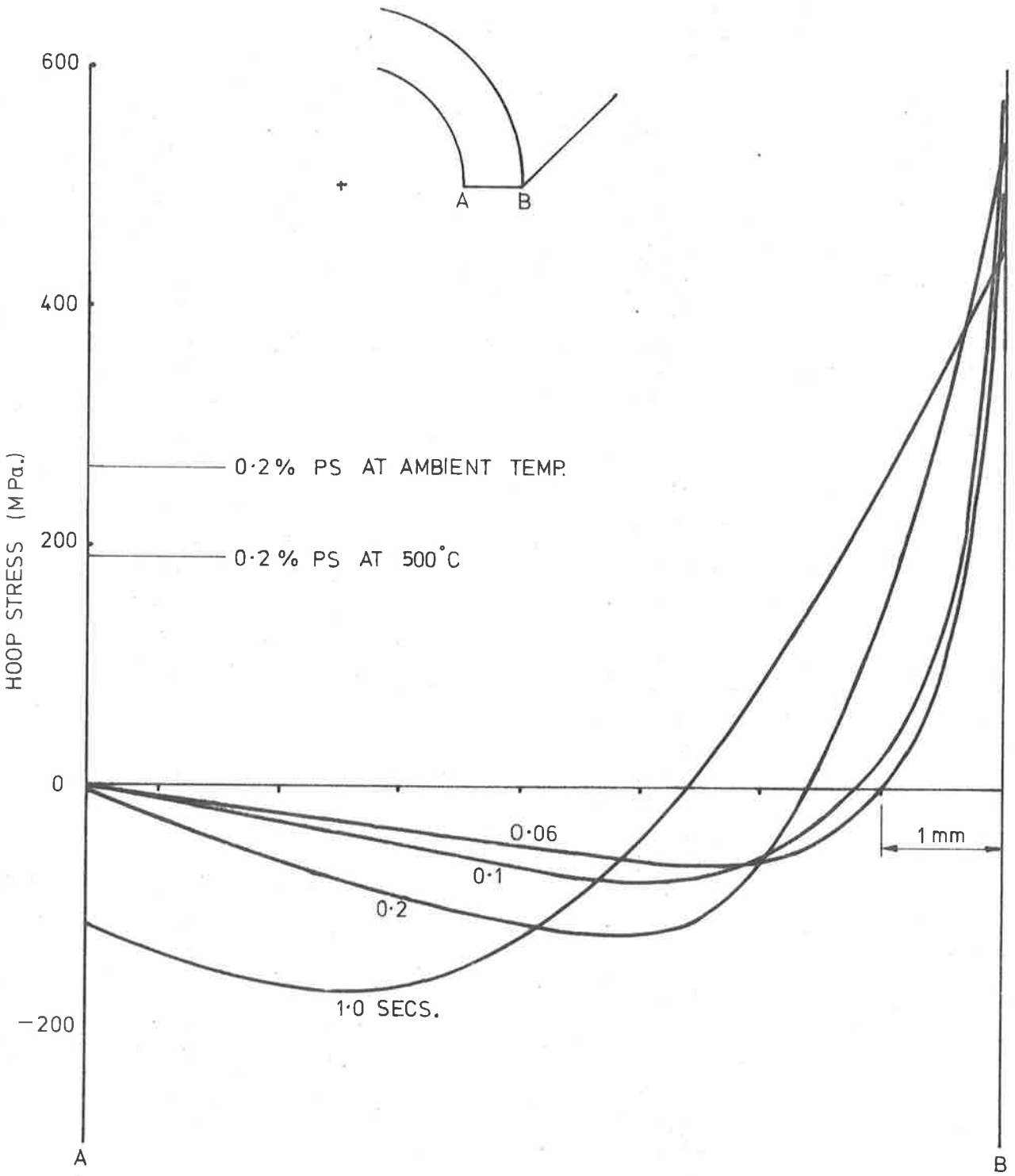

FIGURE 4·14 HOOP STRESS AT A – B

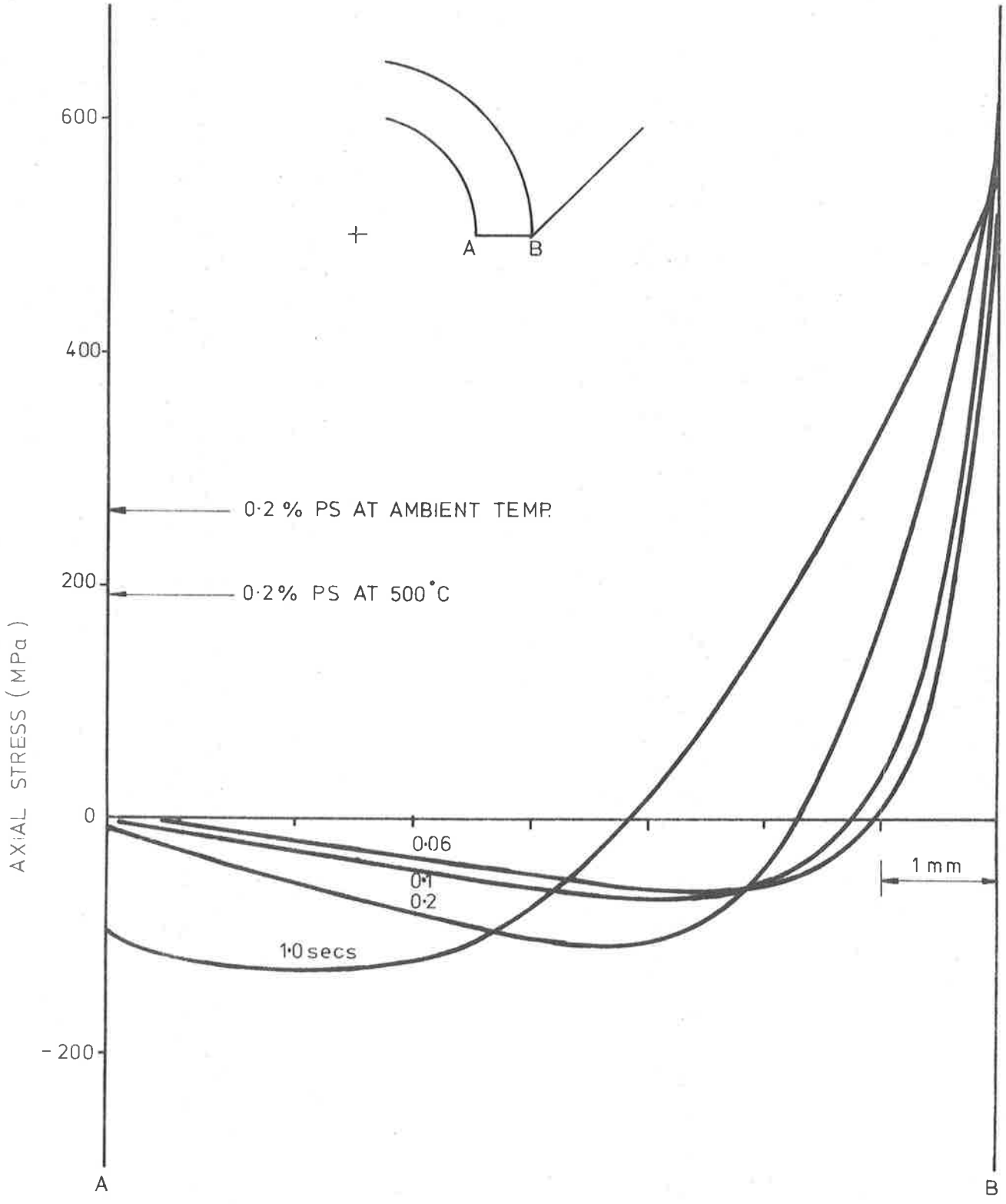

FIGURE 4·15 AXIAL STRESS AT A-B

5 CONCLUSIONS

The 3D heat-conduction analysis carried out using finite elements although time-consuming both in terms of data preparation and computer time, did provide a means of obtaining solutions to a complex transient problem. Such problems can often be simplified, as shown in this case with the 2D and axisymmetric solutions, to give economical and useful results in good agreement with results from a 3D analysis within the limited area that the simplification is applicable.

When a subsequent 3D finite element stress analysis is to be carried out such a simplified temperature analysis would be inadequate. If a 2D thermal stress analysis is contemplated using temperatures from a 2D heat-conduction analysis, complications can arise because of strains occuring in the out-of-plane direction which may require unrealistic assumptions to be made. Generally, if a problem cannot be justifiably simplified by assuming plane strain or plane stress then a 3D analysis becomes necessary, this being the case for the superheater tube subjected to a localised surface cooling.

The approach adopted of applying a harmonic stress analysis, where a 3D solution is obtained by superimposing a number of 2D harmonic solutions, enabled results to be obtained in times equivalent to the heat-conduction computer analysis times. This represents a substantial saving over the time required for a conventional 3D finite element stress analysis. The harmonic technique is not restricted to thermal loading and can be used for applied point loads, line loads

and pressure loading using the Fourier Series representation. The decision as to which approach should be used depends on the particular problem being considered. For a steady-state thermal stress analysis or a single loading-case problem, the conventional direct method of 3D finite element analysis would normally be used, the extra time required for a single solution being offset by avoiding the need for harmonic loads. On the other hand for problems involving numerous solutions, such as transient or multi-loadcase problems, the harmonic approach offers a means of obtaining results more economically. The saving depends largely on the number of harmonics required, which in turn depends on the nature of the applied loading and the degree of accuracy required. The superheater tube problem represents an extreme case involving large temperature gradients requiring 15 harmonics for the analysis, but solutions were still obtained in times comparable to the 3D temperature analysis which had only one variable per node.

Certain conclusions may be drawn from the results which are relevant to the parameters involved in the water washing operating. Figure 4.9 shows that if deslagging can be effectively carried out for quench times of less than 0.1 seconds then lower stresses will be produced in the tube and for a time of 0.01 seconds the elastic limit would not be exceeded. For times in excess of 0.1 seconds the elastic analysis shows high tensile peaks to occur at the quenched surface although in fact such peaks would be cut-off at the yield stress. If it was found that effective deslagging could not be achieved at times less than 0.1 seconds, making yielding at the surface inevitable, then as short a quench time as possible should be used to ensure the minimum depth

over which the elastic limit is exceeded. Figure 4.15 shows that a quench time of 1.0 seconds leads to yielding over a depth twice that reached for a quench time of 0.2 seconds. The shortest quench time necessary could be achieved by a suitable combination of the probe penetration velocity, the speed of rotation and the number of water jets used. The spiral contact path of the water jet results in a progressive quenching along the tubes and the stresses determined by the analysis would apply at the outside boundary of the expanding circular quenched area. The formation of surface cracks leads to an effective reduction in the outside diameter of the tube but would provide a crust giving thermal protection to the underlying layers so that the depth to which the elastic limit was initially exceeded would not be increased further. This means that crack propagation into the tube due to thermal fatigue would be expected to reach a limited depth.

The analysis carried out was for a surface quench initiated at the time $t = 0$ when the tube was assumed to be at a uniform temperature of 500°C. Under normal circumstances there would be a surface deposit on the tube which would be removed by the initial effects of the quench so that when the jet subsequently strikes the cleaned surface the temperature would have been slightly reduced. The analysis therefore represents the severe case of a water jet impinging on a clean, uncooled surface.

The results show the effects of the first quench when no residual stresses were present as a result of previous quenching. After the first quench, when the tube has been reheated to the normal operating temperature, there will be residual compressive stresses at the surface where the elastic limit was exceeded. Subsequent quenching would still produce stresses beyond the elastic limit at the surface, but the depth to which the elastic limit was exceeded should be reduced. An extension to this work could be to consider the elastic-plastic behaviour of the steel and to examine the stress cycling produced by continued quenching.

BIBLIOGRAPHY

1 Zienkiewicz, O C and Cheung, Y K. Finite elements in the solution of field problems. The Engineer, 220, 507-510 (1965).

2 Zienkiewicz, O C and Parekh, C J. Transient field problems : 2D and 3D analysis by isoparametric finite elements. Int. J. Num. Meth. in Engineering, Vol 2, 61-67 (1970).

3 Zienkiewicz, O C. The finite element method in engineering science. McGraw-Hill, London, 1971.

4 Irons, B M. A frontal solution program for finite element analysis. Int. J. Num. Meth. in Engineering, Vol 2, 5-32 (1970).

5 Cheung, Y K and Medwell, J O. The finite element method applied to the solution of heat conduction problems. Rev. Roum. Sci. Techn. - Méc. Appl., Tome 14, No 2, p 361-372, Bucarest, 1969.

6 Donea, J. On the accuracy of finite element solutions to the transient heat-conduction equation. Int. J. Num. Meth. in Engineering, Vol 8, 103-110 (1974).

7 Comini, G., Del Guidice, S., Lewis, R W and Zienkiewicz, O C. Finite element solution of non-linear heat conduction problems with special reference to phase change. Int. J. Num. Meth. in Engineering, Vol 8, 613-624 (1974).

8 Wood, W L and Lewis, R W. A comparison of time marching schemes for the transient heat-conduction equations. Int. J. Num. Meth. in Engineering, Vol 9, 679-689 (1975).

9 Lees, M. A linear three-level difference scheme for quasilinear parabolic equations. Maths. Comp., 20. 516-622 (1966).

10 Wilson, E L. Structural analysis of axisymmetric solids. AIAA Jour., Vol 3, No 12 (1965).

11 Cheung, Y K. Finite strip methods in structural analysis. Pergamon, Oxford, 1976.

12 Timoshenko, S and Goodier, J N. Theory of elasticity. McGraw-Hill, London. 1951

13 Johns, D J. Thermal stress analysis. Pergamon, London. 1965

14 Ellery, A R, Johnson, T R and Newton, J D. Investigation into the likelihood of thermal fatigue damage to furnace and superheater tubes caused by on-load water deslagging. ASME, Jour. Engng. Power, April 1974.